DOCTOR OF PHILOSOPHY

Transparent heterogeneous terrestrial optical communication networks with phase modulated signals

Christopher French

2012

Aston University

Transparent Heterogeneous Terrestrial Optical Communication Networks With Phase Modulated Signals

Christopher R French
Doctor of Philosophy

Aston University

September 2010

ASTON UNIVERSITY

Transparent Heterogeneous Terrestrial Optical Communication Networks With Phase Modulated Signals

Christopher R French
Doctor of Philosophy, 2010

Thesis Summary

This thesis presents a large scale numerical investigation of heterogeneous terrestrial optical communications systems and the upgrade of fourth generation terrestrial core to metro legacy interconnects to fifth generation transmission system technologies. Retrofitting (without changing infrastructure) is considered for commercial applications.

ROADM are crucial enabling components for future core network developments however their re-routing ability means signals can be switched mid-link onto sub-optimally configured paths which raises new challenges in network management. System performance is determined by a trade-off between nonlinear impairments and noise, where the nonlinear signal distortions depend critically on deployed dispersion maps. This thesis presents a comprehensive numerical investigation into the implementation of phase modulated signals in transparent reconfigurable wavelength division multiplexed fibre optic communication terrestrial heterogeneous networks.

A key issue during system upgrades is whether differential phase encoded modulation formats are compatible with the cost optimised dispersion schemes employed in current 10 Gb/s systems. We explore how robust transmission is to inevitable variations in the dispersion mapping and how large the margins are when suboptimal dispersion management is applied. We show that a DPSK transmission system is not drastically affected by reconfiguration from periodic dispersion management to lumped dispersion mapping.

A novel DPSK dispersion map optimisation methodology which reduces drastically the optimisation parameter space and the many ways to deploy dispersion maps is also presented. This alleviates strenuous computing requirements in optimisation calculations. This thesis provides a very efficient and robust way to identify high performing lumped dispersion compensating schemes for use in heterogeneous RZ-DPSK terrestrial meshed networks with ROADMs. A modified search algorithm which further reduces this number of configuration combinations is also presented. The results of an investigation of the feasibility of detouring signals locally in multi-path heterogeneous ring networks is also presented.

Keywords: Fibre Optic Communications, Wavelength Division Multiplexing, Optimization, Chromatic Dispersion Management, RZ-DPSK Modulation Format.

To my dearest family

Acknowledgements

My gratitude to Prof. Sergei K. Turitsyn, my Supervisor, for his view on all things around. I am expanded by your skills, your knowledge and your patience. Thank you for everything.

Dr. Wladek Forysiak from Ericsson UK, my Industrial Supervisor, helped with industry perspective and getting this work up and running.

Dr. Sonia Boscolo taught me new aesthetics to solving problems and how to manage change for which I am deeply grateful.

Dr. Ranjeet Bhamber got me up and running quickly when I arrived at Aston. Thanks for everything.

Dr. Irina Nasievo was another that helped me settle into life at Aston. She pointed out important milestones in the first year.

Thanks to Dr. Thomas Alsop who offered friendship and always provided sound advice as a friend does.

Contents

List of Acronyms

AM	Amplitude Modulation
AMF	Advanced Modulation Format
ASE	Amplified Spontaneous Emission
ASK	Amplitude Shift Keying
AWG	Arrayed Waveguide Grating
BER	Bit Error Rate
CD	Chromatic Dispersion
CT	Cross Talk
DCF	Dispersion Compensating Fibre
DCM	Dispersion Compensation Module
DEMUX	De-Multiplexer
DFB	Distributed Feedback
DPDM	Doubly Periodic Dispersion Map
DPSK	Differential Phase Shift Keying
DQPSK	Differential Quadrature Phase Shift Keying
DSA	Dual Stage Amplifier
DWDM	Wavelength Division Multiplexing
EDFA	Erbium Doped Fibre Amplifier
FBG	Fibre Bragg Grating
FP	Fabry Perot
FSK	Frequency Shift Keying
FWHM	Full Width at Half Maximum
FWM	Four-Wave Mixing
GVD	Group Velocity Dispersion
IFWM	Intra-channel Four-Wave Mixing
IM	Intensity Modulation
IMDD	Intensity Modulated Direct Detection
ISI	Inter-Symbol Interference
ITU	International Telecommunication Union
IXPM	Intra-channel Cross Phase Modulation
LAN	Local Area Network

MAN	Metro Access Network
MSSI	Mid-Span Spectral Inversion
MUX	Multiplexer
MZM	Mach-Zehnder Modulator
NLPN	Nonlinear Phase Noise
NLSE	Nonlinear Schrödinger Equation
NPS	Nonlinear Phase Shift
NRZ	Non Return-to-Zero
OEO	Optical Electrical Optical
OOK	On-Off Keying
OPC	Optical Phase Conjugation
OSNR	Optical Signal to Noise Ratio
OXC	Optical Cross Connect
PAD	Path Average Dispersion
PMD	Polarisation Mode Dispersion
PRBS	Pseudo Random Binary Sequence
PSK	Phase Shift Keying
PTN	Photonic Transport Network
ROADM	Reconfigurable Optical Add Drop Multiplexer
RZ	Return-to-Zero
RZ-DPSK	Return-to-Zero Differential Phase Shift Keying
SE	Spectral Efficiency
SMF	Single Mode Fibre
SPDM	Singly Periodic Dispersion Map
SPM	Self-Phase Modulation
SRS	Stimulated Raman Scattering
SSA	Single Stage Amplifier
TDC	Tuneable Dispersion Compensation
VIPA	Virtually Imaged Phase Array
WAN	Wide Area Network
WD	Waveguide Dispersion
WDM	Wavelength Division Multiplexing
WSS	Wavelength Selective Switch
XPM	Cross-Phase Modulation

List of Figures

List of Tables

Chapter 1

Introduction

Society can now use data, voice, high definition images and video to share ideas and information, whenever they want, in a world where knowledge is at our fingertips via information content which is mobile, transportable and multiplatform. Businesses are pushing for ultra high speed Ethernet technologies through their need for wide ranging applications such as telephony/video, VPN services, fast remote storage access for archival needs / disaster recovery, transparent cloud computing and grid computing power of which data output must be transmitted over local core networks. At the 2008 Ministerial Conference on e-Inclusion held in Vienna, ministers rightly concluded that "broadband is becoming an essential commodity like water or electricity and is today an indispensable service for the effective participation in global trade, economy, education, culture, politics and society" [1]. We are now seeing the introduction of internet televisions, tablets and powerful smartphones which have become computer like, increasing innovation of end user applications which are pushing the current demand for optical fibre bandwidth to unprecedented levels. In the UK we barely meet the bandwidth needs of today rather than being ready for future innovation. Of course a solution to meeting future bandwidth demand is to lay new fibre either across existing routes and/or in "green field". Being a high capital expenditure option, new assets are usually of last resort. Overlays of new technologies which make use of existing fibre in plant, so that new builds are avoided, are cheaper and therefore better fulfil each network operator's business objective of reducing the cost of transmitted bits. After the telecom boom of the later 1990s came a downturn from 2001, fuelled by over deployment of fibre in the past, coupled to an over deployment of optimism in capital markets, and a demand for bandwidth which was less than supply. The result was dark fibres. Today the tide has turned. Without strong investment in optical fibre networks one country's internet and its services may fall behind the capability of others, putting shackles on business that serves for serious economic consequences. Systems and associated components that communicate at high bit-rates must continue to reduce in price to make their wider adoption accessible. Network optimization and simplification is instrumental to the provision of new bandwidth and as such is the top down motivation for this research.

1.1 Fibre Optic Communication Network Topologies

The architecture of fibre optic communication networks is often described by the subdivision of all optical networks into three general types, each of which are characterised by the geographical distance over which the particular network spans. The three types are Core, Metro and Access Networks. The farthest spanning of these are the Core networks also known as Wide Area Access networks (WANs). Core networks are long-distance / long-haul links which can provide inter-city connections over continental distances, crossing international boundaries by land (terrestrial links), or along the ocean beds (submerged links). Core networks tend to transmit digital bits at faster speeds as well as over longer distances, than either Metro or Access networks, they also carry aggregated data from Metro / Local networks between cities and this has lead them to be termed "the Backbone" of modern Photonic Transport Networks (PTNs).

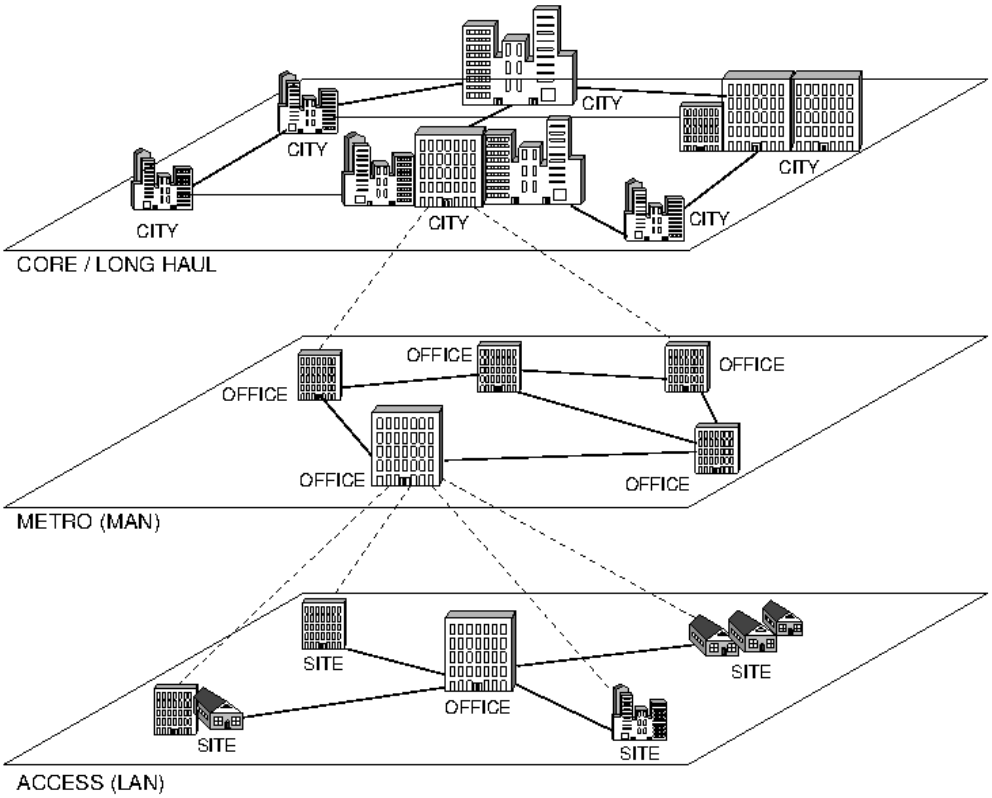

Figure 1.1: Planar View of Terrestrial Network Layers: WAN, MAN and LAN.

Although terrestrial core transmissions can travel thousands of km in the Americas and the Far East, here in Europe they typically cover distances between 300km and 1500km. Fourth generation terrestrial networks were mostly deployed between 1998 and 2001 and typically have 60 to 80 channels. They are 2.5 Gb/s and 10 Gb/s intensity modulated systems with single mode fibre and dispersion compensating fibre (SMF-DCF) infrastructures accompanied by Erbium doped fibre

amplification (EDFA). The major objective of the fifth generation of networks is to increase the fibre spectral efficiency and per channel bit rates whilst economising on costs associated with component inventories. The upgrade of fourth generation terrestrial core / regional to metro interconnects to fifth generation technologies is the central theme of this thesis. More specifically, their upgrade, architecture, simulation, emulation and optimisation are explored. An additional major design trend in fifth generation light wave communication systems is the maximisation of unregenerated transparent transmission distance. An opaque transmission is when signals are converted from the optical domain to the electrical layer for regeneration before returning to the optical domain for re-transmittance and produces message delays due to added signal processing. Regeneration can be cumbersome and adds additional cost however regeneration can be avoided in terrestrial networks by improved dispersion management.

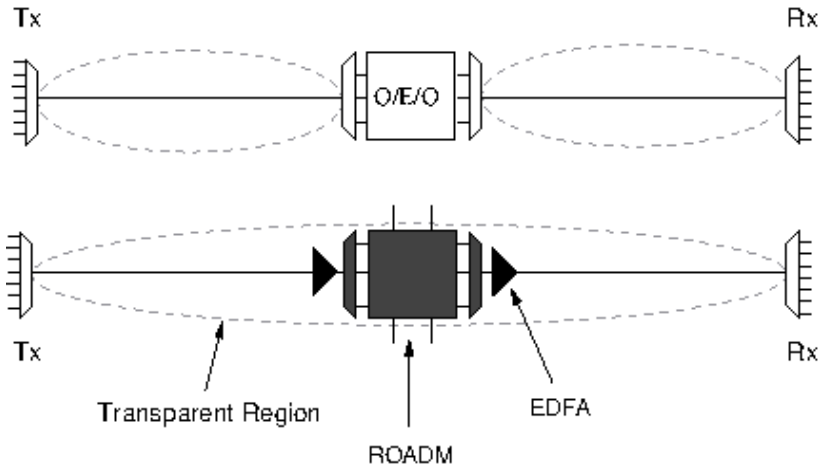

Figure 1.2: ROADMs and EDFAs increase transparent transmission distance

Core network design today aims to reduce the number of opaque transmission paths and increase the length of the transparent transmittable light-path (see Figure 1.2). However as propagation distance is often limited by the accumulation of degradations to signal attributes – amplitude, frequency, phase, polarisation and optical signal to noise ratio (OSNR) – restricting the signal to the optical domain is difficult as the number of optical amplifiers and wavelength switching components increases with propagation distance. The key transparency enabling technologies are the Reconfigurable Optical Add Drop Multiplexer (ROADM), Optical Cross Connect (OXC) and Wavelength Selective Switch (WSS). ROADMs and other switching technologies come at a cost but have the benefit of adding network flexibility and can be used to rescue dark portions of the network (stranded wavelengths), thus better utilising available bandwidth.

Transparent networks require robust systems which feature channels that are robust to the historical path and optical routing of the optical signal. Since ROADMs first appeared in a handful of North American and European vendors' WDM tool cupboards in 2003 they have dramatically changed the management and provisioning of terrestrial Core networks. In 2004, Swisscom / Belgacomm built the first pan-European ROADM network. Today, nearly all Core networks are constructed with ROADMs. This has in-turn driven down prices of these components and for this reason, ROADMs are also starting to appear in Metro access networks (MAN) where their use has been driven by the continued growth of end-user bandwidth demands. Traffic patterns are highly diverse in MANs with wavelengths frequently reconfigured. Future topologies in MANs will likely feature many cascaded ROADMs which places strong emphases on robust dispersion management within each inter ROADM fibre section. Far less focused on transparency, the Local Area networks (LAN) or "distribution rings", implement the "final miles" business and residential connectivity, usually spanning 5 to 50 km, and are characterized by a diverse mix of technologies serving the end-user. Inter-Metro and Local Area Networks are not considered in this work. The main foci of this thesis are the terrestrial WAN to WAN and Wan to Metro all-optical interconnects. The three physical layers of the network are joined via intra layer connections. Figure 1.1 shows a planar view of interconnected terrestrial WAN, MAN and LAN physical layers. The interconnection of point-to-point links in and between layers has led to ring topologies, which when also connected, create interconnected ring structures from which Mesh optical networks are born. Traffic in a mesh network is allocated a particular route itself chosen from several possible routes, thus the mesh facilitates optical transparency and enables shared protection at the wavelength level.

1.2 WDM Systems and Spectral Efficiency

The Wavelength Division Multiplexing (WDM) technique is attractive as it allows a reduced number of channels to achieve a given capacity and provides terabit scalability. Early systems in the 1990s were point to point links and featured 4 to 8 wavelength channels. Each fibre channel has its own transmitter in which the optical carrier is assigned a unique wavelength. Multiplexers (MUX) combine the output of all modulators into a single transmission fibre where the non-overlapping channels propagate together in concert and the demultiplexer (DEMUX) with its wavelength selective mechanisms can separate the multi-wavelength channels back into individual signals.

MUX and DEMUX have been demonstrated using a range of technologies including integrated planar Arrayed Waveguide Gratings (AWG) [2], Thin Film Filters [3] and Fibre Bragg Gratings (FBG) [4]. As thin film filters are really only suitable for large channel spacing's (100GHz +) [4], the AWG

technologies are currently those most commonly deployed as they are suitable for large numbers of channels [2] and therefore better accommodate future scalability.

WDM technology is most useful in mesh architectures allowing dynamic light paths where the signal wavelength can be switched from fibre to fibre. This allows a wider choice of routes, transmission protection by means of protection switching and optical transparency which in turn affords prospect of reconfigurable, flexible, and intelligent / strategic network layers. As the quantity of information transmitted is a function of the wavelength count in a given frequency range, we can quantify bandwidth utilization with spectral efficiency (SE):

$$\text{S.E.} = \frac{B \times H}{\Delta\omega} \left(\text{bits/s} \cdot \text{Hz} \right) \tag{1.1}$$

where B is the symbol rate, H is the number of bits conveyed per symbol, and $\Delta\omega$ is the occupied bandwidth. The ability to increase SE is determined by having stable single-frequency lasers and de-multiplexers which can select individual channels from an array of channels. SE can be increased by tightening channel spacing and / or increasing channel bit rates. The ITU original specification for WDM was a 100 GHz (approx. 0.8 nm) grid spacing in frequencies 186 – 196 THz covering the C and L bands in the wavelength range from 1530 – 1625 nm. The ITU-T G.694.1 (2002) [5] specification upgraded spectral grids for WDM applications to allow 100, 50, 25, and 12.5 GHz spacing's around a nominal central reference of 193.10 THz (1552.52 nm). Current WDM systems mostly use 100 or 50 GHz channel spacing with up to 160 channels in operation. A 50 GHz grid allows for an SE of 80% at 40 Gb/s transmission speeds.

For a given bandwidth, increasing the spectral density can make a system more susceptible to linear and non-linear crosstalk and therefore it is more desirable to pack in 2 x 40 Gb/s channels than 8 x 10 Gb/s channels (20 Gb/s being incompatible with SDH). For this reason, a capacity increase first concerns higher speeds after which tighter channel spacing is considered as the secondary measure.

1.3 Transparency Enabling Technologies for WDM

The current market value of transparent optical networks featuring transparent optical flexibility [6] is now estimated at around US$5 billion per annum, an amount approaching a third of the total value of the global optical networks equipment market (estimated at $16 billion in 2008 [6] and increasing). WDM equipment constitutes the transparent transport part of this market and makes up nearly 50% of the current total value.

This shift to optical transparency began when the EDFA became commercially available in the 1990's after the process of doping silica / fluoride fibres with rare-earth Erbium ions was fully refined [7]. WDM afforded optical signals to be multiplexed within the 1550 nm band in order to profit from the capabilities and low cost of EDFAs, which are practical for use in the C and L bands. EDFAs have replaced and made obsolete per channel SONET/SDH optical-electrical-optical (OEO) regenerators and therefore have become the primary enabling technology of WDM. Before EDFAs, signals had to be regenerated every 35 km to 45 km due to laser, fibre loss and receiver performance limits. EDFAs allowed this distance to approximately double with gains of up to 25dB which improved receiver sensitivity.

An EDFA is an active fibre component which is pumped optically to achieve population inversion in order to amplify the incident light through stimulated emission. Pump-laser power as well as the amplifier structure can limit the maximum power to around 10 to 25dBm. Optical amplification granted the commonly found SMF span lengths found in today's networks of 80 to 90 km (90 km SMF has ~ 20dB fibre loss + insertion loss). Wide bandwidth EDFAs allow bit rate multiplication by increasing transponder numbers at the system edges allowing transmission line / amplifier schemes to remain fixed. EDFAs are deployable over a wide range of modulation speeds however the modulation format does limit signal density. The key requirement of optical amplifiers in WDM systems is flatness in the gain over different wavelengths, with ideally a uniform gain bandwidth, and a high output power. For WDM the uniformity of the gain spectrum is considered to be the most important. Although EDFAs boost signal power they introduce amplified spontaneous emission (ASE) adding noise to the signal. Each subsequent EDFA amplifies this noise in addition to the signal itself and multiplies detrimentally in links where they are used in multiples. The introduction of background noise limits transmission performance by reducing the optical signal to noise ratio (OSNR) and thus the cleanliness of the transmitted signal. Amplifier spacing is often shorter in longer systems to reduce noise build up since the higher the gain, the more noise is amplified with the signal. Remote outside structures which house amplifiers are often referred to as 'huts' and with mixed EDFA/Raman amplification schemes, amplifier 'hut-skipping' is possible. As a central concern of this thesis is on economical upgrades of existing systems, we avoid costs associated with amplification scheme overhauls and make use of the EDFA only amplification type most commonly found in 4th generation systems.

ROADMs provide an important function due to the dynamics and growth of networks. They perform three main faculties, they can (a) direct wavelength channels to any port, (b) power balance and monitor channels and (c) provide a means to controlling stranded wavelength capacity. From a remote office, wavelengths can be switched and redirected, eliminating the need to predict and pre-plan traffic during network installation. ROADMs can support both 10 Gb/s and 40 Gb/s channels [8], and

when placed at intermediate points in the transmission line their demultiplexing, switching and multiplexing capability affords a transition from classic point to point links to multipoint-to-multipoint links. Control plane software which uses routing and wavelength assignment algorithms allow each node to know the resources of other nodes on the network so that the optimal wavelength and path can be determined [9]. This however presents new challenges as multiple channels entering a ROADM can therefore be highly non-uniform.

ROADMs can be two-degree (most common) or multi-degree, where the degree refers to the numbers of WDM fibre pairs entering / exiting the ROADM node. There are now commercially available ROADMs that feature flexible port architectures and multiport WSS [9, 10] giving them the advantage of being both colourless and directionless.

1.4 Single Mode Optical Fibre

In essence, the first major breakthrough in transparent optical communication networks occurred when Charles Kao and George Hockham [11] professed that silica fibres of great transparency could be realised if light-absorbing impurities of primarily water and metals could be omitted from the manufacture of silica glass fibres and in doing so would allow light loss to be reduced from 1,000 decibels to less than 20 decibels per kilometre. Today, the maximum transmission distance and overall general performance of any fibre optic system depends not only on the transparency of the glass, but on fibre linear and nonlinear effects which determine optical signal behaviour in different manors dependent on whether the signal propagates in the low power noise-limited transmission regime or interacts with nonlinear fibre effects in the high power regime.

Standard Single Mode Fibre (SMF) is a step index fibre where the refractive index of the core is uniform throughout and undergoes an abrupt change (or step) at the cladding boundary. SMF is also dispersion unshifted fibre and was specified in the International Telecommunication Union (ITU) standard G.652 (see Figure 1.3). G.652 is the most common installed transmission fibre base in world networks and has a core diameter ~ 5μm and a cladding diameter ~ 125μm.

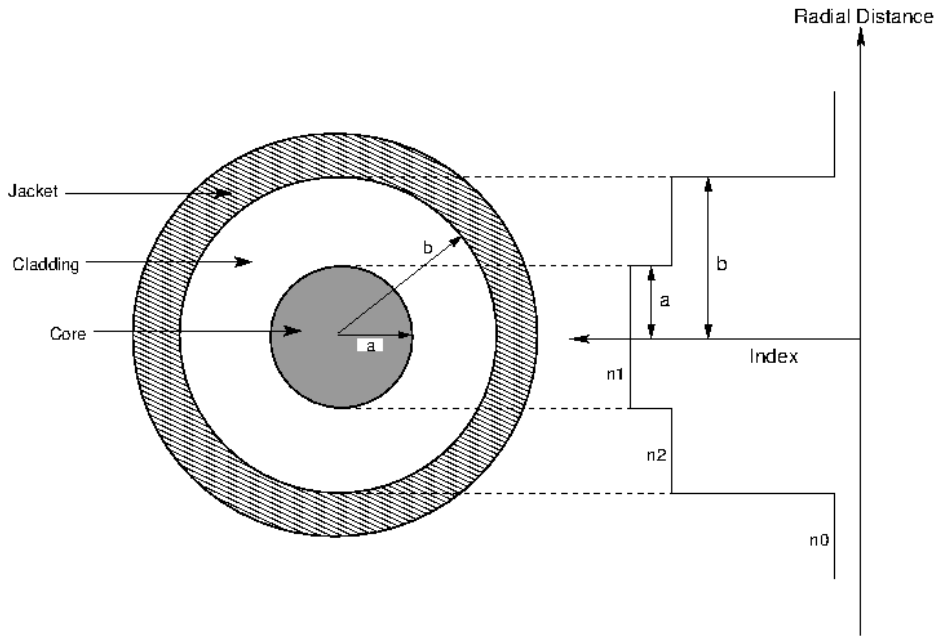

Figure 1.3: G.652 SMF is a Step Index Fibre

At a given wavelength, the number of modes supported by an optical fibre is dependent on the diameter of the fibre core and the difference between the refractive indexes of the core and its cladding. The relative core cladding index difference Δ is given by:

$$\Delta = \frac{n_1 - n_2}{n_1} \tag{1.2}$$

A characteristics measure of fibre profile is the V parameter [12]:

$$V = k_0 \, a \left(n_1^2 - n_2^2 \right)^{\frac{1}{2}} \tag{1.3}$$

where $k_0 = 2\pi / \lambda$ is the wave number, λ is the wavelength of light, a is the core radius and n_1 and n_2 are the refractive indexes of the core and cladding respectively. If $V \leq 2.405$ then the fibre is single mode and guides only the HE_{11} fundamental mode in both orthogonal polarisations whilst all other modes are cut-off at the operating wavelength. The assumption of a linearly polarised field is used in this thesis.

As the intensity of the light and its relation to the impact of nonlinear interactions depends on the cross-sectional area of the fibre core and since power is not distributed uniformly within the cross section of the fibre core, it is convenient to use an effective (cross-sectional) area $A_{\text{eff}} \left[\mu \text{m}^2 \right]$ which is given by:

$$A_{\text{eff}} = \frac{\left(\int_{-\infty}^{\infty} \int |F(x,y)|^2 dxdy \right)^2}{\int_{-\infty}^{\infty} \int |F(x,y)|^4 dxdy} \tag{1.4}$$

A standard single mode fibre has an effective core area $A_{\text{eff}} \sim 80\mu m^2$ at 1550nm.

1.5 Modelling Signal Transmission in Optical Fibres

The propagation effects during light pulse transmission in non-linear dispersive optical fibres can be characterised and modelled numerically through the nonlinear Schrodinger equation (NLSE). The NLSE accurately models various linear and nonlinear processes of fundamental interest in fibre optic communications. By including a nonlinear polarisation term, Maxwell's equations describing electromagnetic wave behaviour and therefore optical fields can be manipulated to obtain the wave equation from which the nonlinear Schrödinger equation can be derived. The wave equation is given as [13]:

$$\nabla^2 \mathbf{E} - \frac{1}{c^2} \frac{\partial^2 \mathbf{E}}{\partial t^2} = \mu_0 \frac{\partial^2 \mathbf{P}_L}{\partial t^2} + \mu_0 \frac{\partial^2 \mathbf{P}_{NL}}{\partial t^2} \tag{1.5}$$

where $\mathbf{E}(\mathbf{r},t)$ is the electric field, c is the speed of light in a vacuum μ_0 is the vacuum permeability and $\mathbf{P}_{\text{L}}$ and $\mathbf{P}_{\text{NL}}$ are the linear and nonlinear parts of the induced polarisation. To solve the wave equation the following assumptions are made. Firstly, as non-linear changes in the refractive index are quite small in practice we can treat $\mathbf{P}_{\text{NL}}$ as a small perturbation of $\mathbf{P}_{\text{L}}$. So that a scalar approach can be used, we also assume that the optical field will maintain its polarisation along the fibre length. Finally, we assume a quasi-monochromatic optical field such that $\Delta\omega / \omega_0 \ll 1$ where $\Delta\omega$ is the spectral width and ω_0 is the central frequency of the pulse spectrum. The electric field is then written in the form:

$$\mathbf{E}(\mathbf{r},t) = \frac{1}{2}\hat{x}\left[E(\mathbf{r},t)\exp(-i\omega_0 t) + \text{c.c.} \right] \tag{1.6}$$

where $\mathbf{E}(\mathbf{r},t)$ is slowing varying with time relative to the optical field and $\hat{x}$ is the polarisation unit vector. The polarisation components $\mathbf{P}_{\text{L}}$ and $\mathbf{P}_{\text{NL}}$ can be expressed similarly as:

$$\mathbf{P}_{\mathrm{L}}(\mathbf{r},t)=\frac{1}{2}\hat{x}\left[P_{\mathrm{L}}(\mathbf{r},t)\exp(-i\omega_0 t)+\text{c.c.}\right] \tag{1.7}$$

$$\mathbf{P}_{\mathrm{NL}}(\mathbf{r},t)=\frac{1}{2}\hat{x}\left[P_{\mathrm{NL}}(\mathbf{r},t)\exp(-i\omega_0 t)+\text{c.c.}\right]. \tag{1.8}$$

The Fourier transform is then defined as:

$$\tilde{E}(\mathbf{r},\,\omega-\omega_0)=\int_{-\infty}^{\infty}E(\mathbf{r},t)\exp\left[i(\omega-\omega_0)\right]t\,dt \tag{1.9}$$

and is found to satisfy the Helmholtz equation:

$$\nabla^2\tilde{E}+\varepsilon(\omega)\,k_0^2\,\tilde{E}=0 \tag{1.10}$$

where $k_0=\omega/c$ and $\varepsilon(\omega)$ is the dielectric constant which has a nonlinear component. The dielectric constant can be used to define the refractive index $\tilde{n}$:

$$\tilde{n}=n+n_2|E|^2 \tag{1.11}$$

where n_2 is the nonlinear index coefficient given by:

$$n_2=\frac{3}{8n}\mathrm{Re}\left(\chi^{(3)}_{xxxx}\right) \tag{1.12}$$

where Re is the real part of the third order susceptibility term $\chi^{(3)}_{xxxx}$, which has only one component in its fourth-rank tensor that contributes to the refractive index. It is such that Eq.1.10 can be solved by using the separation of variables to produce:

$$\tilde{E}(\mathbf{r},\omega-\omega_0)=F(x,y)\,\tilde{A}(z,\omega-\omega_0)\exp(i\beta_0 z) \tag{1.13}$$

where $F(x,y)$ is the modal distribution of the fundamental mode in the case of single mode fibre. The $\tilde{A}(z,\omega)$ term is a slowly varying function of z, and β_0 is the propagation constant. The result in Eq.1.10 allows the following equations for $F(x,y)$ and $\tilde{A}(z,\omega)$ to be obtained:

$$\frac{\partial^2 F}{\partial x^2}+\frac{\partial^2 F}{\partial y^2}+\left[\varepsilon(\omega)k_0^2-\tilde{\beta}^2\right]F=0 \tag{1.14}$$

$$2i\beta_0\frac{\partial \tilde{A}}{\partial z}+\left(\tilde{\beta}^2-\beta_0^2\right)\tilde{A}=0 \tag{1.15}$$

by assuming that $\tilde{A}(z,\omega)$ is a slowly varying function of z, the second derivative of $\tilde{A}(z,\omega)$ in Eq.1.15 is neglected. The dielectric constant in Eq.1.14 is approximated as:

$$\varepsilon=(n+\Delta n)^2\approx n^2+2n\Delta n \tag{1.16}$$

where Δn is given by:

$$\Delta n=n_2|E|^2+\frac{i\tilde{a}}{2k_0} \tag{1.17}$$

and $\tilde{a}=a+a_2|E|^2$ is the absorption coefficient, where a_2 is the two-photon absorption coefficient given by:

$$a_2=\frac{3\omega_0}{4nc}\,\mathrm{Im}\left(\chi^{(3)}_{xxxx}\right) \tag{1.18}$$

which is often relatively small for silica fibres so is often ignored. The Fourier transform $\tilde{A}(z,\omega-\omega_0)$ of $\tilde{A}(z,t)$ satisfies Eq.1.15 and can be written as:

$$\frac{\partial \tilde{A}}{\partial z}=i\left[\beta(\omega)+\Delta\beta(\omega)-\beta_0\right]\tilde{A} \tag{1.19}$$

Eq.1.19 shows that as each spectral component within the pulse envelope propagates along the fibre, it acquires a phase shift whose magnitude is both frequency and intensity dependent. The exact function of $\beta(\omega)$ is rarely known so that it then becomes useful to expand $\beta(\omega)$ in a Taylor series around the carrier frequency ω_0 as:

$$\beta(\omega)=\beta_0+(\omega-\omega_0)\beta_1+\frac{1}{2}(\omega-\omega_0)^2\beta_2+\frac{1}{6}(\omega-\omega_0)^3\beta_3+\ldots, \tag{1.20}$$

where $\beta_0 \equiv \beta(\omega_0)$ and the parameters β_m are defined as:

$$\beta_m = \left(\frac{d^m \beta}{d\omega^m} \right)_{\omega=\omega_0} \qquad (m = 1, 2, ...) \tag{1.21}$$

The term $\Delta\beta(\omega)$ in Eq.1.19 can also be expanded in a Taylor series and defined in the same manner. If the spectral width of the pulse satisfies $\Delta\omega \ll \omega_0$ the cubic and higher order terms in Eq.1.20 can be neglected due to the quasi-monochromatic assumption taken on deriving Eq.1.19.

For some values of ω_0 around the zero dispersion wavelength where $\beta_2 \approx 0$, then β_3 may need to be included. We now make the approximation $\Delta\beta \approx \Delta\beta_0$ and by taking the inverse Fourier transform of Eq.1.19 while replacing $\omega - \omega_0$ with $i(\partial / \partial t)$ we arrive at:

$$A(z,t) = \frac{1}{2\pi} \int_{-\infty}^{\infty} \tilde{A}(z, \omega - \omega_0) \exp\left[-i(\omega - \omega_0)t \right] d\omega \tag{1.22}$$

The equation for $A(z,t)$ then becomes:

$$\frac{\partial A}{\partial z} + \beta_1 \frac{\partial A}{\partial t} + \frac{i\beta_2}{2} \frac{\partial^2 A}{\partial t^2} = i\Delta\beta_0 A \tag{1.23}$$

Here the $\Delta\beta_0$ term is used for loss and nonlinearity, however by using $\beta(\omega) \approx n(\omega)\omega / c$ we can arrive at the propagation equation:

$$\frac{\partial A}{\partial z} + \beta_1 \frac{\partial A}{\partial t} + \frac{i\beta_2}{2} \frac{\partial^2 A}{\partial t^2} + \frac{\alpha}{2} A = i\gamma(\omega_0) |A|^2 A \tag{1.24}$$

where nonlinear effects are taken into account through the nonlinear parameter:

$$\gamma(\omega_0) = \frac{n_2(\omega_0)\omega_0}{c\, A_{\text{eff}}} \tag{1.25}$$

In Eq.1.25, an increase in the refractive index or a decrease in the core effective area A_{eff} leads to an increase of the nonlinearity of the fibre. Here, $n_2\left[\text{m}^2/\text{W}\right]$= nonlinear refractive index coefficient of the fibre, ω_0 $\left[\text{rad}/\text{s}\right]$= carriers' central angular frequency and $c\left[\text{km}\cdot\text{s}^{-1}\right]$= speed of light in a vacuum. To produce a time reference frame moving along with the pulse at the same group velocity v_{g} we make the transformation:

$$T = t - \frac{z}{v_{\text{g}}} = \beta_1 z \tag{1.26}$$

then by substituting Eq.1.26 and Eq.1.25 into Eq.1.24, we can arrive at the propagation equation used in this thesis:

$$i\frac{\partial A}{\partial z} + \underbrace{\frac{i\alpha}{2}A}_{\text{attenuation}} - \underbrace{\frac{\beta_2}{2}\frac{\partial^2 A}{\partial T^2}}_{\text{dispersion}} + \underbrace{\gamma\left|A\right|^2 A}_{\text{non-linearity}} = 0 \tag{1.27}$$

The above version of the NLSE is suitable for pulse widths greater than 5 ps [13]. The four terms on the right hand side of the NLSE govern the effects of dispersion, fibre losses and nonlinearity on pulses propagating inside optical fibres. The NLSE is a scalar propagation and nonlinear differential equation that cannot be solved analytically unless simplified. We take the numerical approach and employ the time efficient split-step Fourier method, which is a pseudo-spectral methodology, to find solution in the NLSE. Here, the split-step Fourier method employs a finite-Fourier-transform (FFT) which we perform numerically through the Fastest Fourier Transform in the West (FFTW) software library. The numerical approach employed works as follows: the optical field is propagated in the spectral domain, by the FFTW library, over a very short distance of $\Delta z/2$, with dispersion and attenuation only. At the point $z+\Delta z$, the field is multiplied by the nonlinear term for the period Δz, applying the nonlinearity in the midpoint of the linear step. The field then propagates the final $\Delta z/2$ with dispersion and attenuation only. This method produces very accurate simulations and is used extensively in optical communications. In this thesis, numerical simulations of scalar optical pulse propagation are performed to test network design models, transmission system performance and monitor signal evolution.

In Eq.1.27, $A = A(z,T)$ is the envelope whose shape is a function of time and propagation distance, $\beta_2\left[\text{ps}^2/\text{km}\right]$ is the second order propagation constant, $\alpha\left[1/\text{km}\right]$= fibre attenuation constant, and

$|A|^2$ [W] = P[W] = optical power. By neglecting the dispersive and nonlinear terms in the given NLSE, the equation can be reduced to show only the effect of optical pulse attenuation when propagating in the fibre:

$$\frac{\partial \mathrm{A}}{\partial z} = -\frac{\mathrm{A}}{2}\alpha \tag{1.28}$$

In terms of optical signal power, attenuation of a bit stream is given by $P_{out} = P_{in}e^{-\alpha L}$ where α is the attenuation coefficient, P_{in} is the input optical power, P_{out} is the output power and L the fibre length. The α coefficient is often expressed in units of dB/km and is referred to as the fibre-loss parameter. It is found through the relation:

$$\alpha\,[\mathrm{dB/km}] = -\frac{10}{L}\log_{10}\left(\frac{P_{out}}{P_{in}}\right) \approx 4.343\alpha \tag{1.29}$$

G.652 standard SMF has an α = 0.22 dB/km at 1550nm. This loss is not constant for all wavelengths.

Nonlinear interactions depend on transmission length and the cross sectional area of the fibre. The longer the link length, the more the interaction and the worse the effect of non-linearity. However most of the nonlinear effects occur early in the fibre span as power decreases along the span due to fibre attenuation. When optical amplifiers are deployed in a transmission line, the signal noise degrades the optical signal to noise ratio (OSNR) such that the input optical power must be raised to preserve sensitivity at the receiver which results in increasing the effect of nonlinearities cumulatively with transmission distance. The effective fibre length L_{eff} then becomes a useful measure of system limitation as it quantifies the impact of nonlinearities with respect to their dependency on fibre length and attenuation. This model assumes that the power is constant over a certain effective length but despite its simplicity it has proven to be quite sufficient in understanding the effects of nonlinearities. L_{eff} depends on link length / amplifier spacing and is found to be:

$$L_{\mathrm{eff}} = \frac{1-\exp(-\alpha L)}{\alpha} \tag{1.30}$$

The measures of dispersion length L_D and nonlinear length L_{NL} provide some insight into system limitations in the various pulse propagating regimes, i.e. linear, nonlinear, and quasi-linear. They are:

$$L_{\mathrm{D}} = \frac{T_0^{\,2}}{|\beta_2|} \qquad L_{\mathrm{NL}} = \frac{1}{\gamma P_0} \tag{1.31}$$

The measures of L_D and L_{NL} help to categorise four main transmission regimes which are characterised as follows:

- $L << L_{NL}$ and $L << L_D$: The fibre length is much shorter than linear and non-linear length so that neither dispersive nor non-linear effects play a role. In this regime transmission is limited only by fibre attenuation.
- $L << L_{NL}$ and $L \geq L_D$: Nonlinear effects can be neglected and pulse evolution is governed by the fibre dispersion.
- $L \geq L_{NL}$ and $L << L_D$: Pulse evolution is governed by nonlinear effects which results in phase modulation and a spectral broadening of the signal spectrum.
- $L \geq L_D$ and $L \geq L_{NL}$: Both dispersion and fibre non-linearity's act together and the performance of the transmission is limited by their interplay.

1.6 Nonlinear Optical Effects

The nonlinear processes which impinge the transmitted bit streams in optical fibres can be generally split into two distinct classifications: stimulated scattering of light and the Kerr effects. Theses effects and related processes are shown in Fig. 1.4:

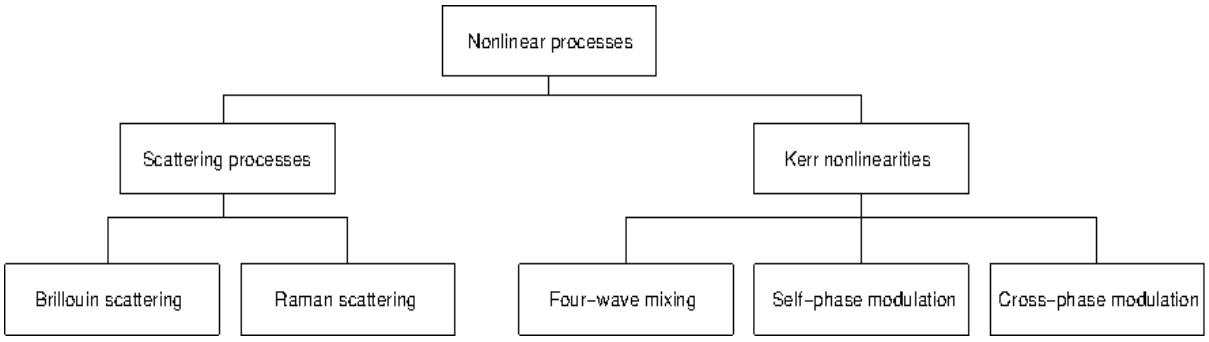

Figure 1.4: Nonlinear Processes in Optical Transmission

There are two general types of Stimulated Scattering and these are Stimulated Brillouin Scattering (SBS) and Stimulated Raman Scattering (SRS). Both are examples of inelastic scattering which cause a shift in the frequency of scattered light. Stimulated Brillouin Scattering (SBS) occurs as signal power reaches a certain point and starts to generate acoustic vibrations which change the core's refractive index causing light to scatter thus generating more acoustic waves. Brillouin scattering sends a light wave slightly shifted in frequency back toward the light source, creating attenuation on

the link. By shortening the pulse length, more power is needed to cause Brillouin scattering. Stimulated Raman Scattering (SRS) occurs when light strikes an atom that's vibrating and the light absorbs an amount of energy that is equivalent to the atoms vibration. This results in a scattering of the light and also a change in the lights wavelength. When Raman scattering occurs, the result can be cross-talk between two waves in the fibre. In single mode fibres the main differences between SRS and SBS [12] are as follows: (a) SBS occurs only in the backward direction but SRS can occur in both directions; (b) the frequency shift of scattered light is about 10 GHz for SBS but by 13 THz for SRS; (c) the Brillouin gain spectrum (bandwidth < 100 MHz) is very narrow compared to the Raman-gain spectrum (bandwidth ~ 20 - 30 THz). Both scattering processes result in a loss of power at the incident frequency but this loss is negligible at low power levels. At higher powers both SBS and SRS can become important, however, as channel spacing's no smaller than 50GHz and no more than 8 channels are used in this work, both effects are assumed negligible. This negligence is afforded as large channel spacing's makes inter-channel crosstalk due to SBS negligible, while the small number of channels means that the power shift down the spectrum due to SRS can also be neglected.

The Kerr nonlinear effects are elastic processes and originate from the dependence of the refractive index of silica on the intensity of propagating light confined in the small core area of the transmission fibre. This result of the Kerr effect can produce an intensity dependent phase shift of the optical field and dependent on whether the refractive index fluctuations are caused by power in a single channel or from the signal powers in co-propagating neighbouring channels, this can lead to intra- and inter-channel nonlinear optical effects. It is such that SPM, IFWM and IXPM are the single-channel (or intra-channel) nonlinearities, while XPM and FWM are multi-channel (or inter-channel) nonlinearities.

Self Phase Modulation (SPM)

Self-phase modulation is the major non-linear limitation in a single-channel system [14]. As the refractive index is intensity dependent it leads to self-focussing and phase modulation within a single pulse. This phase shift causes frequency broadening and leads to a change in the propagation constant of the fundamental mode. The power dependant propagation constant can be written as:

$$\beta' = \beta + k_0 \bar{n}_2 P / A_{eff} \equiv \beta + \gamma P \tag{1.32}$$

with the nonlinear parameter γ given as:

$$\gamma = \frac{2\pi \bar{n}_2}{A_{\text{eff}} \lambda} \tag{1.33}$$

whose value in SMF can vary depending wavelength λ and on the effective mode area A_{eff}. In this thesis the non-linear coefficient $\bar{n}_2 = 2.6 \times 10^{-20}\,\text{m}^2/\text{W}$. High intensity light increases the refractive index which slows the group velocity and causes a phase delay in the centre of a pulse with respect to its tails. The new frequencies result in an increased occupied bandwidth through broadening of the power spectrum and the extended frequency range leads to pulses that spread to a greater extent from group velocity dispersion. As self-phase modulation causes pulse spreading through chromatic dispersion it can limit WDM channel density depending on filter bandwidths.

For each amplifier span of length L with attenuation α, where $P(z) = P e^{-\alpha z}$ and $P = P(0)$ is the launch power, then the nonlinear phase shift ϕ_{NL} is given by:

$$\phi_{\text{NL}} = \int_0^L \left(\beta' - \beta\right) dz = \int_0^L P(z)\, dz = \gamma\, P\, L_{eff} \tag{1.34}$$

The term L_{eff} was defined in Eq.1.30 and is the effective fibre interaction length which gives the length over which the power decreases by a factor of *e* in passive fibres. The drop in pulse power with propagation reduces the local contribution of non-linear effects as the length of the fibre increases, so that the effect of fibre nonlinearities depends on inter-amplifier spacing. The quantification of the total ϕ_{NL} across a phase modulated communication system is an important measure when determining the systems performance of a new network configuration.

Cross Phase Modulation (XPM)

Cross-phase modulation is one of the most detrimental impairments in high-bit-rate wavelength division multiplexing systems. The spectrum broadening effect caused by SPM can produce inter-channel cross talk between channels in WDM systems through interactions between co-propagating channels at different frequencies. This results in a phase modulation of the light producing XPM [15, 16] where the nonlinear phase shift for a specific channel depends not only on the power of that channel but also on the power of the other channels. The phase shift for the jth channel is given by:

$$\phi_j^{\text{NL}} = \gamma\, L_{eff} \left(P_j + 2 \sum_{m \neq j} P_m\right) \tag{1.35}$$

where the nonlinear parameter is defined in Eq. 1.33 and L_{eff} as defined in Eq. 1.30. The factor of 2 in Eq. 1.35 indicates that XPM is twice as effective as SPM for the same amount of power. In WDM systems, the total phase shift depends on the powers in all channels and will vary from bit to bit in OOK systems, however this is not the case with DPSK modulation as 'one' bits are present in every bit slot. Assuming equal channel powers the phase shift for the worst case scenario in DPSK systems in which all pulses overlap is given by [17]:

$$\phi_j^{\mathrm{NL}} = (\gamma/\alpha)(2M-1)P_j \tag{1.36}$$

where *P* is power, *a* accounts for losses, (2M – 1) is a 2M – 1 channel system. The phase shift due to XPM can only occur when two pulses overlap in time as they propagate at different speeds in neighbouring channels. Dispersion converts the phase noise into signal distortion. It is such however that a select choice of dispersion map can help to reduce the effects of XPM but cannot eliminate it completely.

Four Wave Mixing (FWM)

The nonlinear phenomenon known as four-wave mixing (FWM) originates from the third-order nonlinear susceptibility $\chi^{(3)}$ [13]. FWM manifests when two or more channels propagate in concert through an optical fibre. For example if three optical fields co-propagate with carrier frequencies ω_1, ω_2 and ω_3 then $\chi^{(3)}$ will generate a fourth field with frequency ω_4 which is related to the other frequencies as follows:

$$\omega_4 = \omega_1 \pm \omega_2 \pm \omega_3 \tag{1.37}$$

Due to a phase matching requirement many of the several frequencies corresponding to different plus and minus signs in Eq. 1.37 do not build up. However of those that do, it is frequency combinations of the form $\omega_4 = \omega_1 + \omega_2 - \omega_3$ that are troublesome in WDM systems as they can become nearly phase-matched when the channels lie close to the zero-dispersion wavelength. Four-wave mixing is dependent on chromatic dispersion, input optical power, channel spacing and channel count, and in phase modulated channels it would result in distortion of both the amplitude and phase of the optical pulses, reducing receiver sensitivity and overall system performance. However, the effects of FWM can sometimes be reduced by using dispersion management where GVD is kept locally high in each fibre section [18].

Nonlinear Phase Noise (NLPN)

Nonlinear phase noise (NLPN) is a serious impairment in phase modulated communication systems as it can lead to errors during differential phase detection. The impact of nonlinear phase noise on system performance is mainly determined by an intricate interplay between Kerr nonlinearity, chromatic dispersion and ASE noise.

Due to the Kerr effect, the wave propagation constant of a lightwave propagating in an optical fibre depends on the field amplitude and any type of amplitude fluctuation will result in corresponding phase fluctuations. One such source is the amplitude fluctuations from ASE noise added by optical amplifiers. Amplifier noise in the signal intensity introduces non-linear phase noise to the linear SPM-induced nonlinear phase shift so that the received phase becomes a combination of these linear and nonlinear phase components. It such that it is not only ASE-induced amplitude fluctuations of the channel itself that can create nonlinear phase noise but the amplitude fluctuations of adjacent channels.

The Kerr effect is also responsible for self-phase and cross-phase modulation (SPM, XPM), and four-wave mixing (FWM), where SPM and XPM convert intensity fluctuations into phase fluctuations. Nonlinear phase noise gets its name due to the nonlinear origins of these fluctuations. The first study of nonlinear phase noise was performed by Gordon and Mollenuer [19] who studied a long-haul phase-shift-keyed (PSK) modulated optical communication system in their seminal paper. They argued that nonlinear phase noise due to the amplitude-to-phase noise conversion effect arising from the interaction of ASE noise from the optical amplifiers and the nonlinear Kerr effect imposed a severe limitation on systems employing phase modulation. They concluded that optimal system performance would be achieved when the launch power for every span was chosen such that the total mean nonlinear phase shift for the whole link was around 1 rad. Gordon and Mollenuer studied a single channel only and ignored the effects of fibre dispersion.

In the presence of dispersion where dispersive effects broaden optical pulses, pulses in neighbouring symbol slots overlap and interact through intra-channel XPM [16] which can also introduce nonlinear phase noise to the signal phase. In WDM systems pulses belonging to different channels overlap periodically, while co-propagating in the fibre at different speeds, leading to phase noise through inter-channel XPM. This can limit the performance of phase encoded systems quite severely.

1.7 Advanced Modulation Formats

Over the last decade there has been an enormous interest in increasing system reach and aggregate WDM transport capacity due to growing volume and bandwidth demand of data services. High spectral efficiency, high capacity optically routed terrestrial networks are enabled by low loss optical components, low noise amplifiers, advanced optical fibres and advanced modulation formats. Modulation technologies encode incoming electrical data streams onto an optical signal by changing optical field elements such as the amplitude, phase (including frequency) and polarisation. Advanced optical modulation formats refer to modulation formats which use advanced modulation and detection technologies operating at high bit rates. Advances in high-speed electronics and optoelectronics allow increasingly sophisticated transponder hardware meaning that systems no longer rely only on binary modulation of the optical intensity but a transition to other modulation formats such as binary and multilevel phase modulation and partial response formats. Some advanced formats employ phase modulation only or a mix of phase and amplitude modulation and others also make use of information encoding using the polarisation of light.

The choice of signal modulation format affects the choice of system parameters and vice versa. The task of selecting a format depends on required system specification such as compatibility with the desired data rate, channel spacing, fibre characteristics, amplification scheme, noise resilience, receiver bandwidth, unregenerated transparent transmission distance and dispersion maps. In 40 Gb/s transmission, there has been no advanced modulation format which has simultaneously afforded high capacities, has a narrow spectral width, demonstrates superior robustness (over other formats) to non-linear fibre effects, has a large dispersion tolerance, is resistant to PMD, is tolerant to noise accumulation and has a cost effective transmitter configuration [20-23]. However, it is such that the proper selection of a more complex modulation format than binary On-Off-Keying (OOK) can to an extent, improve a systems performance by minimising the overall combined effects of sources of signal degradation. Constellation diagrams of popular modulation techniques are shown in Figure 1.5.

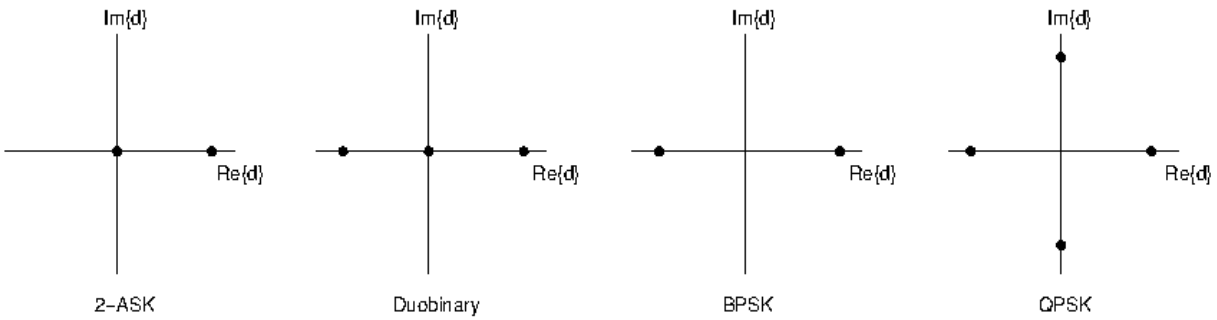

Figure 1.5: Constellation diagrams of popular modulation techniques.

Widespread research efforts have focussed on the development of optical communication systems that employ modulation formats which encode information in the differential phase shifts between successive symbols. Although Phase Shift Keying (PSK) provides a highly bandwidth efficient modulation scheme, Differential Phase Shift Keying (DPSK) [24] was seen as an improvement on PSK since the absolute phase was not required at the receiver. For differential-phase modulation formats each bit acts as a phase reference for another bit where the transmitted information is encoded on the binary phase change between adjacent bits. This technique can be accompanied by pulsed modulation such as return to zero (RZ) where data information is imprinted on a periodic optical pulse train. RZ-DPSK is characterised by periodic optical pulses in each bit slot whereas NRZ-DPSK features a constant optical intensity.

OOK and DPSK are two of the most common formats found in terrestrial systems. NRZ-OOK and RZ-OOK are components of Intensity Modulated Direct Detection (IMDD) systems. For many years, NRZ was the dominant modulation format in 10 Gb/s IMDD terrestrial systems. This was mostly due to its relatively low electrical bandwidth requirements (compared to RZ) of the transmitter and receiver, its simple transmitter and receiver configuration and its tolerance to non-linear effects over short distances [12]. The NRZ spectral width is half that of RZ, which makes it potentially attractive for WDM. However as transparent transmission distance requirements grew so did the need for high receiver sensitivity. RZ with its reduced pulse width produces a greater tolerance to fibre non-linear effects over long distances [25, 26] and polarization-mode dispersion (PMD) [27] than NRZ. At bit rates of 40 Gb/s the penalties due to nonlinearity in signal transmission are primarily associated with the effects of IFWM and IXPM [28 - 30]. Signals distort during propagation as timing jitter due to IXPM is acquired by 1-bits. More serious is the performance degradation in ultra-high speed transmission when amplitude variations caused by the generation of ghost pulses in 0-bit slots [31–32] is initiated by IFWM.

Like OOK, DPSK can be implemented in RZ and NRZ format. DPSK has been demonstrated excellent capacity-reach performance in 40 Gb/s transmission systems [33]. As the symbol spacing for DPSK is increased by $\sqrt{2}$ compared to OOK, this leads to a theoretical 3dB advantage compared to OOK for a fixed average optical power. This allows DPSK to accept a $\sqrt{2}$ larger standard deviation of the optical field noise than OOK for equal BER translating into ~ 3-dB reduction in OSNR [34] which can be used to extend transmission distance. As DPSK power is homogenously distributed due to the constant amplitude of its bit stream, this facilitates a reduction in pulse distortion from self-phase modulation (SPM) and pulse pattern related cross-phase modulation (XPM) [34, 35]. DPSK's improved tolerance to the efficiency of nonlinearities can be attributed to correlation between nonlinear phase shifts acquired by adjacent bits due to propagation in similar conditions [36]. RZ-

DPSK has also been reported to be more robust than OOK in terms of narrow-band optical filtering and PMD [34] making it very attractive for high spectrally efficient transmission. It is such that good receiver sensitivity and tolerance to fibre nonlinearity combined make possible robust systems with an S.E. of 0.4 or greater. RZ-DPSK has been shown to be highly robust over 40 Gb/s terrestrial distances and is more economical in bandwidth to deploy than 4 x 10 Gb/s OOK channels. DPSK formats have outperformed all OOK based formats at 40 Gb/s [28, 34, 37, 38].

Historically, advanced modulation formats have nearly always used some form of phase modulation of the bit stream to reduce the detrimental effects of nonlinearity. A common technique was to alternate the phase of neighbouring bits by a value $\Delta\phi$. The phase alternation can be imposed by a separate phase modulator after RZ modulation. CSRZ is such a format where the phase of the optical field of a return to-zero (RZ) intensity-modulated bit stream is changed by π every bit to beneficially influence the optical spectrum. By changing the π-phase shifts to $\pi/2$ phase shifts, the resulting modulation format is called $\pi/2$-APRZ. Depending on the configuration of the system, the APRZ phase shifts may benefit from optimisation (to $\leq \pi/2$) by optimising the amplitude of phase modulation [39] which has been reported to yield an improvement in IFWM tolerance compared to CSRZ and standard RZ. Another solution when upgrading 10Gbit/s WDM systems to 40Gbit/s transmission speed is to deploy duobinary modulation formats. The classical duobinary formats [40, 41] are designed to have a low spectral occupancy which reduces the channel bandwidth in WDM systems. They are also known for high tolerance to residual chromatic dispersion [42]. These transmitters employ differential encoding as found in DPSK systems, electrical filtering based on the delay-and-add method and a three-level coding scheme comprising of "0", "+1" and "-1" symbols. The intensity profile is normally the same as that of the NRZ format. Typically, in duobinary, a π-phase shift takes place between two groups of "1"s when the number of "0"s in-between is odd which assists resistance to inter-symbol-interference (ISI) in the neighbouring "1" blocks [43]. This resistance to ISI in "1" blocks (which neighbour "0"s) does not materialise when the number of "0"s is even.

Another type of duobinary format, phase-shaped binary transmission (PSBT) [44, 45, 46, 47], gets its name as the small amount of light that remains after modulation in the zero bit slots (which have π-phase shifts at their centre) has been found to contain the spreading of the "+1" and "-1" symbols, limiting ISI in dispersive fibre, as a result of the phase shift occurring in their neighbouring "0"s during transmission. Unlike classical duobinary, with PSBT, each group of "1"s is protected from the ISI generated by its neighbours irrespective of the number of zeros between "1"s. A drawback of the light which remains in the zero bit-slots is a poor eye-opening of PSBT which leads to a low tolerance to noise. Due to PSBTs low tolerance to noise and in order to improve the formats back-to-back

OSNR sensitivity, Enhanced-PSBT (E-PSBT) [48] was proposed where a second MZM with NRZ modulation was used to carve away most of the light in the zero bit slots while the π-phase shifts remain. This had the effect of improving the signal eye and hence noise tolerance.

High bit-rate PSBT formats have also been demonstrated with optical filtering [49] as opposed to the classical method of using electrical filters, in order to overcome the complexities inherent to high speed electronics [50]. Similarly, to improve the OSNR sensitivity of PSBT formats, the so called "Optimum" PSBT format [51] was recently proposed. This format also displays some resistance to residual CD and importantly for WDM applications has the narrowest optical spectrum of all PSBT formats, however its practical implementation is complex due to the presence of three electrical and optical filters located in both the transmitter and receiver whose transfer function profile and bandwidth have to be optimised.

Interestingly, duobinary and DPSK are related in that DPSK can be converted into duobinary by narrow optical filtering [52]. It is also such that the two output ports of a DPSK delay interferometer modulator produce partial response signals: the DI constructive port converts DPSK into conventional duobinary whereas the DI destructive port produces an alternate mark inversion (AMI) signal. If the MZ is fed with RZ-DPSK data, these formats, as above, are turned into the so-called RZ duobinary and RZ-AMI formats, respectively. Though lacking the robustness of PSBT to chromatic dispersion, RZ-AMI benefits from the effect of π phase-shifts separating mark symbols against intrachannel nonlinearities [53].

Both duobinary and DPSK can achieve the high spectral efficiency required to transmit 40Gb/s channels on a 50GHz channel spacing. DPSK has better OSNR tolerance than duobinary, where duobinary is well known to have good tolerance to chromatic dispersion and narrow optical filtering. Recently a balanced detection scheme was proposed for duobinary as a substitute for traditional detection using a single photodiode. The proposed balanced detection scheme allows duobinary to approach the performance of NRZ-DPSK [54].

Today, many transmission systems have a 50GHz WDM channel spacing, which implies a 0.8 bit/s/Hz spectral efficiency for 40Gb/s transmission. As binary formats, duobinary and DPSK edge closer to their theoretical limit, much attention has turned to multi-level formats. One such format is Differential Quadrature Phase Shift Keying (DQPSK) modulation [55 - 57] which is a spectrally efficient multilevel version of the DPSK technique and has gained much attention for its application in ultra-high bit-rate systems [58 - 63]. To generate a 40Gb/s RZ-DQPSK signal the optical signal from a continuous wave (CW) laser source is split into two parts. The phases of the signals, one of which is phase shifted by π/2 with respect to the other, are differentially encoded [64] with two 20

Gbit/s independent NRZ data streams and then re-combined with a y-coupler producing a 40Gb/s DQPSK signal. The signal is then re-modulated with the 20 GHz clock synchronized with the data streams. The resultant RZ-DQPSK signal has an RZ-like intensity waveform with a 50% duty cycle while the data is encoded in the optical phase of each RZ pulse in a four-level differential phase format. DQPSK makes it possible to double spectral efficiency (b/s/Hz) by encoding two bits within each symbol. In comparison to binary modulation formats this halves the symbol rate from 40G-symbol/s to 20G-symbol/s for 40Gb/s line speeds. Phase shifts of 0, $\pi/2$, π or $-\pi/2$ are often used to represent 00, 01, 10, 11 binary pairs. As the bit stream is a series of "1" bits, the DPSK and DQPSK eye diagrams are the same. However, the DQPSK optical spectrum is around half the width of DPSKs affording transmission of 40Gb/s signals over existing 10Gb/s network infrastructure with either 50GHz or 100GHz channel spacing and has high tolerances to chromatic and polarization-mode dispersion when compared at the same line rate as binary modulation [65 - 67].

The search for efficient modulation formats able to support the highest possible single channel bit rate in optical networks continues. The non-wavering increase in network traffic load means that that an increasing number of existing metro and regional networks which currently operate at 10Gb/s or 40Gb/s (some do already run at 100Gb/s) will eventually require upgrading to 100Gb/s channels. In many cases these existing lower rate channels will not be taken out of service, but will remain on the same terrestrial routes in operation either in different fibres, or co-propagating with 100Gb/s payload channels in the same fibre [68] despite the presence of strong cross-phase modulation [69].

As the vast majority of internet traffic is generated by end systems with Ethernet interfaces the demand for carrier-grade 100Gb/s Ethernet [70 - 74] has led to large scale research efforts into multilevel modulation formats which incorporate more than 2 bits per symbol. The focus has been to take these technologies beyond short-reach interconnects and LAN connections, in order to take 100Gb/s Ethernet technologies into metropolitan area networks (MAN) and wide area networks (WAN). This would lead to Ethernet frames transmitting over wavelength-division multiplexing (WDM) optical backbone networks (Ethernet-over-WDM), so that the ultimate goal of removing several layers of other technologies can be achieved in the process.

On a practical perspective, 100Gb/s channels must be able to provide a price point of less than twice a 40Gb/s channel. If a metro or regional system has only a few spans the major system cost contribution comes from the transponders and in some cases the right price point may only be achieved if complicated transmitter or receiver structures are avoided. Furthermore, in metro systems in particular, channels on a 100 GHz grid can be cost efficient for some operators who require systems with low complexity and power consumption and simple upgradability of existing 10Gb/s

infrastructures. This is also the typical case when configuring lines to the many geographical areas with lower population densities than major cities.

Advanced modulation formats such as DPSK, PSBT and DQPSK have reduced the nonlinear performance gap between 10 and 40Gb/s line speeds. Demonstrations of DQPSK modulation combined with polarisation-multiplexing (PDM) have produced a further reduction of the symbol rate to a quarter of the bit-rate by encoding 4 bits/symbol instead of DQPSKs 2-bits/symbol. As such, the POLMUX-RZ-DQPSK signal format has established itself as a strong candidate for implementation at a data rate of 111Gb/s [75 - 80].

Coherent detection [81 - 84] affords both the amplitude and the phase of the complex envelope of the electromagnetic field to be directly measured. This allows the receiver to make both I and Q components of the carrier signal available, so theoretically, any multilevel modulation format can be demodulated. This technology has afforded the prospect of developing advanced modulation formats with M levels such as M-PSK or M-QAM (Quadrature Amplitude Modulation). The combination of a digital coherent receiver with state of the art high speed electronics and analogue to digital converters (ADC) can also be used to help equalise linear transmission impairments such as CD and PMD. Coherently detected polarisation-multiplexed-quadrature-phase-shift-keying (POLMUX-QPSK) modulation format has recently been demonstrated at a data rate of 111Gb/s (100Gb/s of payload and 11 Gb/s of forward error correction and Ethernet overheads) [85].

By coding information over four phase levels in the QPSK format and over two orthogonal polarization states using PDM while decoding using coherent detection and digital signal processing at the receiver, the format named Coherent-POLMUX-RZ-QPSK (CP-RZ-QPSK) can be produced. To generate a CP-RZ-QPSK signal, DFB lasers are used to co-propagate wavelength-division-multiplexing (WDM) channels which are grouped into odd and even channels using two array waveguide gratings (AWGs). After the AWGs, the two channels groups are pulse carved using two Mach–Zehnder modulators (MZM) driven with a clock signal at a quarter of the bit rate, then the two wavelength combs are QPSK modulated using two nested-MZMs again operating at a quarter of the bit rate. Then the two wavelength combs of resulting RZ-QPSK modulated channels are combined using a 50/100-GHz interleaver. At the output of the interleaver, a polarization multiplexing stage consisting of a 50/50 splitter, a delay line and a polarization beam splitter is used to polarization multiplex the signals. The signal is then transmitted and detected with a digital coherent receiver. In order to further increase spectral efficiency, POLMUX-16QAM could be deployed in either in single-carrier or multicarrier (orthogonal frequency-division multiplexing, OFDM) configurations but this is likely to be a technology only deployed commercially in future systems with operating at speeds much greater than 100Gb/s, due to the complexity and costs of realising these transponders.

The choice of modulation technologies is widening and the choice between them in the commercial environment will depend on optical networking aspects, hardware maturity, desirable price point and availability of components.

1.8 DPSK Signal Generation

At bit rates of greater than 2.5 Gb/s, the direct modulation of a laser results in frequency chirp which reduces the possible transmission distance of an optical communication system. For this reason the direct modulation of a laser is rarely used in modern transmitters. The solution is to use a continuous wave (CW) source such as a Distributed Feedback Laser (DFB) and an external modulator. DFB lasers can be biased at well-controlled DC bias and temperature which results in a very stable optical power output both in amplitude and wavelength. The external modulator then impresses input electrical data provided by a pulse generator onto the CW light resulting in the modulation of the optical carrier.

Nearly all modern modulation techniques make use of an external $LiNbO_3$ Mach-Zehnder Modulator (MZM). The MZM device exploits the material properties of Lithium niobate ($LiNbO_3$) which is characterised by a uniform, highly consistent piezoelectric transducer single crystal and is used extensively in the production of optical modulators and optical waveguides. Electro-optic crystals are a solid-state material and used to make active devices due to the presence of an electro-optic effect, known as the Pockels effect.

This effect manifests through the variation of an externally applied electrical field which causes a change in the refractive index of the material. To utilise the electro-optic effect, RF electrodes are fabricated directly onto the $LiNbO_3$ surface or an optically transparent buffer layer to reduce losses [17]. Signal voltages can then be applied to the waveguides so that the propagation constant within each waveguide can be modulated. $LiNbO_3$ has a Curie temperature of around 1140 C, allowing Titanium (Ti) to be diffused into the $LiNbO_3$ substrate to create the low-loss waveguides. The waveguides are connected to splitter / combiners in the form of passive Y-junction couplers (see Figure 1.6).

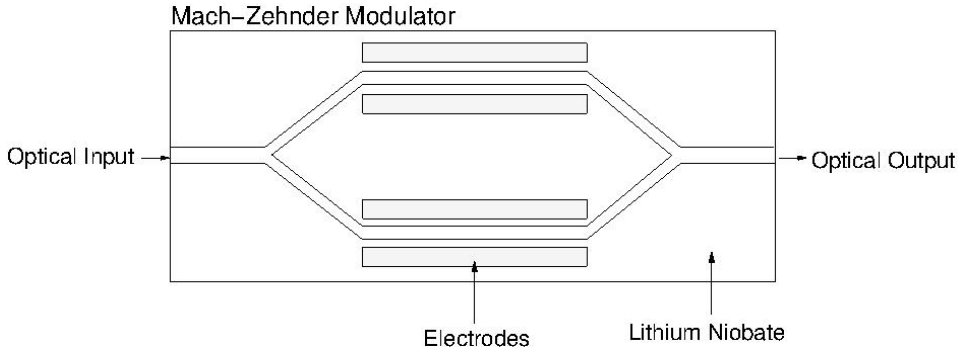

Figure 1.6: MZM Modulator

By using transfer matrices, the basic operational principles of an MZM are now demonstrated through modelling the device as a splitter (T_s), phase shifter (T_ϕ) and combiner (T_c) as follows:

$$T_S = \begin{bmatrix} \sqrt{\rho} & -i\sqrt{1-\rho} \\ -i\sqrt{1-\rho} & \sqrt{\rho} \end{bmatrix} \tag{1.38}$$

$$T_\phi = \begin{bmatrix} e^{i\phi_1} & 0 \\ 0 & e^{i\phi_2} \end{bmatrix} \tag{1.39}$$

$$T_c = \begin{bmatrix} \sqrt{\rho} & i\sqrt{1-\rho} \\ i\sqrt{1-\rho} & \sqrt{\rho} \end{bmatrix} \tag{1.40}$$

Here ρ denotes the power splitting ratio at the Y-junction. If we set ρ = 0.5 to produce a 50/50 splitter/combiner and let ϕ_j = phase in modulator arm j (for j=1,2), then the transmitted field A_t can be obtained through multiplying the input field A_i by the transfer matrices as such:

$$A_t = A_i \cdot T_s \cdot T_\phi \cdot T_c \tag{1.41}$$

After multiplying out and simplifying algebraically, the transmitted field A_t can be presented in terms of the two phase shifts as [17]:

$$A_t = \frac{1}{2} A_i \left(e^{i\phi_1} + e^{i\phi_2} \right) \tag{1.42}$$

We can see from E.q.1.42 that if $\phi_1 = \phi_2 = 0$, so that no phase shift occurs, then $A_t = A_i$. The modulator transfer function t_m is then derived as:

$$t_m = \frac{A_t}{A_i} = \cos\left[\frac{1}{2}\left(\phi_1 - \phi_2\right)\right] e^{i\left(\frac{\phi_1+\phi_2}{2}\right)} \tag{1.43}$$

The transfer function in Eq.1.43 shows that the MZ modulator can affect both the amplitude and phase of the light incident upon it.

Different phase shifts can be applied to the equally split input fields in each of the upper and lower branches by applying various voltages across the two waveguides that form the two arms of the modulator. These phase shifts can be represented in terms of applied voltages as:

$$\phi_j = \frac{\pi\, v_j(t)}{v_\pi} \tag{1.44}$$

where $v_j(t)$ = voltage applied across arm j (for j=1,2), and v_π = voltage to produce a π phase shift (typically under 5V). Eq.1.44 substituted into Eq.1.43 allows an analysis of the phase shifts and hence amplitude modulation as a function of the applied voltages from the pattern generator. By further introducing the condition:

$$v_2(t) = -v_1(t) + v_b \tag{1.45}$$

where v_b is a constant bias DC voltage then the power transfer function $T_m(t)$ of the modulator can then be derived as:

$$T_m(t) = \left|t_m\right|^2 = \cos^2\left(\frac{\pi}{2v_\pi}\left[2v_1(t) - v_b\right]\right) \tag{1.46}$$

Introducing the bias v_b effectively moves the zero bias point allowing control over the output optical power. It is such that the condition $v_2(t) = -v_1(t) + v_b$ also allows the modulator to be used as a *pure amplitude modulator*. This is achieved when the voltages are applied in such a way that the summation of $\phi_1 + \phi_2$ reduces the phase in the transfer function to a numerical constant so that the modulator acts as pulse carver, i.e. it shapes the pulses while the phase remains constant. In the absence of losses, the modulator can also act as a *pure phase modulator* when the same voltage is

applied to each arm such that $\phi_1 = \phi_2$, with the exception of the condition $\phi_1 = \phi_2 = 0$ where $A_t = A_i$. In the *push-pull regime* where we impose the condition $\phi_1 = -\phi_2$, the applied voltages are such that transfer function t_m gives the values ± 1, thus producing phase shifts of 0 and π.

In the previous models losses have been ignored. As losses do exist, one of the most important parameters of the modulator is the extinction ratio ε which is related to losses through the γ parameter:

$$\gamma = \frac{\sqrt{\varepsilon} - 1}{\sqrt{\varepsilon} + 1} \tag{1.47}$$

The extinction ratio is the ratio of the maximum output optical power and the minimum output optical power. To realise an infinite extinction ratio a modulator would need splitting/combining ratios that are exactly 50/50 and an equal amount of loss through each arm of the device. The resulting combining fields would have identical amplitudes and therefore the device would be classed as an 'ideal' modulator where $\gamma = 1$, i.e., the resultant would be along the real axis. When the device is not 'ideal' i.e. when $\gamma < 1$, the consequence is a time-varying residual phase which manifests itself as residual chirp.

It can be seen that the MZM is a versatile device which can act as an Amplitude Modulator and/or Phase Modulator. The device has paved the way for many of the advanced modulation formats in the literature, some requiring more than one modulator. Differential Phase Shift Keying (RZ-DPSK) formats encode information on the binary phase change between adjacent bits. This can be performed with either a Phase Modulator (PM) or a MZM. Both are now discussed.

A Phase Modulator (PM) only modulates the phase of the optical field which results in a constant envelope. However as the phase change is not instantaneous, transient chirp occurs across bit transitions. The optical phase directly follows the electrical drive signal. The phase transitions can be limited by driver bandwidth and any drive waveform imperfections get mapped directly onto the optical phase and are reflected in phase distortions. Dependant on the severity the distortions can potentially degrade performance at the receiver.

When employing an MZM, the bias is set to the minimum transmission point of the modulator and the data amplitude adjusted to $2V_\pi$ (see Figure 1.7). The MZM allows switching the phase between consecutive symbols precisely by π but introduces residual amplitude modulation in the form of intensity dips. This means that the constant envelope that the PM can produce is not achieved with the

MZM. However a major advantage of the MZM is that the two neighbouring transmission maximum points, which are symmetrically driven around zero transmission, have opposite phase. This means the MZM modulates straight along the real axis (the phase changes its sign as it goes through zero) as opposed to the PM which modulates the phase around the unit circle in the complex plane (see Figure 1.8). This allows the MZM to create a phase shift of π regardless of drive voltage imperfections.

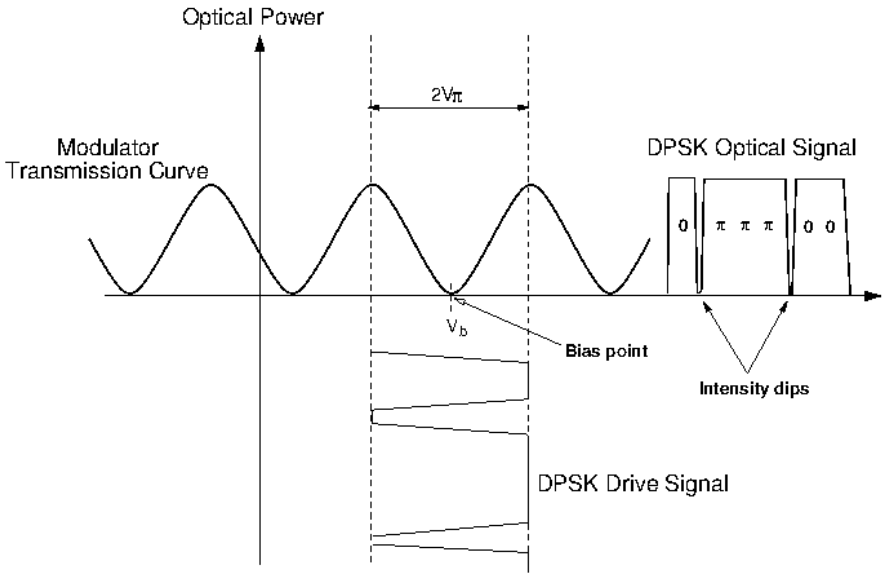

Figure 1.7: DPSK Modulation – operational characteristics of single drive MZM.

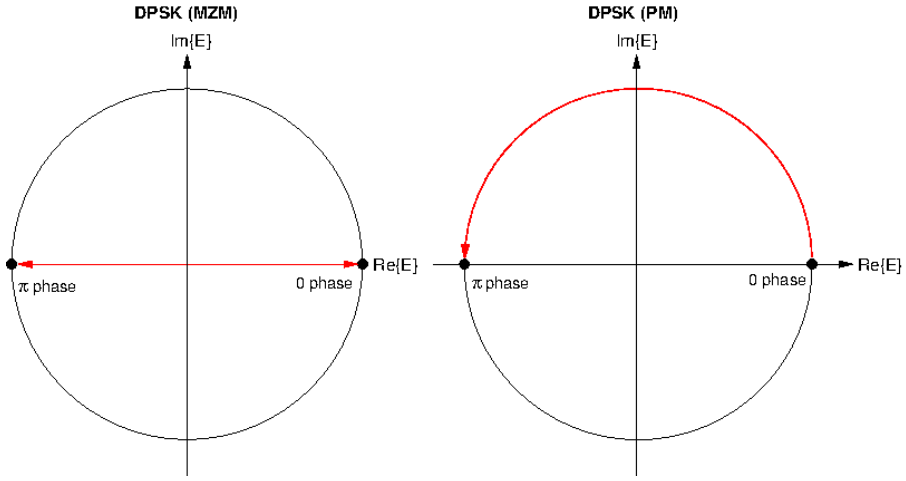

Figure 1.8: DPSK modulation - MZM vs. PM.

The lack of constant envelope in DPSK modulation is less important than perfect phase transitions, as it is the information-bearing optical phase that must remain intact to ensure good receiver performance. For this reason the MZM is used more often in these transmitters than the straight line phase modulator. For RZ-DPSK in particular, the residual intensity dips at the edge of the bit slots are largely eliminated when a pulse carver cuts the pulse width leaving only the centre portions of each bit. Pulse carvers usually come in the form of dual-drive MZMs which require perfect push-pull operation where the sinusoidal drive amplitudes have to be exactly equal and of opposite phase. Furthermore this modulator is required to have an infinite DC extinction to avoid phase distortions through chirp. While using only MZMs, the chirp or fluctuations in intensity can largely be suppressed when producing the RZ-DPSK format.

1.9 DPSK Receiver

At receiver the optical signal is converted back into a replica of the original electrical signal. There are two types of optical receiver configurations: power detecting receivers and coherent detection receivers. Power detecting receivers are often called direct detection (DD), or non-coherent receivers. EDFA technologies, used as low noise preamplifiers, have made it possible for DD systems to match the sensitivity performance of coherent systems [28], a highly desirable outcome as DD receivers offer the key attraction of simplicity and low cost. Fast photodiodes covert the optical intensity to electrical current and often a trans-impedance amplifier follows so to convert the current to a voltage which itself replicates the pre-modulated signal albeit with noise added mostly from optical amplifiers and the receiver circuits.

Balanced detection in DPSK systems (see Figure 1.9) is used to make a decision at the receiver where the current symbol is demodulated by using the phase of the previous symbol as a reference.

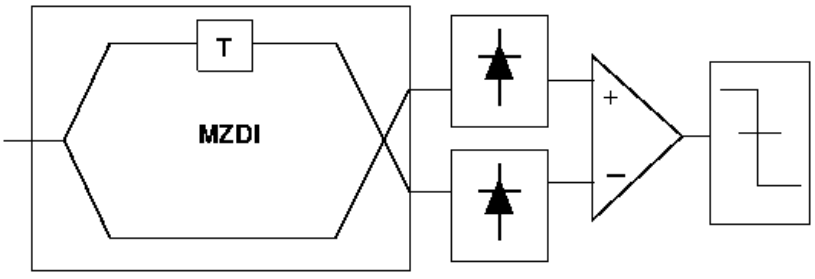

Figure 1.9: MZDI and Balanced Detection.

A balanced receiver includes a MZ delay interferometer whose two arms differ in lengths so that the signal in the longer arm is delayed in time equal to the duration of a single bit ($T = 1/B$). On leaving each arm, the two adjacent bits interfere at the two output ports in order that phase-to-intensity modulation conversion is performed. The powers at the two output ports are given by [17]:

$$P_{\pm}(t) = \frac{1}{4}\left|A(t) \pm A(t - T_s)\right|^2 \tag{1.48}$$

To detect both $P_{\pm}(t)$ two photo detectors are employed and the resulting currents are subtracted. By using $A(t) = \sqrt{P_0}\exp[i\phi(t)]$ in Eq.1.48, and using $I_{\pm} R_d P_{\pm}(t)$ where R_d is the detector responsivity, then the two currents at the photo detectors can be written as:

$$I_{\pm}(t) = \frac{1}{2} R_d P_0 [1 \pm \cos(\Delta\phi)] \tag{1.49}$$

The phase difference between the two neighbouring symbols is given by $\Delta\phi(t) = \phi(t) - \phi(t - T_s)$ where in the case of DPSK $\Delta\phi = 0$ or π. The currents are then subtracted and the original bit stream can be reconstructed from temporal variations in the electrical signal.

1.10 Monitoring and Measuring System Performance

Numerical performance evaluation tools are critical in providing an estimate of optical communication system performance and the effectiveness of both network new build and retrofit designs. They can help determine and separate out the dominant system limitations and transmission ailments which disturb a propagating optical signal. Such measures are introduced and described in this section. The measures presented in this section are used for the evaluation of optimisation methodologies and non-linear system performance. They are often used before, during and after transmission to monitor modulation parameters, input power limitations, dispersion map performance, amplifier location and optimisation of receiver filter bandwidths.

A challenge in numerical simulations is to provide a reliable estimate of the bit error rate (BER). Instead of simulating over 10^9 bits and calculating the BER via a direct error count (which is too costly even with modern computing resources) an alternative is to use smaller bit streams and to calculate the BER from statistical fluctuations of the received signal. These fluctuations are characterised by the *Q*-factor which gives a measure of the quality (*Q*) of the opening of the signal eye. For OOK, the standard Q-factor is based on Gaussian statistics and is defined as:

$$Q = \frac{|\mu_1 - \mu_0|}{\sigma_1 + \sigma_0} \tag{1.50}$$

where $|\mu_1 - \mu_0|$ denotes the separation between the intensity levels of the "0" and "1" bits. The mean values for the zeros and ones are subtracted giving the height of the eye at the sampling time when the sum of the bit amplitudes is at maximum. The random noise statistic $\sigma_1 + \sigma_0$ is the sum of the standard deviations of the intensities around the levels of "1" and "0" and varies between simulations.

The relation between the BER and Q assumes a Gaussian approximation of the noise distribution in the received signal even although it is recognised that the noise distribution in the intensity domain is not exactly Gaussian [86]. This approximation does however provide a good estimation of performance. The BER is derived through its relation to Q and found to be:

$$\text{BER} = \frac{1}{2} erfc\left(\frac{Q}{\sqrt{2}}\right) \approx \frac{1}{Q\sqrt{2\pi}} \exp\left(-\frac{Q^2}{2}\right) \tag{1.51}$$

This model can however lead to inaccurate prediction of the BER in DPSK simulations due to the no-Gaussian nature of the noise distribution in the output signal of the DPSK balanced receiver. In [34, 87], a Q model is proposed which allows an estimate of the BER for DPSK systems. To highlight this method a linear optical transmission system and a field of *N* return to zero (RZ) pulses is considered. At the end of the transmission the field $F(t)$ can be described as:

$$F(t) = \left[\sum_{n=0}^{N-1} a_n u(t - nT) + z(t)\right] e^{-i\omega_c t} + c.c. \tag{1.52}$$

The $u(t - nT)$ term provides the location of the envelope of the RZ pulse in time, $z(t)$ represents additive Gaussian noise and ω_c is the angular frequency of the optical carrier. The term a_n is the complex amplitude of the *n*-th pulse where for DPSK pulses the relative phase change is encoded with respect to the a_{n-1} pulse. In this case $a_n = \pm 1$ is chosen, and a "0" is represented by a phase change of π, whereas a "1" is represented by no phase change.

The transmitted signal is pre-filtered to optimise receiver performance. This matched optical filter is characterised by its impulse response function $h(t)$ as:

$$h(t)=\left[\frac{1}{\sqrt{E_b}}\right]u(-t)e^{i\omega_c t}+c.c. \tag{1.53}$$

where E_b is the energy per bit defined by:

$$E_b=\int_{-T/2}^{T/2}u^*(t)u(t)dt \tag{1.54}$$

Convolution of $F(t)$ and $h(t)$ gives the filtered signal, and near the centre of the n-th timeslot the filtered signal is given as:

$$F_n(t)=f_n e^{-\omega_c t}+c.c. \tag{1.55}$$

$$f_n=a_n\sqrt{E_b}+z_n \tag{1.56}$$

$$z_n=\int_{(n-1/2)T}^{(n+1/2)T}z(t)u^*(t-nT)dt \tag{1.57}$$

The filtered noise amplitude is given by $z_n=x_n+iy_n$ where both real and imaginary parts are independent zero-mean Gaussian-distributed quantities with the equal variance such that:

$$\left\langle x_n^2\right\rangle=\left\langle y_n^2\right\rangle=\sigma^2 \tag{1.58}$$

After filtering the DPSK signal it is decoded with an optical delay interferometer so that either destructive or constructive interference takes place depending on the relative phase between f_n and f_{n-1}. The two resultant fields measured are then found as:

$$\begin{aligned} I_+&=\left|\frac{f_n+f_{n-1}}{2}\right|^2 \\ I_-&=\left|\frac{f_n-f_{n-1}}{2}\right|^2 \end{aligned} \tag{1.59}$$

In the case of balanced detection it is necessary to find the balanced output I_{bal}, thus the fields in Eq.1.59 are subtracted to give:

$$I_{bal} = I_+ - I_- = \frac{f_n f_{n-1}^* + f_n^* f_{n-1}}{2} \tag{1.60}$$

By expanding z_n in eq.1.56 with $z_n = x_n + iy_n$ and substituting the result into Eq.1.60, I_{bal} is reducible to:

$$I_{bal} = \left(a_n\sqrt{E_b} + x_n\right)\left(a_{n-1}\sqrt{E_b} + x_{n-1}\right) + y_n y_{n-1} \tag{1.61}$$

Under the assumption of only small Gaussian noise amplitude remaining after filtering, I_{bal} can be further reduced to:

$$I_{bal} \approx a_n a_{n-1} E_b \tag{1.62}$$

From Eq.1.62 we can see that depending on the phase change between bits a_n and a_{n-1} then $I_{bal} \approx E_b$ or $I_{bal} \approx -E_b$ for a "1" or "0" respectively. As x_n and y_n are zero-mean Gaussian-distributed quantities with the same variance, then by using the Gaussian probability density function of each, the BER, which is the probability of I_{bal} having the wrong sign, can be calculated analytically as:

$$\text{BER} = \frac{1}{2}\exp\left(-\frac{E_b}{2\sigma^2}\right) \tag{1.63}$$

On re-analysing Eq.1.62, the balanced receiver output $I_{bal} \approx \pm E_b$ which corresponds to $\left|\mu_1 - \mu_0\right| \approx 2E_b$, and since x_n and x_{n-1} are independent, the standard deviation of I_{bal} becomes $\sigma_1 = \sigma_2 \approx \sigma\sqrt{2E_b}$. Putting these values into the Q of Eq.1.50, gives a Q-factor of:

$$Q \approx \frac{\sqrt{E_b}}{\sqrt{2}\sigma} \tag{1.64}$$

By substituting this Q model into the original BER formula in Eq.1.51, then the BER then becomes:

$$\text{BER} = \frac{1}{2}\text{erfc}\left(\frac{Q}{\sqrt{2}}\right) \approx \sqrt{\frac{\sigma}{\pi E_b}} e^{-\frac{E_b}{4\sigma^2}} \tag{1.65}$$

A comparison of Eq.1.63 and 1.65 shows that the predicted BER in Eq.1.65 is ~3dB worse meaning that this method is not suitable for DPSK as it would put DPSK performance on par with OOK. The issue arises due to the non-Gaussian nature of the noise distribution (as opposed to the assumption above) at the output of the balanced receiver. To compensate the $\sqrt{2}$ (or 3dB) deviation, it was proposed that the variance of the field amplitude is evaluated before the delay interferometer and an alternative *amplitude-Q*, or Q_A, was given as:

$$Q_A = \frac{\langle |f_n| \rangle}{\sigma |f_n|} \approx \frac{\sqrt{E_b}}{\sigma} \tag{1.66}$$

Note that this model will overestimate the performance of transmission in the high power regime as non-linear penalties are assumed to be insignificant, i.e., the model assumes DPSK is propagating in a linear channel. Due to the presence of phase noise in nonlinear systems it has been proposed [87] that the Q-factor be evaluated in the phase domain. This is achieved by first switching to polar co-ordinates where:

$$f = |f_n| e^{i\phi_n} \tag{1.67}$$

Then by replacing Eq.1.56 (which was originally substituted into Eq.1.59) with Eq.1.67, and simplifying Eq.1.60 in the same manner as before, the following relation for I_{bal} is obtained:

$$I_{bal} = |f_n f_{n-1}| \cos \Delta\phi_n \tag{1.68}$$

where $\Delta\phi_n$ is the differential phase and defined as:

$$\Delta\phi_n = \phi_n - \phi_{n-1} \tag{1.69}$$

which takes the value of $\Delta\phi_n = 0$ (for "1" bits) or $\Delta\phi_n = \pi$ (for "0" bits). If phase noise is such that a deviation of $\pi/2$ or greater from the ideal value of $\Delta\phi_n$ occurs, then an error is realised. This allows the introduction of an alternative Q measure, the differential-phase-Q, or $Q_{\Delta\phi}$ [34, 87] which takes the form:

$$Q_{\Delta\phi} = \frac{\pi}{\sigma_{\Delta\phi,0} + \sigma_{\Delta\phi,\pi}} \tag{1.70}$$

The $\sigma_{\Delta\phi,0}$ and $\sigma_{\Delta\phi,\pi}$ terms in the differential phase $Q_{\Delta\phi}$ are the standard deviations of the optical differential phase on the 0 and π rails. $Q_{\Delta\phi}$ can be employed to observe signal phase margins. In [88] it was shown that by applying $Q_{\Delta\phi}$ to DPSK systems, it provided a relatively good estimate of nonlinear phase noise penalties where such phase noise was the dominating source of nonlinear penalty. They also show that compared with the direct error counting BER method, the differential phase Q method can reduce the computation time tremendously. Both $Q_{\Delta\phi}$ and Q_A are used in this thesis and the smaller measure is used as the overall Q for BER estimation. This allows us to take into account the contributions of both the amplitude noise and the phase noise as the optical power levels are varied in the numerical simulations The final *Q*-factor measure is a unit-less quantity and is converted to dB using: $20\log_{10}Q = Q$[dB] where Q^2 denotes Q[dB] in this thesis.

Amplifier noise limits the *Q*-factor at low power levels whereas nonlinear effects limit the *Q*-factor at high power levels (see Figure 1.10). System performance is determined by a trade of between nonlinear impairments and noise. The Q-factor increases with launched power, reaches a peak, then decreases with increased launched power due to the onset of nonlinear effects.

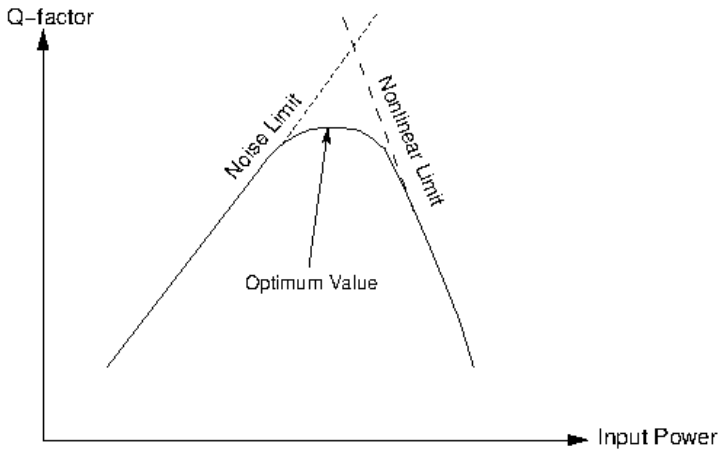

Figure 1.10: Q-factor variation with launch power in terrestrial systems with lumped amplification

Another useful measure is the optical signal to noise ratio (OSNR) which is used to monitor the mixture of signal power to noise power in the optical channel. The ASE noise added by each amplifier to the optical signal reduces the OSNR and makes it more difficult for the receiver to detect the signal accurately. The input signal should be well above background noise to give an adequate OSNR. Noise power can be suppressed by a band pass filter which allows the removal of the out-of-band noise while permitting the optical signal to pass through free from intervention. However complete removal of noise is not possible, thus the OSNR measure is a useful evaluation tool during transmission system design. The ASE power added by any amplifier in a chain is attenuated in

succeeding fibre sections; however it is also amplified by all following amplifiers. The net effect allows us to simply add the ASE powers of all amplifiers at the end of a fibre link [17]. In terrestrial systems the distance between lumped optical amplifiers depends on network geography and leads to unequal amplifier spacing. The gain G of the i-th amplifier where (i = 1, 2, ..., N) is:

$$G_i = \frac{P_{out}}{P_{in}} = \exp(\alpha L_i) \tag{1.71}$$

Assuming a transparent line such that the input power to the transmission line is equal to the output power of the system, and that all EDFAs in the system have the same noise figure, then the total ASE power [89, 90] for a chain of N amplifiers unequally spaced is given by:

$$P_{ASE}^{tot} = 2 n_{sp} h \nu \left(\sum_{i=1}^{i=N} \left(G_i - 1 \right) \right) B_O = 2 n_{sp} h \nu \left(\sum_{i=1}^{i=N} (\exp(\alpha L_i) - 1) \right) B_O \tag{1.72}$$

where the factor of 2 takes into account the unpolarised nature of ASE, n_{sp} is the spontaneous emission factor, h is Planck's constant, $h\nu$ is photon energy and B_O is the optical filter bandwidth. The output OSNR of the system can then be approximated through:

$$OSNR_{OUT} = \frac{P_{out}}{P_{ASE}^{tot}} = \frac{P_{out}}{2 n_{sp} h \nu \left(\sum_{i=1}^{i=N} \left(G_i - 1 \right) \right) B_O} \tag{1.73}$$

For the typical launch power levels required in terrestrial systems, an increase in input signal power at the input of the system increases the OSNR but also increases optical fibre nonlinearities. Thus the achievable OSNR at the receiver is severely limited by fibre nonlinearities so that system design is complicated by the interrelationships between signal power evolution during transmission, topology of the amplifier scheme and deployed dispersion maps.

Chapter 2

Dispersion Management

In the 1980s, transmission rates of ≈2.5 Gb/s (OC-48 rate) were an industry standard for signal transmission over the 1310nm-optimised G.652 single-mode fibres. However in these systems, maximum repeater / link length was limited by transmission loss of ~ 0.34 dB/km at this 1310nm wavelength. Transmission was then shifted to the lowest loss (approx 35% to 40% less loss) wavelength window at 1550nm where chromatic dispersion was in the region of 17 ps/(km-nm). This level of chromatic dispersion in G.652 originates from, and is sufficiently defined as, the summation of material dispersion (positive at 1550nm) and waveguide dispersion (negative in general) [91] where material dispersion is the major contributor.

In terrestrial networks, dispersion management entails finding a dispersion scheme that not only compensates accumulated dispersion but simultaneously optimises the interaction between non-linear Kerr processes and the optical signal. The interplay between SPM and group velocity dispersion leads to changes in the intensity waveform (pulse narrowing and broadening) and can result in substantial waveform distortion. Chromatic dispersion (CD) produces signal eye closure by lowering the height of light pulses while simultaneously spreading pulse energy into adjacent bit slots causing neighbouring symbols to interfere with one and other. As short optical pulses at high bit rates have larger spectral content there exists a greater difference in the velocities. It is such that the penalty due to CD grows approximately quadratically proportional to an increase in bit-rate and is around 16 times more severe at 40Gb/s than at 10Gb/s. This leads to acute workable margins in dispersion management at 40Gb/s line speeds. These margins are explored in depth in later chapters. Discussed in this chapter, are some of the fundamental issues in dispersion management, such as the physical origin of chromatic dispersion, residual dispersion, dispersion compensating technologies and various arrangements of distributing dispersion along a link, also known as dispersion mapping.

2.1 Refractive Index of Silica Glass

The index of refraction of glass is the ratio of the speed of light in a vacuum (free space) relative to the speed of light in the glass. If a single mode glass fibre has a refractive index of 1.467 then light travels through the fibre at approximately 68% (1/1.467 = 0.68) the speed of light in a vacuum. The refractive index of silica glass is a function of optical frequency and optical intensity, and determines the optical propagation properties of each wavelength. The Sellmeier series [92] measures the

relationship between the refractive index of the fibre core and wavelength. The general form of the equation for glasses is given by:

$$n(\omega) = \sqrt{1 + \sum_{i=1}^{K} \frac{A_i \lambda^2}{\lambda^2 - B_i}} \tag{2.1}$$

with λ is wavelength and A_i and B_i are the Sellmeier coefficients. Sufficient accuracy can be obtained employing only the first three terms although additional terms are sometimes added to make the calculation even more precise.

2.2 Dispersion, Slope and Curvature

The Chromatic Dispersion (CD) of an optical medium is the phenomenon that the phase velocity and group velocity of light which, when propagating in a transparent medium, are dependent on the optical frequency. If we let the effective index n_{eff} represent the effective index of the fundamental mode then the propagation constant β can be written as [13]:

$$\beta = \frac{\omega}{c} n_{eff}(\omega) \tag{2.2}$$

where c is the speed of light and ω is the frequency. The velocity of the propagation of the phase front through the medium is given by:

$$v_p = \frac{\omega}{\beta} = \frac{c}{n_{eff}(\omega)} \tag{2.3}$$

and the modal group velocity v_g can be defined as:

$$\frac{1}{v_g} = \frac{d\beta}{d\lambda} = \frac{1}{c}\left[n_{eff}(\lambda_0) - \lambda_0 \frac{dn_{eff}}{d\lambda_0} \right] \tag{2.4}$$

where λ is the wavelength. For optical fibre, the effective index n_{eff} depends on the core and cladding refractive indices as well as the waveguide parameters. CD in optical fibres is due to the frequency dependent nature of the propagation characteristics for both the material (the refractive index of glass) and the waveguide structure profile.

Light spreads in time as a result of different frequency components of the pulse travelling at different velocities, with a group velocity v_g given by [12]:

$$v_g = \frac{c}{n_g} = \frac{d\omega}{d\beta} = \left(\beta_1\right)^{-1} \tag{2.5}$$

where n_g is the group refractive index parameter given as:

$$n_g = n_{eff} + \omega\left(\frac{dn_{eff}}{d\omega}\right) \tag{2.6}$$

The propagation constant β can also be written as:

$$\beta = n_{eff}\ \frac{\omega}{c} = n_{eff}\ \frac{2\pi}{\lambda} \tag{2.7}$$

In SMF of length L the arrival as a time delay of a spectral component at frequency ω can be written as:

$$T = \frac{L}{v_g} \tag{2.8}$$

If we assign $\Delta\omega = \left(\omega - \omega_0\right)$ as the spectral width of the pulse, then:

$$\Delta T = \frac{dT}{d\omega}\left(\omega - \omega_0\right) = \frac{d}{d\omega}\frac{L}{v_g}\left(\omega - \omega_0\right) = L\frac{d^2\beta}{d\omega^2}\left(\omega - \omega_0\right) = L\beta_2\Delta\omega \tag{2.9}$$

where $\beta_2 = d^2\beta / d\omega^2$ is the group velocity dispersion (GVD) parameter which gives the rate of optical pulse broadening when propagating inside SMF. When $\beta_2 > 0$ (normal dispersive medium), the low frequency components travel faster than those with a higher frequency causing temporal pulse spreading, SMF is an example of this type of fibre. Although dispersion has to be compensated in WDM systems, SMF has to have some amount of dispersion in order to minimise the effect of fibre nonlinearities as nonlinear FWM severely limits systems that operate near the zero dispersion wavelength of the fibre [93]. This is a result of a nonlinear mixing effect induced by the phase matching of channels co-propagating around the same speed while they are on different wavelengths. When $\beta_2 < 0$ (anomalous dispersive medium), the low frequency components travel slower than those with a lower frequency.

To find the relation between the GVD parameter and the dispersion parameter D, we can switch from frequency to wavelength where $\omega = 2\pi c / \lambda$ to show that:

$$\Delta T = \frac{d}{d\lambda}\frac{L}{v_g}(\lambda - \lambda_0) = DL\Delta\lambda \quad \text{where} \quad D = \frac{d}{d\lambda}\left(\frac{1}{v_g}\right) = -\frac{2\pi c}{\lambda^2}\beta_2 \tag{2.10}$$

The effect of dispersion on the bit rate B can be estimated by using ΔT from equation 2.10 and via the criterion:

$$BL|D|\Delta\lambda < 1 \tag{2.11}$$

This equation offers an estimated measure of the BL product offered by SMF. The dispersion length L_D is another useful measure and indicates the distance pulses must propagate to be significantly affected by the GVD. It is defined as:

$$L_D = \frac{T_0^2}{|\beta_2|} \tag{2.12}$$

where T_0 is the 1/e pulse width. Higher order dispersive terms are modelled by a Taylor series expansion around the central wavelength:

$$D(\lambda) = D(\lambda_0) + D'(\lambda_0)(\lambda - \lambda_0) + \frac{1}{2}D''(\lambda_0)(\lambda - \lambda_0)^2 + \ldots \tag{2.13}$$

where, D is the dispersion, $D' = S = dD/d\lambda$ is the dispersion slope and D'' is the dispersion curvature. The slope S is also called the differential dispersion parameter and by using D from equation 2.10, S can also be written as:

$$S = \left(\frac{2\pi c}{\lambda^2}\right)^2 \beta_3 + \left(\frac{4\pi c}{\lambda^3}\right)\beta_2 \tag{2.14}$$

where $\beta_2 = d^2\beta_2 / d\omega \equiv d^3\beta / d\omega^3$ is the third order dispersion parameter. As S is positive for most fibres, neighbouring channels in WDM systems have slightly different GVD values making it difficult to compensate for all channels simultaneously.

2.3 Material and Waveguide Dispersion

In G.652, Chromatic Dispersion is positive (at 1550nm) and is sufficiently defined as the summation of material dispersion (positive at 1550nm) and waveguide dispersion (negative in general) where material dispersion is the major contributor. To find the equations for D_m and D_w, we use the dispersion parameter in the form:

$$D = \frac{d}{d\lambda}\left(\frac{1}{v_g}\right) = -\frac{2\pi c}{\lambda^2}\beta_2 \tag{2.15}$$

which can be re-written using n_g in Eq. 2.6 as:

$$D = -\frac{2\pi c}{\lambda^2}\frac{d}{d\omega}\left(\frac{1}{v_g}\right) = -\frac{2\pi}{\lambda^2}\left(2\frac{dn_{eff}}{d\omega} + \omega\frac{d^2 n_{eff}}{d\omega^2}\right) \tag{2.16}$$

then by substituting [17]:

$$n_{eff} = n_2 + b\left(n_1 - n_2\right) \approx n_2\left(1 + b\Delta\right) \tag{2.17}$$

where n_1 is the core index, n_2 the cladding index, b is the normalised propagation constant and by using:

$$V = k_0 a\sqrt{\left(n_1^2 - n_2^2\right)} \approx \left(\frac{2\pi}{\lambda}\right) a n_1 \sqrt{2\Delta} \tag{2.18}$$

then D is sufficiently described by:

$$D = D_M + D_W = D_{material} + D_{waveguide} \tag{2.19}$$

As material dispersion D_M originates from the physical properties of the silica which gives rise to the frequency dependence of the refractive index, the slope of the group mode index n_g over wavelength can be used to define material dispersion as such:

$$\mathrm{D_M} = -\frac{2\pi}{\lambda^2}\frac{dn_{2g}}{d\omega} = \frac{1}{c}\frac{dn_{2g}}{d\lambda} \tag{2.20}$$

Waveguide dispersion D_W reduces dispersion from its material value at 1550nm and arises from the waveguide structure profile of the fibre such as the core radius. The effective index of the mode depends on the fraction of power in the core and the cladding at a particular wavelength, so that when the wavelength changes this fraction also changes. Waveguide dispersion can be defined as [17]:

$$D_W = -\frac{2\pi\Delta}{\lambda^2}\left[\frac{n_{2g}^2}{n_2\omega}\frac{Vd^2(Vb)}{dV^2} + \frac{dn_{2g}}{d\omega}\frac{d(Vb)}{dV}\right] \tag{2.21}$$

The term inside the brackets is usually positive so that D_w is negative. The sign of material dispersion is dependent on the wavelength region operated within and therefore material dispersion and waveguide dispersion can cancel each other out to produce the so called zero-dispersion wavelength at $\lambda_D = 1.27\mu m$.

2.4 Dispersion Compensating Technologies

CD compensation is a critical task in WDM system design and has profound implications in fibre optic system performance. While transmission distances and speeds have increased over the years, dispersion management has become a major challenge for network designers to contend with. The spreading of neighbouring pulses produces inter-symbol-interference (ISI) and can lead to a reduction of the optical signal-to-noise ratio (OSNR), a loss of information and a higher Bit Error Rate (BER).

Dispersion Compensating Fibres

Dispersion compensating fibres (DCF) [93] are the dominant dispersion compensating device in world networks. DCF based optical compensation has the advantages of being broadband, passive and can be used with any modulation format and at any channel spacing. Fibre based Dispersion Compensating Modules (DCM) are usually presented as DCF-for-SMF [km] modules rather than DCF by the metre. A finite number of modules are available commercially and have large granularity which leads to a reduction in dispersion map accuracy. Desired properties of DCF are a low nonlinear coefficient to reduce nonlinear impact, and a low attenuation in order to limit amplifier induced noise accumulation following the DCF. To limit DCF loss a large negative dispersion value D is preferable in order to reduce the DCFs length. To generate a large negative D, a large effective central core area is required. The larger the effective area the greater the reductions in both bend induced losses and the sensitivity to nonlinear optical effects. Bend losses are important as DCF is normally collocated on a spool with EDFAs. The DCF must be wound on the spool at a precise tension not only to the reduce bend loss but to ensure thermal uniformity. DCMs are sometimes constructed with EDFAs on each side of the DCF, creating dual stage amplification. This type of assembly allows the power levels in

the DCF to be optimised separately from the transmission fibre and can reduce the impact of DCF insertion loss on noise accumulation in the system. Splitting the gains between amplifiers also results in lower power stages which is sometimes beneficial for economic reasons as EDFA pump prices are positively correlated with their output power capabilities and are the most expensive part of the amplification stage (this cost is dependent on the uncompensated lossy fibre length prior to the DCM).

The length of DCF needed to compensate an SMF link is given by:

$$L_{DCF} = -\frac{D_{SMF}}{D_{DCF}} L_{SMF} \tag{2.22}$$

This measure quantifies the compensation of dispersion described by the D parameter of the SMF and by slope S matching the DCF to the transmission fibre we can compensate for $D' = S$ also:

$$S_{DCF} = -\frac{S_{SMF}}{L_{DCF}} L_{SMF} = \frac{S_{SMF}}{D_{SMF}} D_{DCF} \tag{2.23}$$

However despite dispersion in SMF being accounted for adequately by including the first two dispersion terms in the NLSE, this does not guarantee 100% dispersion compensation at the end of the link. In DCF, higher order terms are significant and lead to a residual dispersion. Slope matching the DCF only ensures that residual dispersion is minimised. However, it is such that residual dispersion is often required to have a value different from zero to suppress penalties from, e.g., cross-phase modulation. However, in system design it is often unclear whether to have a slight over or under compensation to nullify residual dispersion as this measure depends on an often unknown bandwidth vs. residual dispersion variation ratio. Although the path average dispersion (PAD) for the centre channel may be close to zero, the dispersion curvature of DCF is wavelength dependent so that when broadband compensation is sought, i.e., the number of channels increases, the residual dispersion is larger in channels which are closer to the edge of the wavelength grid. This dispersion compensation error accumulates with propagation distance. In 40Gb/s WDM transmission systems, fine granularity dispersion detuning / tuneable dispersion compensation (TDC) is a necessity directly before or within the receiver to optimise the signal eye. Per-channel TDCs are expensive but provide a way to tackle the low residual dispersion tolerance inherent in high bit rate systems.

There have been many alternative dispersion compensating devices proposed in the literature such as Gires-Tournois etalons [94 – 97], Virtually-Imaged Phased-Arrays (VIPA) [98], Fibre Bragg Gratings (FBG) [99], Optical Phase Conjugation (OPC) [100] and Electronic Dispersion Compensation (EDC)

[101]. The latter three technologies are now introduced due to their potential for application in phase modulated optical systems.

Fibre Bragg Gratings

Dispersion management can be performed with fibre Bragg gratings (FBG). The basic characteristics of a Bragg grating can be understood and modelled by using coupled-mode theory. In a fibre grating the refractive index of the fibre mode can be written as:

$$\tilde{n}(\omega, z) = \bar{n}(\omega) + \delta n_g(z) \tag{2.24}$$

where $\delta n_g(z)$ accounts for periodic index variations inside the grating. Most fibre gratings involve very short lengths of fibre so that optical nonlinear interactions are considered to be negligible. The $\delta n_g(z)$ term in Eq.2.24 can be expanded in a Fourier series to produce [17]:

$$\delta n_g(z) = \sum_{m=-\infty}^{\infty} \delta n_m \exp\left[2\pi i m (z/\Lambda)\right]. \tag{2.25}$$

Next we use the Helmholtz equation in the form:

$$\nabla^2 \tilde{E} + \tilde{n}^2 k_0^2 \ \tilde{E} = 0 \tag{2.26}$$

and solve using the refractive index in Eq.2.24, then, taking into account both forward (*f*) and backward (*b*) propagating waves, the approximate solution for $\tilde{E}$ is given by:

$$\tilde{E}(\mathbf{r}, \omega) = F(x, y)\left[\tilde{A}_f(z, \omega)\exp(i\beta_B z) + \tilde{A}_b(z, \omega)\exp(-i\beta_B z)\right] \tag{2.27}$$

where $\beta_B = \pi/\Lambda$ is the Bragg wave number for a first-order grating. Assuming $\tilde{A}_f$ and $\tilde{A}_b$ slowly vary with z and keeping only the nearly phase matched terms, the frequency-domain coupled-mode equations take the form [17]:

$$\frac{\partial \tilde{A}_f}{\partial z} = i\delta(\omega)\tilde{A}_f + i\kappa\tilde{A}_b \tag{2.28}$$

$$-\frac{\partial \tilde{A}_b}{\partial z} = i\delta(\omega)\tilde{A}_b + i\kappa\tilde{A}_f \tag{2.29}$$

where ∂ is a measure of detuning from the Bragg frequency and defined as:

$$\delta(\omega) = (\overline{n}/c)(\omega - \omega_B) \equiv \beta(\omega) - \beta_B \tag{2.30}$$

The grating induced-coupling between the forward and backward waves is governed by the parameter κ, where for a first order grating κ is given by:

$$\kappa = \frac{k_0 \int\int_{-\infty}^{\infty} \delta n_1 \left|F(x,y)\right|^2 dxdy}{\int\int_{-\infty}^{\infty} \left|F(x,y)\right|^2 dxdy} \tag{2.31}$$

which in this form allows for transverse variations of δn_g when the photo induced index change is not uniform over the core area. In the case of a CW beam the frequency-domain coupled-mode equations have the general solution:

$$\tilde{A}_f(z) = A_1 \exp(iqz) + A_2 \exp(-iqz) \tag{2.32}$$

$$\tilde{A}_b(z) = B_1 \exp(iqz) + B_2 \exp(-iqz) \tag{2.33}$$

where q is to be determined. The constants A_1, A_2, B_1 and B_2, are interdependent and satisfy the relations:

$$(q-\delta)A_1 = \kappa B_1 \qquad (q+\delta)B_1 = -\kappa A_1 \tag{2.34}$$

$$(q-\delta)B_2 = \kappa A_2 \qquad (q+\delta)A_2 = -\kappa B_2 \tag{2.35}$$

which are satisfied for nonzero values of A_1, A_2, B_1 and B_2 if the values of q obey the dispersion relation:

$$q = \pm\sqrt{\delta^2 - \kappa^2} \tag{2.36}$$

By introducing an effective reflection coefficient $r(q)$, the coupled mode equations can be re-written as:

$$\tilde{A}_f(z) = A_1 \exp(iqz) + r(q) B_2 \exp(-iqz) \tag{2.37}$$

$$\tilde{A}_b(z) = B_2 \exp(-iqz) + r(q) A_1 \exp(iqz) \tag{2.38}$$

where

$$r(q) = \frac{q-\delta}{\kappa} = -\frac{\kappa}{q+\delta}. \tag{2.39}$$

The range $|\delta| \le \kappa$ is the photonic bandgap, or the stop band, since light stops transmitting through the grating when its frequency falls within the photonic bandgap. The stop band is a spectral region where incident light is reflected back. This stop band is centred at the Bragg wavelength $\lambda_B = 2\bar{n}\Lambda$ where $\bar{n}$ is the effective mode index and Λ is the grating period. What happens to optical pulses incident on a grating depends on the location of the pulse spectrum with respect to the stop band. If the spectrum is entirely inside the stop band the whole pulse is reflected, whereas if part of the spectrum is outside the stop-band, then that part will be transmitted through the grating. The grating period can be varied or constant however most gratings have a varied grating period due to the difficulty of producing constant period gratings with a wide stop band.

During grating inscription, numerous physical parameters of the grating may be varied such as index changes, length, apodization, and period chirp. By varying these parameters, gratings can be produced that have very wide or very narrow bandwidths, extremely sharp spectral features, and specific dispersive characteristics. Gratings can also be produced with low losses and a small footprint.

Non-uniformities can be created along the grating length so that the two grating parameters κ and δ become z-dependent. Gratings can be 'chirped' to reflect different wavelengths at different locations by varying the optical period $\bar{n}\Lambda$ along the grating (z-axis). Typically, the grating period Λ is designed to vary linearly along the grating and $\delta(z) = \delta_0 + \delta_c z$, where δ_c is a chirp parameter. Alternatively, chirping can be induced by changing the effective mode index $\bar{n}$ along z. When a pulse, whose spectrum is inside the stop band, is incident on a chirped grating, different spectral components of the pulse are reflected by different parts of the grating. This results in the pulse experiencing a large amount of GVD whose nature (normal or anomalous) and magnitude can be controlled by the chirp, hence chirped fibre Bragg gratings (CFBG) are used as dispersion compensators [99, 102 - 108]. CFBGs can be designed to produce anomalous GVD so that the reflection of lower frequency components takes place further into the grating than the reflection of the higher frequencies. Different frequencies can be made to reflect at different locations within the

grating due to the shifting Bragg wavelength along the grating. In essence, the stop band of a chirped fibre grating results from overlapping of many mini-stop stop bands.

Advancements in recent years have produced long FBGs [109] able to compensate for large quantities of dispersion and multi-channel chirped fibre Bragg gratings (MC-CFBG) [110] with broadband functionality. High bit-rate phase modulated signals have also been successfully dispersion managed using FBGs [111, 112], whilst tuneable chromatic dispersion compensation has been demonstrated in 40-Gb/s systems using nonlinearly chirped fibre Bragg gratings [113]. Dynamic or tuneable operations are possible since the transfer function of FBG-based devices can be made adaptive through temperature or stress control [114, 115].

Optical Phase Conjugation

Optical Phase Conjugation (OPC) for chromatic dispersion compensation is typically called "mid-link OPC" or mid-span spectral inversion (MSSI), and is an interesting concept where the spectrum of the signal is inverted in the middle of the transmission system. This spectral inversion has the effect of compensating accumulated dispersion from the first half of the link as the signal propagates through its second half. In essence, OPC is a lumped dispersion compensating scheme. It has been shown that OPC can compensate for GVD and SPM simultaneously [100, 116, 117] in the absence of fibre losses but this benefit disappears when attenuation is introduced as SPM is power dependent. In a recent experiment on a 40Gb/s DPSK system [118] it was shown that OPC could be deployed to reduce SPM-induced nonlinear phase noise in phase-shift-keyed transmission systems. Other benefits of OPC are transparency to data rate, low losses and broadband capability which would potentially make it an attractive dispersion compensation technology. Although it does have its merits in subsea systems [119], OPC is a complex method to implement and its appearance in heterogeneous terrestrial networks is currently unlikely.

Electronic Dispersion Compensation

Progress of semiconductor technology has afforded a platform for signal processing techniques in the electrical domain and advancements in electronic dispersion compensation (EDC). These techniques are an attractive replacement of optical dispersion compensation units in future networks due to the lower costs involved and small footprint. The losses in DCF have to be recovered using optical amplifiers which introduce noise, for this reason EDC has been seen as potential way to improve OSNR in a system.

EDC using electronic pre-distortion involves precompensating for dispersion experienced in the fibre link, at the transmitter [101, 120]. An electronic pre-distortion transmitter uses a digital predistortion

device programmed to compensate for the desired amount of signal distortion. The data stream to be transmitted is converted into digital samples representing real and imaginary parts of the pre-distorted optical field. The digital waveforms are then subject to signal processing and digital-to-analogue conversion (DAC) to determine the exact amplitude and phase of each bit so that the entire bit stream can be generated by applying the resulting electrical signal to modulators such as a dual-drive Mach Zehnder or an I/Q modulator.

The feedforward equaliser (FFE) and decision feedback equaliser (DFE) were the first analog processing structures which were realized originally for 10 Gb/s and since have been recently demonstrated at 40 Gb/s [121]. An FFE consists of a transversal filter in which the incoming electrical signal $x(t)$ is split into a number of branches using multiple tapped delay lines and their outputs are then combined back together to obtain:

$$y(t) = \sum_{m=0}^{N-1} c_m x(t - mT_c) . \tag{2.40}$$

where N is the total number of taps, T_c is the delay time (~ 50% of the bit slot) and c_m is the relative weight of the *m*th tap. To improve receiver performance the tap weights can be optimised using control algorithms. In the case of a DFE, the device makes use of feedback provided by a decision circuit whereby the voltage provided by the decision circuit is subtracted from the incoming signal. These circuits are often combined with an FFE.

A maximum likelihood signal estimator (MLSE) is another type of electronic equaliser which is based on digital signal processing and requires an analogue-to-digital converter (ADC) after the photodetector. This technique uses the Viterbi algorithm which analyses multiple bits and finds the most likely bit sequence for them. The main point here is that it is not based on specific types of distortion so can compensate for both GVD and PMD simultaneously.

In [122] two types of EDC techniques were tested on DPSK signals, these were a DFE with feedforward filter of 4 delay-taps and a feedback filter of 2 delay-taps, and an MLSE with memory of 2. The authors concluded that EDC performance with pre-distortion methods is limited in DPSK systems by the conversion from phase to intensity with a delay-interferometer and balanced detection.

In 40Gb/s transmission systems PMD induced distortion is hard to equalise adaptively by optical devices as it is a statistical phenomenon and time variant effect. However electrical compensation

using a receiver side electrical compensator has been successfully demonstrated [123] using an ultra-wideband IC module after 40Gb/s RZ-DPSK transmission.

In differential phase modulated formats, receiver decoding is performed optically using a delay-and-add structure to avoid the need for generating a coherent local oscillator. This technique is known as self-coherent as a delayed replica of the optical signal itself is used in place of the local oscillator required for coherent detection. This scheme can also be used for RZ and NRZ systems to recover the optical phase at the receiver and used to construct the full optical field [124].

The successful implementation electronic dispersion compensating technology will depend on particular optical network aspects, modulation format, historical signal path (signal may be non-deterministic), and of course the performance margins between 'suboptimal' dispersion maps and corresponding 'globally optimal' maps which are often found to have some amount of inline dispersion compensation to reduce nonlinear degradation, which deterministically, depends upon the deployed dispersion map.

Although many technologies are capable of dispersion compensation, only DCF with its simplest form is at such an advanced stage of technology that it is deployed in a very widespread manner in current optical networks. Although not the smallest device or the most tolerant to nonlinearities (as compared to FBG), its abundant supply, low cost and continued improvement means it has a strong position as the state-of-the-art technology. However the use of FBGs is increasing as this attractive technology is now mature and available commercially. For this reason DCF and FBG dispersion compensation are considered in this thesis.

2.5 Dispersion Compensating Schemes

A dispersion map provides a visual representation of how fibres with different dispersion characteristics give rise to dispersion variations along a given link. As a desirable aim is to upgrade systems without complete infrastructure overhauls, only localised dispersion compensation (as opposed to diffused compensation with dispersion managed fibres) is considered in this work and therefore propagation length, when DCF is used, exceeds transmission distance by approximately 17%. Dispersion compensation can take place at the transmitter (pre-compensation or D_{pre}), along the transmission line (inline-compensation or D_{inl}) or at the receiver (post-compensation or D_{post}). This often leads to a very large number of ways to implement the dispersion scheme, where the task of identifying optimal dispersion maps for a given system is a nontrivial and a resource expensive problem to solve. To achieve an adequate OSNR at the end of a system, the launch power must be somewhat above that of ASE power which at high enough levels affects the onset of fibre

nonlinearities. It follows then that nonlinear distortions in an optical link depend critically on the dispersion map while the optimal dispersion map depends on the system length, data rate, modulation format and the number and density of channels. Optimising a dispersion map is akin to finding the system configuration which operates at the highest possible launch power to maximise a systems output OSNR while simultaneously minimising fibre nonlinearities in order to reduce signal distortion.

In the absence of dispersion compensation, the dispersion accumulates in a constant manner with propagation distance. Without regenerating the original digital signal this method is only suitable for very short links and /or very low bit rate systems. Over longer lengths / higher rates any single pulse can spread over several bit periods causing multiple errors. A transmission line can be configured so that positive or negative dispersion accumulates first in any dispersion map period with the net impact of dispersion dependant on how dispersion is allowed to accumulate within each period for all fibre sections. Subsequently there have been many techniques proposed for the compensation of dispersion in a variety of scenarios / systems. Historically dispersion maps have often followed simple rules and periodic patterns to simplify network design. Some of these maps are now discussed.

To use only pre-dispersion compensation at the transmitter / line input (see Figure 2.1a), involves calculating and compensating for all dispersions present in the link before propagation through the system, then after encountered transmission dispersions, the net residual dispersion at the end of the link will be zero or close to zero. Previous studies have shown that using partial pre-compensation can extend the error-free transmission distance [125 – 127]. In [125] they show that an optimum value of pre-compensation helped reduce distortion due to intrachannel nonlinear effects.

Another possibility is to employ only post compensation immediately before the receiver, where pulses are permitted to fully disperse through all fibre sections before dispersion compensation takes place (see Figure 2.1b). This technique leads to ISI during transmission where extreme bit overlapping of neighbours will take place.

The Singly Periodic Dispersion Map (SPDM) [126] is a distributed dispersion management scheme (see Figure 2.1c) where dispersion compensation takes place at the system input (D_{pre}) thereafter all further compensation takes place at repeater sites at the end of each transmission fibre span. Thus in an SPDM, the positive dispersion of each transmission fibre span is compensated by negative dispersion directly before propagation through that span.

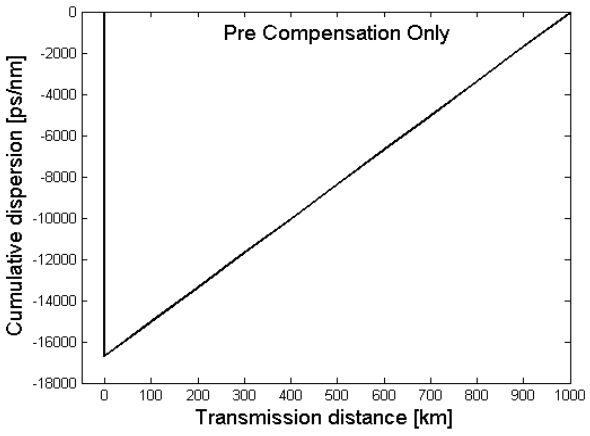

(a)

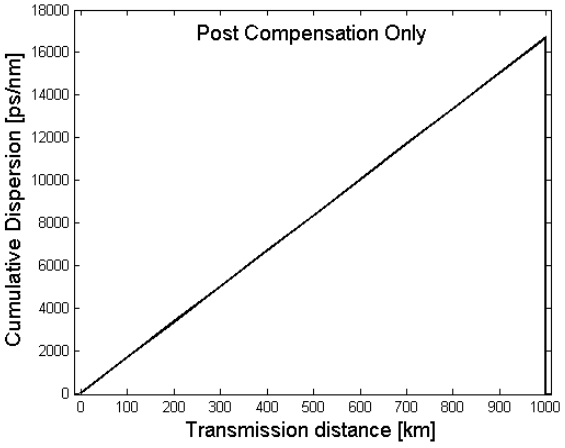

(b)

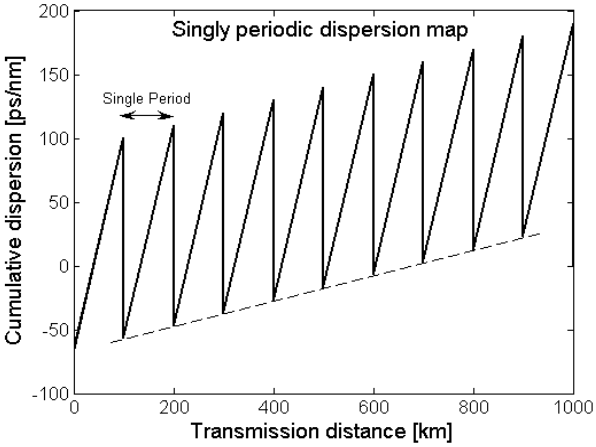

(c)

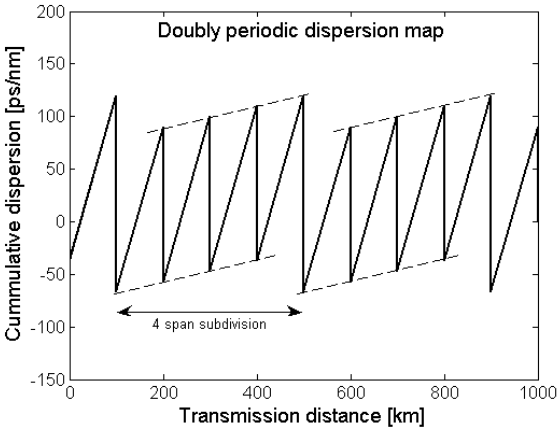

(d)

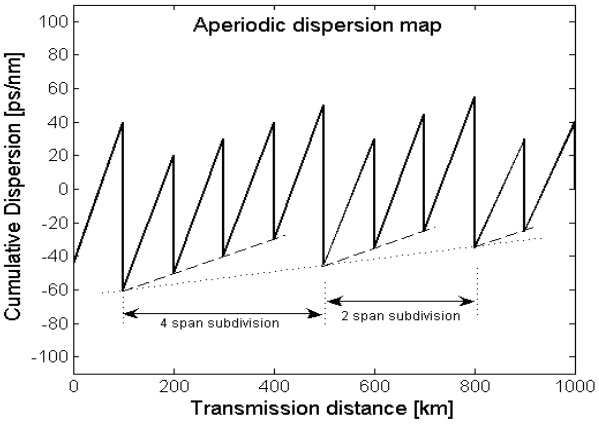

(e)

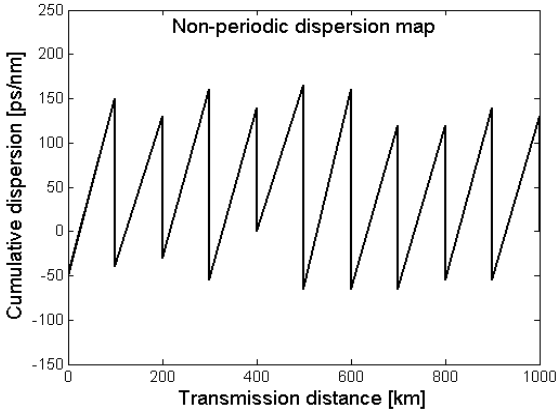

(f)

Figure 2.1: (a)-(f) Various arrangements of dispersion maps.

Each span does leave some amount of residual dispersion uncompensated which is allowed to accumulate and summate along the link and accumulates until a postcompenstion device is used to counter it along with the dispersion accumulation from the final span.

A very popular class of dispersion map is called the doubly-periodic dispersion map (see Figure 2.1d) which can be viewed as a concatenation of singly periodic maps of equal lengths over N spans and is defined by the amount of pre-compensation, the residual dispersion per span, the residual dispersion per subdivision of N spans and the final postcompensation before the receiver. In Figure 2.1d, the doubly-periodic dispersion map features a zero residual dispersion per subdivision of N spans, i.e., the map brings the residual dispersion in the link to zero every few spans [128 – 130]. This method reduces the dependence on predispersion and postdispersion compensations on distances for 40Gb/s channels.

Derived from doubly-periodic dispersion maps, the aperiodic map (see Figure 2.1e) has subdivisions of unequal lengths, i.e., varied number of spans in each subdivision. This is usually the case due to the geographical location of inline nodes. The target residual dispersion from node to node can be set to zero, or some other amount. If set to zero, then accumulated dispersion will not depend on light path which can be particularly useful in ROADM networks.

Non-periodic maps (see Figure 2.1f) can feature dispersion compensation after the Tx, at repeater sites, before the Rx and have varied inline compensation. Unlike the previous methods, in a heterogeneous terrestrial network with varying fibre spans an optimum non-periodic map will be the ‘global optimum’ dispersion map for a given system configuration since increased degrees of freedom are used (the map is not restricted to a pattern). Furthermore dispersion compensation need not take place at all repeater sites. A system complexity / performance trade-off can take place if system margins are identified. Of course when employing non-periodic dispersion maps the number of possible maps for a link increases exponentially as the number of transmission fibre spans increases. The global map can only be found by multitudinous numerical simulations, which falls outside the capability of normal computing power. Multi-node supercomputers themselves can take weeks and months to run such quantities of numerical calculations while searching for an optimum.

These are the most widely sited and deployed dispersion compensating schemes. Some of these compensation techniques are used as benchmarks for comparison to the heterogeneous dispersion maps presented in Chapter 4 of this thesis. In the third chapter, the focus turns towards another dispersion management method called lumped dispersion mapping and explores the technique in the context of a 40Gb/s RZ-DPSK terrestrial system.

Chapter 3

Lumped Dispersion Management in 40 Gb/s Terrestrial Point to Point Links

3.1 Introduction

New optical fibre lines were deployed in vast numbers during the mid to late 1990s when the most popular type of modulation / detection scheme, whether on land or submerged was Intensity Modulation with Direct Detection (IMDD). In this chapter, our concern is with the most widely deployed type of terrestrial transmission system from this era which are those characterised by an SMF / DCF infrastructure and EDFA only amplification schemes. These links were mostly installed as 10Gb/s, RZ or NRZ, WDM systems which had fixed amplifier sites with non-uniformly spaced inter-amplifier distances determined by network geographics.

When 40Gb/s channels are used in the upgrade of 10Gb/s systems these upgrades need not involve resorting to the sizeable capital investment associated with rebuilds or system overhauls. A quicker and cost efficient solution is to retrofit new technologies to these ageing systems so that existing amplifier spacing can be used and the SMF in plant can remain fixed. A 40Gb/s line speed is then achieved by switching to modulation formats which are robust to this transmission speed then carefully reconfiguring the systems dispersion compensating scheme within the transmitter, the amplifier huts and at the receiver. In particular, high spectral efficiency can be maintained by using phase modulated data formats such as RZ-DPSK [34]. A key issue then is whether differential phase encoded modulation formats are compatible with the cost optimised dispersion schemes employed in current 10Gb/s systems. Another important practical issue which is dealt with in this chapter is how robust the transmission is to inevitable variations in the dispersion mapping and how large the margins are when suboptimal dispersion management is applied. This leads to the aim of finding a pragmatic trade-off between inventory count and system performance once the optimal system configurations and acceptable performance margins have been established for the target system. The main objective of this chapter therefore is to study of the effects of lumped dispersion management in an RZ-DPSK system where the dispersion compensation is concentrated at specific points along the dispersion map—lumped mapping [131, 132], as opposed to deploying a larger number of smaller dispersion compensators placed periodically along the map – distributed mapping.

The aim here is to employ the simplest dispersion management configuration with the minimal number of dispersion compensators to increase system availability and to show the performance for a

wide range of signal powers. This can lead to dispersion compensation schemes with large Q variation. Another important aspect in this chapter is exactly to show under what conditions the Q for different schemes varies little to reduce the component count and potential cost of the system.

Various arrangements of dispersion management are investigated through large scale numerical simulations of an existing terrestrial link connecting two German cities. This link in particular was chosen as it is representative of the commonly found links that connect most of the major European cities. The 838 km installed terrestrial link is described in [131]. The system was initially a 10Gb/s line employing the non-return to zero (NRZ) modulation format. We replace OOK modulation with the return-to-zero differential phase-shift keying (RZ-DPSK) modulation format, which is used throughout this chapter.

3.2 Terrestrial System Configuration

The terrestrial system investigated is schematically depicted in Fig. 3.1. The link and has ten amplifier nodes, which are non-uniformly spaced between the transmitter and receiver. The total link length spans 838 km of SMF as dispersion compensation is localised (using DCF) at the transmitter, within amplifier huts, and at the receiver. The G.652 SMF parameters at 1550 nm are: D = 16.7 ps/nm/km, Slope S = 0.06 ps/nm^2/km, Aeff = 80 μm^2 , loss = 0.22 dB/km.

Dispersion compensation can be based on different technologies such as those discussed in Chapter 2, in this system, we use dispersion compensating fibre. Dispersion compensating fibres are followed by EDFAs. Each of the EDFAs has a noise figure of 4.5 dB and recovers losses from the previous fibre. All dispersion compensating fibres are sloped matched with the transmission fibre (SMF). This matching of the dispersion slope improves the usable bandwidth, and reduces residual dispersion levels when multiple wavelength channels are multiplexed together. The notation in this work is such that a DCF-150 signifies compensation for 150 km of SMF. The DCF fibre parameters at 1550 nm are: D = −100 ps/nm/km, S = −0.36 ps/nm^2/km, an effective Aeff = 30 μm^2 and loss = 0.65 dB/km.

While we leave the SMF spans fixed, we investigate seven schemes of the 838km link. Each scheme is such that there are multitudinous possible dispersion maps since removing DCF (leaving only the EDFA), and relocating the dispersion compensation to other sites, creates many ways to implement the dispersion management.

a)

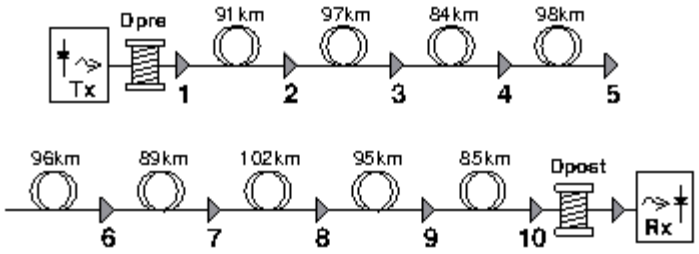

b)

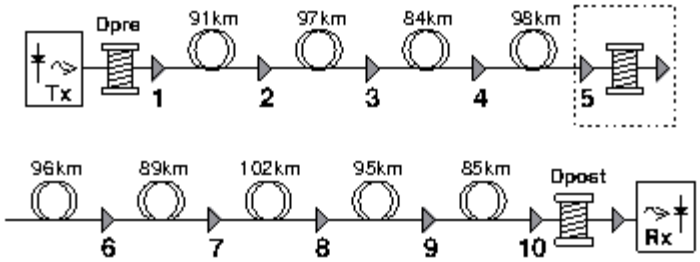

c)

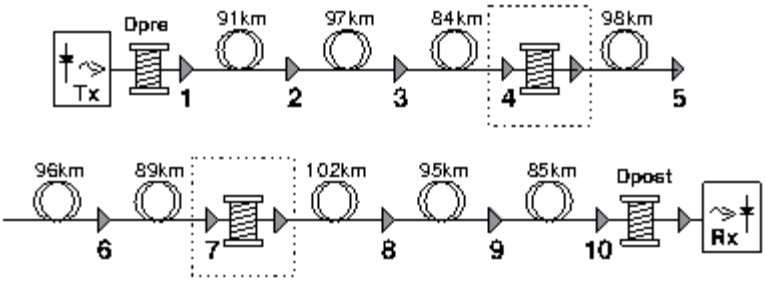

d)

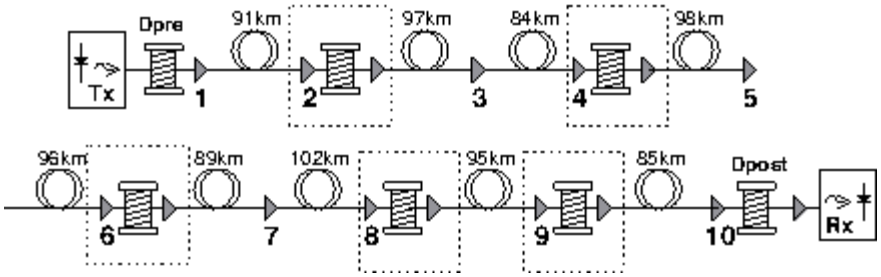

Figure 3.1: Schematic diagram of target terrestrial link, a) no inline DCF, b) 1 DCF-150 located at site 5, c) 2 DCF-150's located at sites 4 and 7, d) 5 DCF-150's are located at sites 2, 4, 6, 8 and 9.

We consider schemes with 0, 1, 2, 3, 4, 5 and 8 DCFs. The notation k = 0, 1, 2..., 8 denotes the number of DCFs deployed in line at amplifier sites 2 – 9. Variable pre-compensation (DCF-pre) and post-compensation (DCF-post) lengths of DCF are placed at sites 1 and 10 respectively. The inline DCF lengths are equal in the systems with more than one inline DCF. During the dispersion map optimisation the size of these DCF lengths is reassigned while simultaneously optimising the pre- and post-compensation DCF lengths and the signal launch power. After the last span in the transmission line, an additional dispersion compensator optimises the residual dispersion in order to obtain an optimal eye opening.

Some of these dispersion schemes are presented In Figure 3.1. In scheme 0, which has no in-line DCF, Erbium-doped fibre amplifiers are situated at sites 2 – 9, and pre- and post-compensation DCF is housed at sites 1 and 10 respectively. As this scheme has pre- and post-compensation only, all dispersion must be compensated between these sites and the optimisation consists of optimising these lengths at each end of the transmission line while simultaneously optimising the signal launch power. In this configuration, when longer lengths of DCF are used the losses are very high so that additional Erbium-doped fibre amplifiers (max. gain = 25dB) are required directly after the pre- and post-compensation DCF. In the other schemes additional amplifiers are also added as and when required.

The system in Figure 3.1(b) has only 1 in-line DCF at site 5 and EDFAs at amplifier sites 2 – 4 and 6 – 9. As in all other dispersion scheme configurations, when DCF is inserted at an amplifier node, an additional amplifier is used directly after the DCF at that node to recover the losses from propagation through the DCF. In this type of configuration it is such that the launch powers into each of the SMF spans are equal irrespective of the dispersion map.

3.3 Discussion of Results

The numerical simulations were averaged results over 10 runs to eliminate minor statistical variations. Each RZ-DPSK Gaussian pulse had a 50% duty cycle and the transmitted signal was comprised of $2^{\wedge 11}$ - 1 PRBS bits. Both single channel and 8 x 100 GHz spaced WDM channels were simulated. Simultaneous optimization of DCF-pre, DCF in-line, and launch power parameters led to a very wide choice of suitable configurations. The size of the DCF-post length was calculated such that the total residual dispersion of the map would be close to zero. The DCF-post was then numerically fine-tuned to maximize the *Q* factor. The *Q* factor was measured by a differential phase technique similar to that introduced in [133]. As a result of massive multi-parametric optimizations, we have determined the optimal parameters for each of the considered lumped mapping schemes as presented in Table 3.1.

Table 3.1. Optimal Parameters of Dispersion Management Schemes

	Scheme0	**Scheme1**	**Scheme2**	**Scheme3**	**Scheme4**	**Scheme5**	**Scheme8**
Pre-compensation (ps/nm)	-7181 (SMF 430km)	-4342 (SMF 260km)	-3006 (SMF 180km)	-2839 (SMF 170km)	-2505 (SMF 150km)	-1670 (SMF 100km)	-2171 (SMF 130km)
Inline compensation (ps/nm)	-	-5177 (1x310km)	2 x -3841 (2x230 km)	3 x -2839 (3x170 km)	4 x -2171 (4x130km)	5 x -2171 (5x130km)	8 x –1169 (8x70km)
DCF placement (amplifier node)	-	5	4,7	2,6,9	2,4,7,9	2,4,6,8,9	2,3,4,5,6,7,8,9

The granularity of DCF lengths used in these simulations was 10 SMF-km and is often typical of packaged DCF available commercially. A granularity of 5 SMF-km was tested in initial runs to compute margin measurements. When using 5 SMF-km steps the choice of optimal map would not change as the Q-factor difference between steps was very small around the optimal region (less than 0.1dB)**.** For this type of optimization, where the optimization space is already very large, a granularity of 10 SMF-km is not only suffice but often necessary even with modern computing resources.

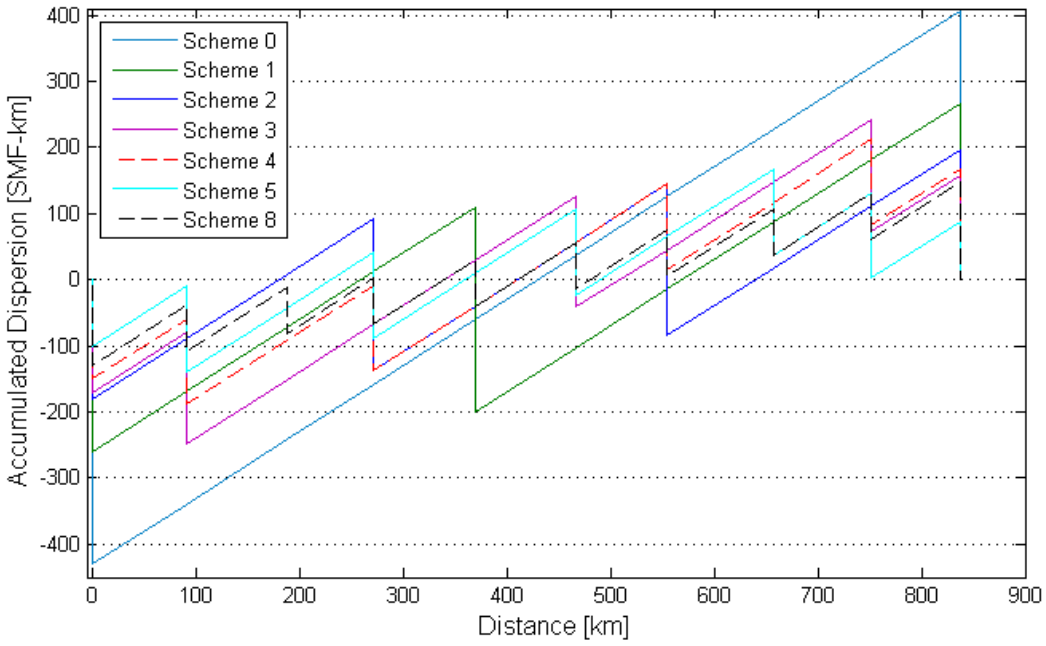

Figure 3.2: Dispersion maps for each optimised dispersion management scheme

Figure 3.2 shows a regular map of the dispersion management (scheme 8 – distributed map), and other configurations where dispersion compensation is lumped together at specific sites. The dispersion map shows the dispersion variations along the link for the optimal schemes presented in Table 3.1.

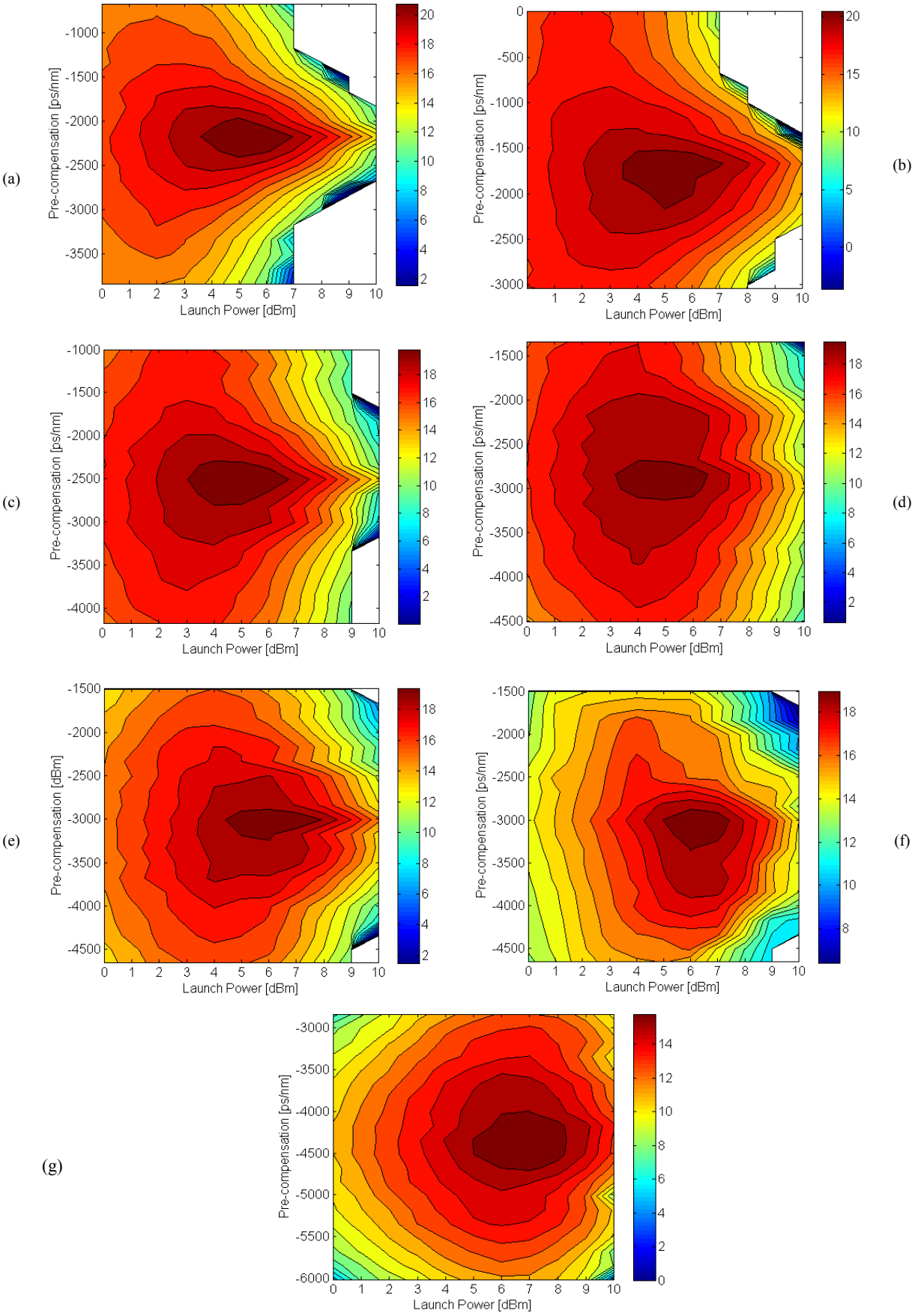

Figure 3.3: Q^2 for DCF-pre vs. launch power: a) Scheme 8, b) Scheme 5, c) Scheme 4, d) Scheme 3, e) Scheme 2, f) Scheme 1, g) Scheme 0.

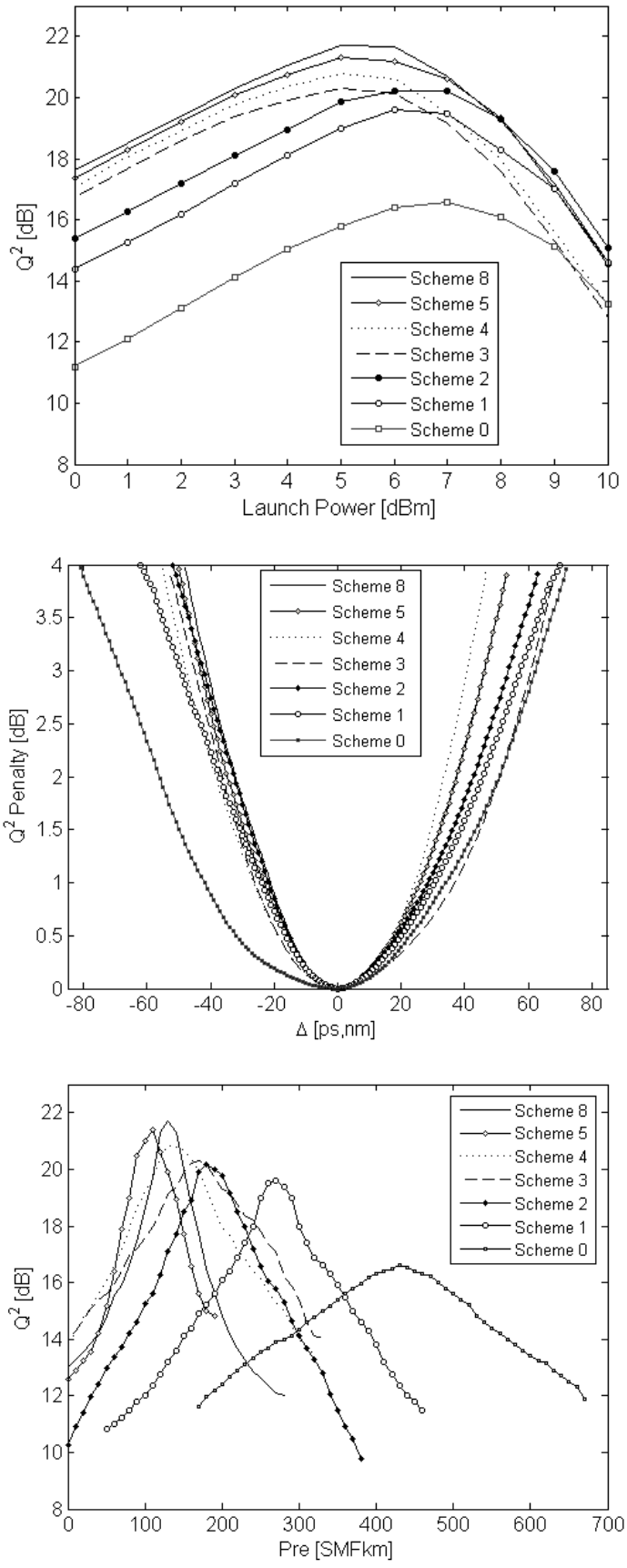

Figure 3.4: (a) *Q*-factor versus peak power for optimal dispersion management schemes,
(b) *Q*-penalty versus post compensation (DCMpost) detuning margins,
(c) *Q*-factor versus DCM-pre with optimum peak power and in-line DCMs.

Figures 3.3 (a)–(g) show the *Q*-factor (decibel) topology of DCF-pre (SMF-km) versus launch power (dBm) for each of the dispersion maps. The poorest performing scheme (Scheme 0) has no in-line DCF (dispersion compensation here is split equally between the DCF-pre and DCF-post modules). Compared to the best performing scheme the drop in receiver sensitivity is just under 5dB. A more attractive solution however is Scheme 1 which compared to the optimal lumped dispersion map (Sch. 5), has a 1.7 dB *Q* penalty and of course a lower inventory count.

The tolerance of the system performance of the optimal schemes to variations in (a) peak power, (b) post-compensation detuning margins, and (c) pre-compensation are illustrated in Figs. 3.4 (a)–(c) respectively. Figure 3.4 (b) illustrates that approximately up to 80 ps/nm dispersion tolerance fluctuations are allowable in the post-compensation detuning at the receiver before a 1 dB penalty in *Q* factor is generated.

The optimal input signal power for Schemes 8, 5, 4 and 3 is 5dBm, for Schemes 2 and 1 it is 6dBm and for Scheme 0 it is 7dBm, while the optimal pre-compensating dispersion, in-line dispersion corresponding to the chosen scheme, and the location of the DCFs for each configuration are listed in Table 1. The *Q*-factor for the optimal map in each scheme is presented in Figure 3.5.

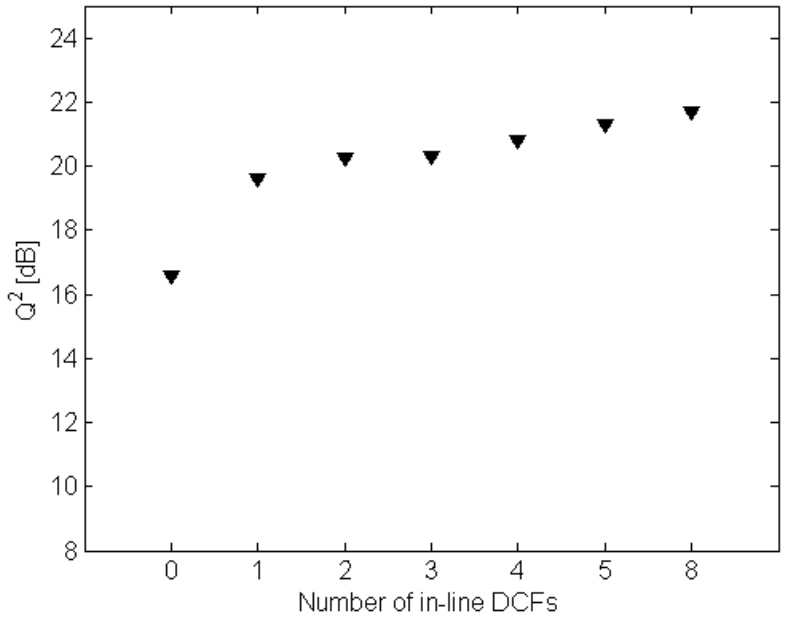

Figure 3.5: Q^2 at Rx for the optimal map in each scheme.

Presented in Figure 3.6 are numerical simulations of 8 x 40 Gb/s WDM channels spaced 100 GHz apart and centred around 1550.52 nm (ITU-C 100GHz grid) with the best dispersion maps identified from the single channel simulations. Efforts were concentrated to the cases of 5, 2 and 1 in-line DCFs.

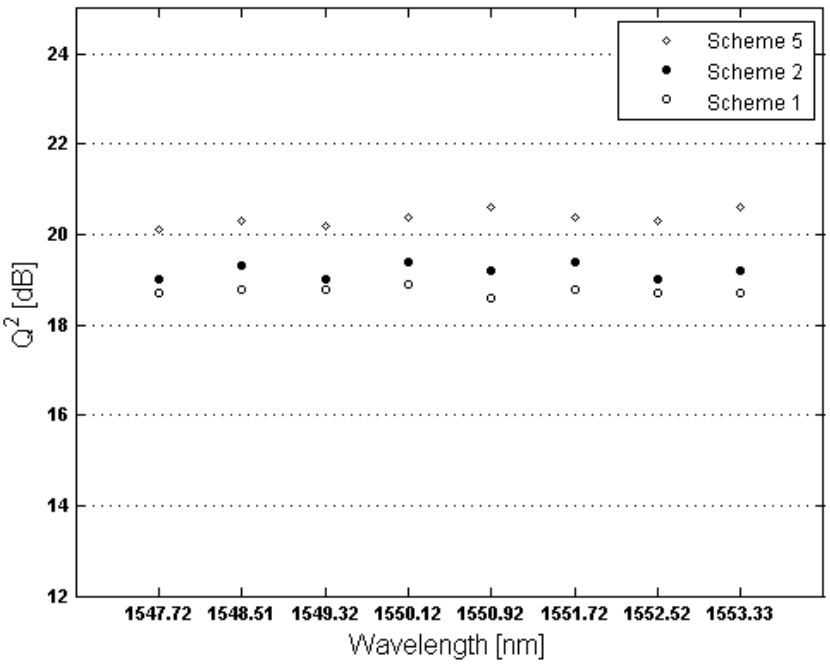

Figure 3.6: Q^2 at Rx - RZ-DPSK WDM channels on 100GHz grid.

Summary measurements for the WDM simulations compared to the single channel results are presented in Table 3.2. For Scheme 5 the difference between single channel performance and the average WDM channel is 0.9dB and the difference in *Q*-factor for the worst and best channel for this scheme is 0.5dB. Both the other schemes have a 1dB difference between single channel and WDM and both have a 0.4dB difference in *Q*-factor between the worst and best channel.

Table 3.2: WDM measurements - Optimal Dispersion Management Schemes

Scheme	**5 x DCF in-line**	**2 x DCF in-line**	**1 DCF in-line**
Single Channel Q[dB]	21.3	20.2	19.6
WDM – average channel Q[dB]	20.4	19.2	18.6
Difference between best and worst channel - Q[dB]	0.5	0.4	0.4

Each channel had been pre-filtered before multiplexing in order to reduce inter-channel crosstalk. The same filters were used at the DEMUX. The filter transfer function is given by:

$$H(f) = \exp\left[-\frac{1}{2}\left(\frac{(f-f_0)}{B}\right)^N\right] \tag{3.1}$$

where the filter steepness parameter N = 4 was optimal. The optimal bandwidths for these Super-Gaussian filters were typically around 0.07 THz. The optimisation of these filters followed processes detailed in [134]. Scheme 8 was optimised first (see Figure 3.7), then bandwidths for other schemes were verified to be either the same or between 0.06 THz and 0.07 THz but the Q-factor was unaffected (as shown below) to any significant extent.

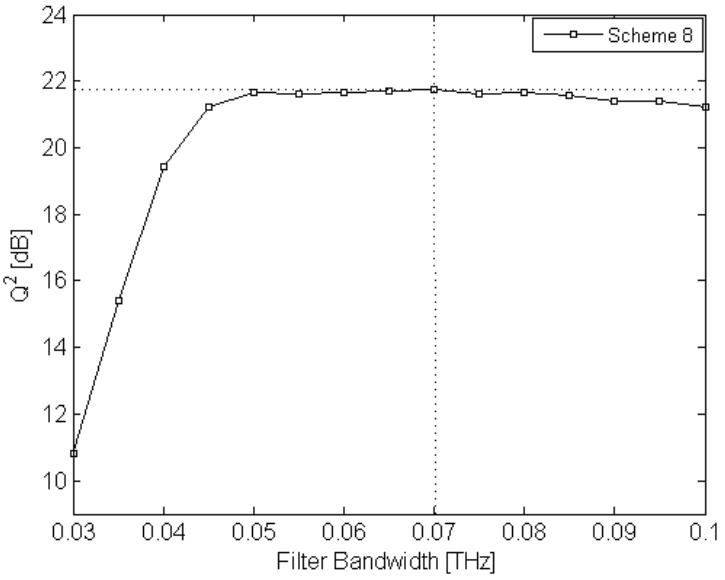

Figure 3.7: Optimal Filter Bandwidth

3.4 Systems Analysis

For each scheme the optimal launch power for that scheme is equal to the SMF and DCF launch powers as amplifiers recover losses from the previous fibre span. The optimal launch powers for Schemes 8, 5, 4 and 3 is 5dBm, for Schemes 2 and 1 it is 6dBm and for Scheme 0 it is 7dBm.

In the case of the worst performing optimal map, Scheme 0, the optical pulses spread far outside their assigned bit slot due to the very high accumulated dispersion, overlapping considerably and interacting with each other through the non-linear term in the NLS equation. A consequence of this pulse spreading is that it helps to lower the overall impact of fibre non-linearity and allows a slightly higher launch power into the link. Despite this scheme having the highest optimal launch power into the link the *Q*-factor is the lowest. This is a result of a combination of factors. Firstly when there is large dispersion and significant pulse overlap IFWM induced ghost pulses produce a phase noise variance increase with fibre dispersion. This results in the distortion of both the phase and amplitude of the DPSK RZ-optical pulses. Scheme 0 results in more accumulated dispersion in the signal than any other scheme by the time it reaches the 700km point in the line (see Figure 3.2), 137km before the line end and the next dispersion compensator. Secondly, the signal propagating through the Scheme 0 map carries more noise loading than any other scheme whilst travelling over the first four SMF spans. This is due to the recovery of losses from the very large optimum DCF-pre. This loss recovery was very high and required additional amplifiers. This high noise loading results in phase fluctuations introduced by the conversion of amplified spontaneous emission (ASE) noise into phase noise through SPM and IXPM (the latter having a lesser effect). These effects create greater distortions earlier in the transmission line than for any other scheme. For these reasons Scheme 1 benefits greatly from its one inline DCF and a smaller DCF-pre length and requires one less dB of launch power to achieve its 3.1 dB better *Q*-factor at the receiver. The Q-factor of the optimal lumped schemes rises as the number of in-line DCFs increases above one but at a slower rate partly due to the absence of such extreme bit overlapping and partly due to lower noise loading by amplifiers at the pre-compensation node.

When optimised lumped dispersion schemes are employed, system performance levels are determined by a trade-off between nonlinear transmission impairments and optical amplifier noise. Nonlinear degradation deterministically depends upon the deployed dispersion map and signal power.

3.5 Conclusion

In a comprehensive manner, this research systematically identifies the optimal dispersion compensating configurations for the outlined 40Gb/s WDM point-to-point system. Considering the existing terrestrial SMF–DCF link of 838 km, we demonstrate that the performance of a WDM 40Gb/s RZ-DPSK transmission system is not drastically affected by reconfiguration from periodic dispersion management to lumped dispersion mapping. It is shown that excellent performances can be achieved not only by using similar dispersion maps as used in 10Gb/s systems but that the number of inline dispersion compensating fibres (DCFs) can be reduced dramatically whilst imposing only small Q-factor penalties. Demonstrated results for lumped dispersion mapping afford large granularity without greatly compromising system performance. We have shown that for a particular considered system it is possible to replace five to eight existing DCMs with just one compensating module with a penalty of 1.7 dB. This work demonstrates that RZ-DPSK is a very robust modulation format at 40Gb/s and its compatibility with the cost optimised, in-field, 10Gb/s dispersion managed system is superb.

This chapter demonstrates that the transmission of 40Gb/s return-to-zero differential phase-shift keying (RZ-DPSK) signals is robust to lumped dispersion mapping on a typical installed terrestrial single-mode fibre/dispersion compensating fibre (SMF–DCF) link and in this case will withstand propagation over 800 km of SMF with zero in-line group-velocity dispersion compensation. Upgrading similar point-to-point links, with lumped dispersion maps and 40 GB/s RZ-DPSK signals can be achieved while incurring relatively low performance penalties.

Chapter 4

Dispersion Management in Heterogeneous Optical Networks

4.1 Introduction

Technologies such as the reconfigurable optical add drop multiplexer (ROADM) and optical cross-connect (OXC) make possible a reduction in the number of opaque nodes and increase transparent transmission distance and therefore form crucial enabling components for future core network developments [135 - 137]. ROADMs provide flexibility in access bandwidth by dynamic allocation of wavelengths at non-terminating nodes in the network. Transparent OXCs can be remotely reconfigured and cross-connect traffic from various directions while supporting network restoration during partial network failure. Together, these technologies make possible a transition from point to point links to mesh networks creating optically transparent paths (direct- and indirectly-routed) over many hundred, and indeed thousands of kilometers of fibre.

At 40Gb/s, DPSK has shown to be very robust in the terrestrial regime, providing very high Q-factor performance sustained over medium haul distances (<1500km) at readily accessible optical signal to noise ratios (OSNRs) due to its ability to support high launch powers [138,139]. Consequently, high-performing and cost-efficient upgrades of systems to 40Gb/s can be achieved by making use of the existing fibre and equipment infrastructure. It is advantageous to optimise the dispersion management for best performance, which if not constrained to follow a standard engineering rule, can require many thousands of time expensive numerical simulations.

Dispersion management in single-mode fibre based communications has been studied extensively including systems in which amplifier spacing is very large [140,141], and where various approaches have been used such as doubly periodic dispersion maps of compensation in optical mesh networks [129] and dense dispersion management with two-fold periodicity [130,128]. On the optimisation of dispersion management at 40Gb/s, several methods have been proposed, some of which are the conditioning of the dispersion management through adjusting the signal power evolution [142], suppressing XPM by optimising the pre-compensation and residual dispersion per span [143, 144], and recently, reducing the number of zero crossing points in the dispersion map [145]. In terms of reducing the optimisation computation time a recent technique demonstrates a parameter space reducing algorithm [146].

In this chapter the general problem of optimising dispersion maps for 40Gb/s transmission in heterogeneous optical networks using lumped dispersion management is considered. Lumped

dispersion mapping was proven to be a highly effective and economical technique of dispersion management in RZ-DPSK terrestrial point to point links [131, 138, 139, 147 and 148]. Here, this approach is re-examined in the context of 40Gb/s meshed networks, while adding the constraint due to the presence of ROADMs and OXCs, which requires that the residual dispersion for all paths within the optical network is returned close to zero at such nodes. A computationally efficient approach for optimising these maps is identified, and its effectiveness is demonstrated in detailed examples versus standard approaches, such as fixed level of pre-compensation for each inter-ROADM/OXC section.

Lumped dispersion management if applied correctly, results in only a small transmission penalty with respect to conventional maps while reducing the overall system noise and facilitating the deployment of fewer dispersion compensation devices and simpler Er-doped amplifiers. However, if simple engineering rules specifying for instance, the amount of pre-compensation each ROADM/OXC or maximum accumulated residual dispersion are not adopted then, obtaining the best performance requires one to perform a parameter sweep of all viable input power and dispersion compensating fibre length combinations. When performing this task on a heterogeneous transmission line such as System 1 in Fig. 1, it is reasonable to perform a parameter sweep of ~11 launch power levels, say between 0 to 10 dBm (in steps of 1dBm). The total number of numerical simulations required is equal to the eleven launch power levels multiplied by an array of possible DCF combinations. This array is vast, however we reduce the problem by considering each network as a concatenation of "sections", e.g., System 1 comprises section 1, which spans from the transmitter to the first ROADM, section 2, which spans from ROADM-1 to ROADM-2, and the third section, which spans from ROADM-2 to the receiver. Due to the presence of two ROADMs in System 1, the cumulative dispersion requires precise or near precise cancellation, and fibre losses regained, before the signal reaches either a ROADM or the end destination receiver, i.e., as the traffic can enter this link at the ROADMs it is beneficial to have a uniform way to deal with dispersion and losses inherent in each "section" for all signals irrespective of the historical path taken. When applying lumped dispersion management to System 1, DCF is positioned only at positions Di, for i = 1 to 6, therefore in each "section" there are only three ways to deploy the dispersion management: (1) section precompensation only, (2) section postcompensation only or (3) both pre and post section compensation. Obviously the latter method requires optimisation and methods (1) and (2) are simply special cases of (3). Note that although optimisation in this way provides a scheme with good performance, the derived dispersion maps are not the global optimal maps for these systems. Such maps can only be achieved within a distributed dispersion management scheme where one can exercise more degrees of freedom through the inclusion of inline dispersion compensators positioned at intermediary repeater sites. The goal here (and the general goal of lumped dispersion mapping) is to avoid such schemes whilst realising only a very small impairment to system performance.

4.2 Dispersion Map Optimisation Strategy

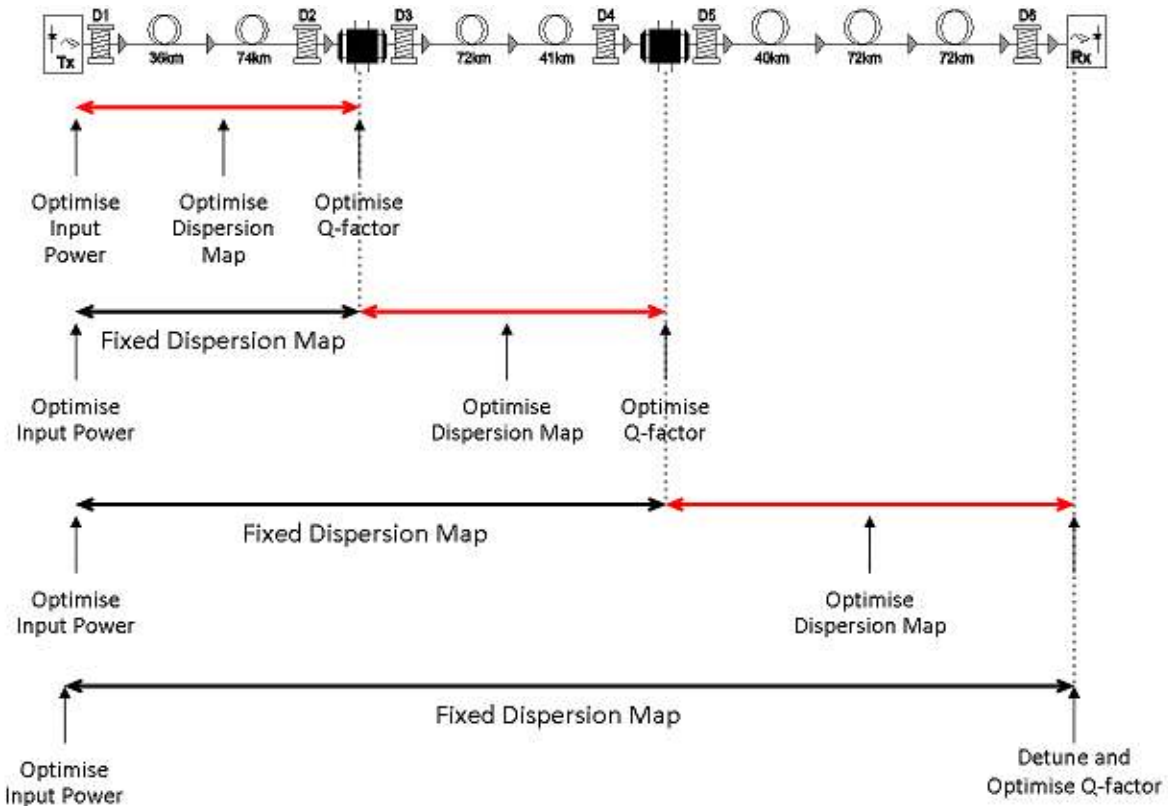

Figure 4.1: Dispersion Map Optimisation Methodology Applied to a Transparent Network

A dispersion management method suitable for optimising 40G lumped dispersion compensating schemes in the standard mono mode fibre (G.652) sections of heterogeneous terrestrial optical networks is now presented. The technique is as follows:

1. Bit patterns are repeatedly propagated at various power levels along the 1st section of the line.
2. The launch power and dispersion compensating scheme are optimised based on the *Q*-factor at the end of section 1 (in the case of System 1, at the 1st ROADM).
3. Once identified, the optimal dispersion map for the 1st section is set up for use (and fixed) for the remainder of the optimisation.
4. We then relaunch "fresh" bit patterns of various power levels from the Tx and propagate them through both of the first two sections. The launch power (into the first two sections) and dispersion compensating scheme (for the second section only) are optimised based on *Q*-factor at the end of section 2 (in System 1, the 2nd ROADM).
5. The best dispersion compensation scheme for the second section is identified and the dispersion map is fixed.
6. This process of optimising the launch power/dispersion scheme combination is performed as before for all subsequent sections throughout the line until the final section of the line is reached.

7. In the final section, dispersion detuning is performed in combination with the optimisation of the launch power/dispersion scheme combination.
8. The full dispersion map for the path chosen is fixed and an optimal signal launch power identified.

4.3 Test Systems and Parameters

The first link under consideration is the 407 km installed terrestrial link depicted in Fig. 4.2(a). There are 11 conventional single-stage EDFAs non-uniformly spaced to compensate for fibre loss, each with a noise figure of 4.5dB. Each EDFA recovers losses from the previous fibre section (i.e., usually losses incurred since the last EDFA). All inline ROADM components have an insertion loss of 20dB. The SMF G.652 fibre parameters at 1550 nm are: D = 16.7 ps/nm/km, Slope = 0.06 ps/nm^2/km, Aeff = 80μm^2, loss = 0.22dB/km. Each DCF fibre has D = -100 ps/nm/km, is slope matched with the SMF, has an Aeff = 30μm^2 and loss = 0.65dB/km. D_1 to D_6 denote the locations where DCF fibre can be installed and optimised. The second link in Fig. 4.2 (b) has the same fibre parameters and D_1 to D_{16} denote the locations housing the dispersion compensating devices. To explore the robustness of the proposed optimisation methodology, two SMF configurations are considered in System 2 (2A and 2B). The SMF lengths for System 2A are non-uniform as shown in the diagram. These distances are representative span lengths which connect towns and cities in the UK outer ring network. System 2A has a total length of 1086km. For the second configuration, System 2B, we switch the heterogeneous SMF lengths in System 2A for 18 uniform 70km SMF spans so that the total length of the system is 1260km. The rest of the configuration parameters are unchanged. The simulation of equal span lengths allows us to check for the effect of resonances between sections. In the numerical simulations we numerically transmit either 33% or 67% RZ-DPSK signals of 1024 bits at 40 Gb/s.

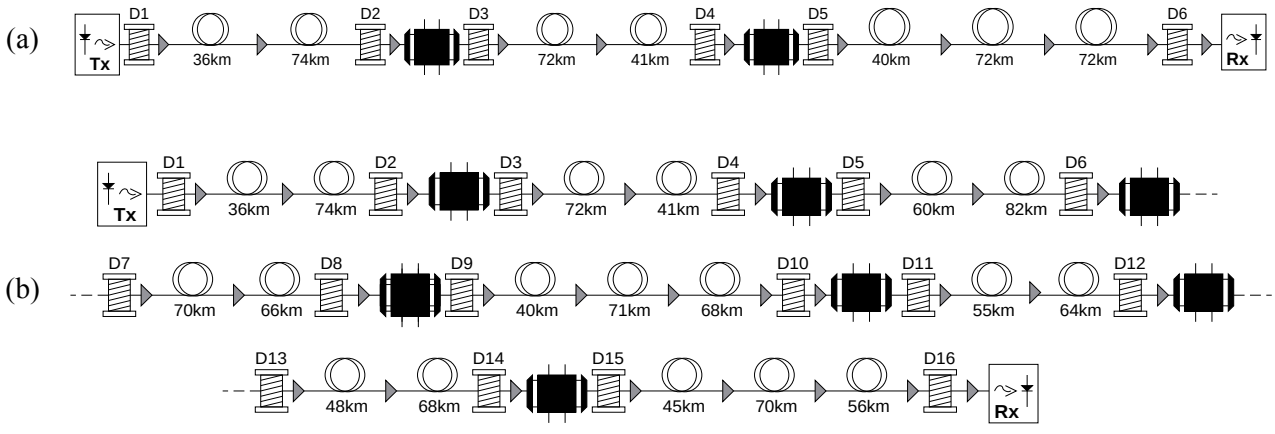

Figure 4.2: (a) System 1, (b) System 2A; in System 2B we switch SMF lengths in 2A for 18x70km spans

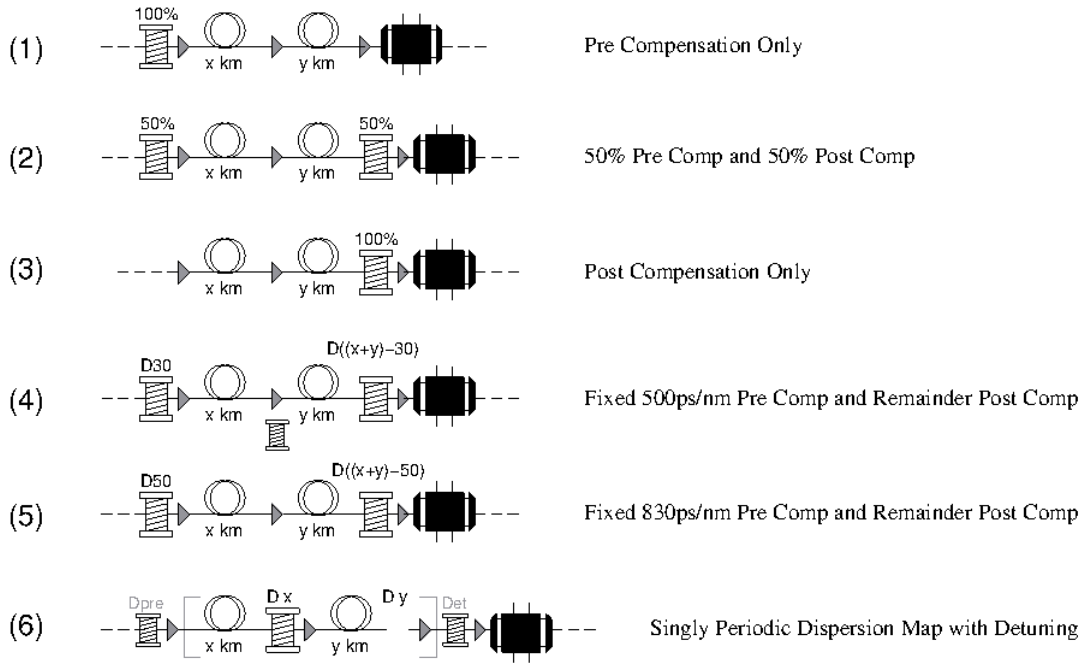

Figure 4.3: Benchmark Dispersion Maps.

4.4 Benchmarking the Proposed Method

To determine the performance of the proposed methodology and the dispersion schemes it found, we chose six benchmarks (see Figure 4.3):

1) Each section has only one precompensation DCF module which is placed directly after either the transmitter or a ROADM and before the primary EDFA of that section.
2) Two DCF modules are used in each section. One DCF module is positioned at the precompensation site (as in (1)) and the other at the postcompensation site. The postcompensation module is placed directly before the final EDFA of the section.
3) Each section has only one postcompensation module placed directly before the final EDFA of the section.
4) Each trunk has only one 500 ps/nm (compensates 30 SMF-km) precompensation DCM which is placed directly after either the transmitter or a ROADM and before the first EDFA in that section.
5) Each trunk has only one 835 ps/nm (compensates 50 SMF-km) precompensation DCM which is placed directly after either the transmitter or a ROADM and before the first EDFA in that section.
6) Singly Periodic Dispersion Map (System 2B only): DCF modules are added directly before the second EDFA in sections 1, 2, 3, 4, 6, 7 and directly before both the second and third EDFAs in sections 5 and 8.

Table 4.1: Proposed method: best dispersion scheme for each system / duty cycle

DCF [SMF-km]	D1	D2	D3	D4	D5	D6	D7	D8	D9	D10	D11	D12	D13	D14	D15	D16
System/DutyCycle	Section 1		Section 2		Section 3		Section 4		Section 5		Section 6		Section 7		Section 8	
1 / 33%	110	0	50	63	70	114	-	-	-	-	-	-	-	-	-	-
1 / 66%	110	0	10	93	20	164	-	-	-	-	-	-	-	-	-	-
2A / 33%	110	0	50	63	142	0	100	36	20	159	40	79	60	56	70	101
2B / 33%	140	0	110	30	100	40	120	20	50	160	140	0	140	0	20	190

4.5 Results of Numerical Simulations

Presented in Table 4.1 are the best dispersion maps found by the proposed method when applied to each system (1, 2A and 2B). The granularity of DCF lengths used in these simulations was 10 SMF-km after *Q*-margin measurements verified these lengths suffice (as per Chapter 3). DCF lengths are given in terms of the quantity of SMF-km compensated. Each section's $D_i + D_{i+1}$ pair compensate 100% of the dispersion accumulated in that section. At the receiver, the *Q*-factor and detuning tolerance is measured for each scheme, they are illustrated in Fig.4.4. The *Q*-factor detuning at the receiver is presented relative to 100% dispersion compensation of the transmitted signal. The *Q*-factor vs. launch power curves in Figure 4.4, illustrate the performance of our "best maps". These maps (see Table 4.1 for DCF lengths) are non-symmetric and perform better than the 50/50 map or indeed any of the other test maps. This result holds for all three system configurations. If we turn to System 1, and the 33% RZ-DPSK simulation (Figure 4.4(a),(b)) we show that at the optimal launch power of 6dBm our method allows for a ~2dB *Q*-factor improvement over the 50/50 split (the best performing benchmark) and up to 5.8 dB better than the worst of the others. Detuning parameters inferred from Fig 4.4 show that an under compensation of ~10ps/nm in the last trunk of System 1 leads to the optimal *Q*-factor at the receiver. Here a detuning deviation of 20ps/nm either side of the optimal *Q*-factor is possible before incurring a 1dB *Q*-factor penalty, a result which is echoed in the detuning tolerances of the 33% RZ-DPSK transmission over Systems 2A and 2B due to identical duty cycle and fibre characteristics. On System 1 only, we also test the robustness of the proposed method to an increase in duty cycle (67% RZ-DPSK). We can see from Figure 4.4 (c) that at the optimal power of 3dBm the proposed method provides a 1.3 dB improvement in *Q*-factor over the 50/50 split whilst figure 4.4 (d) illustrates an under compensation of -55 ps/nm relative to 100% dispersion compensation is required to obtain an optimal. Naturally detuning tolerance for the 67% RZ-DPSK signal is far greater than that of the 33% RZ-DPSK signal. In our longer networks, Systems 2A and 2B, we propagate only 33% RZ-DPSK signals. System 2A is the 1086km heterogeneous terrestrial line. For this system we find that for an optimal launch power of 6dBm, the proposed method allows for ~3dB *Q*-factor improvement over the 50/50 split.

(a)

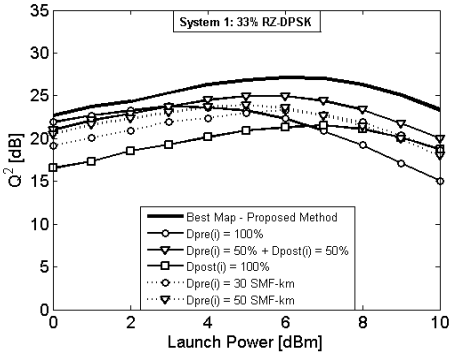

(b)

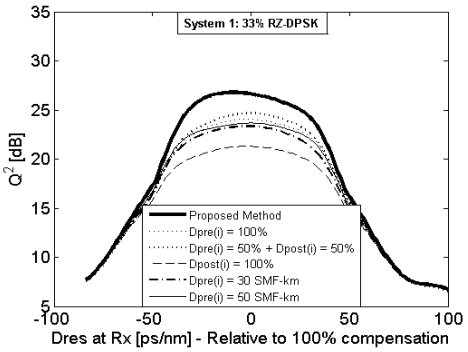

(c)

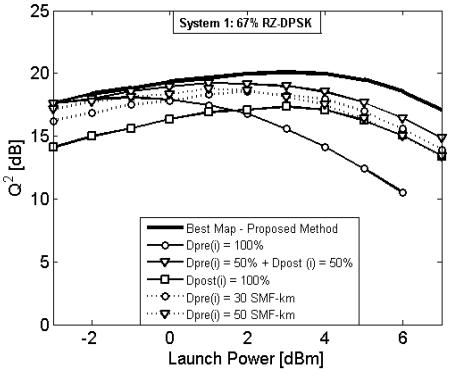

(d)

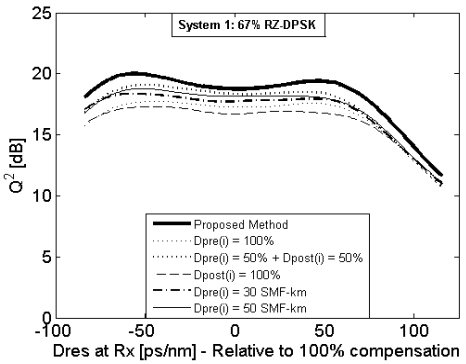

(e)

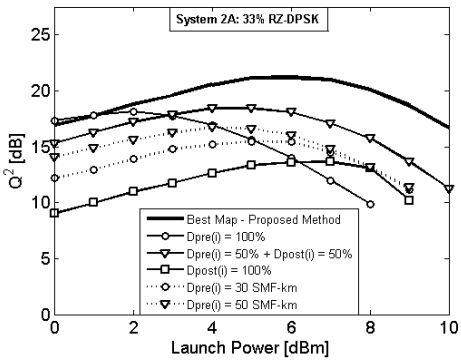

(f)

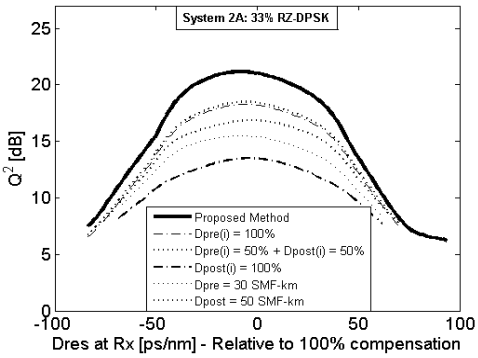

(g)

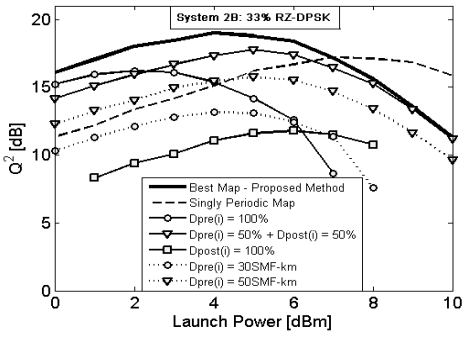

(h)

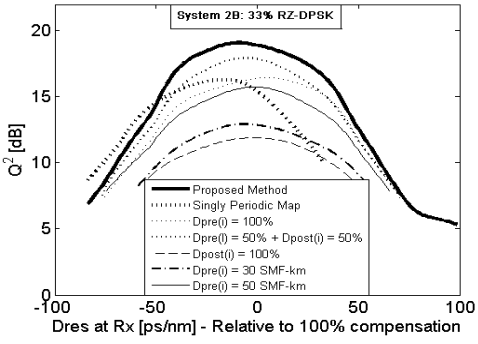

Figure 4.4: Receiver Qfactor vs. Launch Power and Receiver Detuning Tolerance

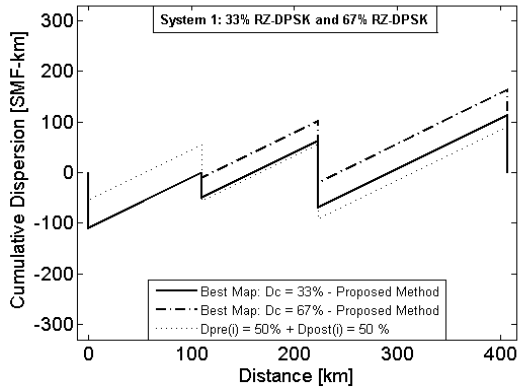

(a)

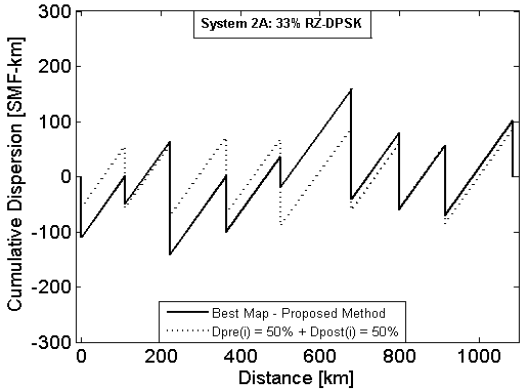

(b)

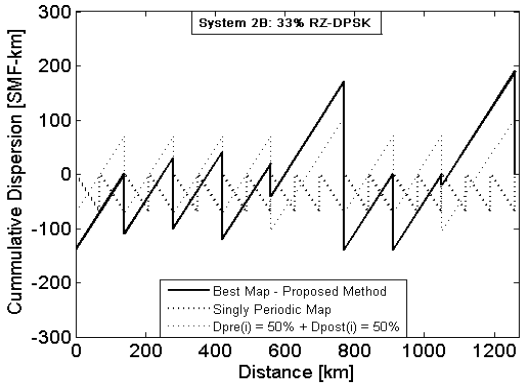

(c)

Figure 4.5: Dispersion Maps across each link.

The sixth benchmark is deployed in System 2B (1260 km homogeneous line with 18 x 70km uniform SMF spans) and is based on a Singly Periodic Dispersion Map [149] as this configuration features equal SMF lengths of 70km in each amplifier span and thus led to a periodic map as can be seen in Figure 4.5 (c). We realise ~2dB *Q*-factor improvement over the50/50 split and a 2.8dB the Singly Periodic Map by employing the proposed method. A detuning deviation of 20ps/nm either side of the optimal *Q*-factor for 2A and 2B is possible before incurring a 1dB penalty in *Q*-factor at the receiver.

In Figure 4.5, we present the dispersion maps for each system configuration. The periodic 50/50 split and the non-periodic maps from the proposed method are shown in contrast to one another. For each of our three systems, the best dispersion schemes have fewer zero-crossing points within their dispersion maps than the 50/50 split benchmark. This agrees with the results in [85], which found that the performance of RZ-DPSK systems strongly depends on the number of zero-crossing points combined with inherited self-phase modulation (SPM). Note that for System 1 we were able to verify that the best dispersion map found by our search method is indeed the optimum via an exhaustive grid-search over the entire parameter space of P_{in} x D1 x D3 x D5 $\approx 2^{15}$ combinations. However, even with our modern computer resources, this was not possible in a reasonable time for Systems 2A and 2B for which there are more than 2×10^{10} and 6×10^{10} possible combinations, respectively.

4.6 Modified Search Technique (Method B)

Finally, we investigate the performance of a modified search algorithm (Method B) which allows for further reduction in the number of calculations required. Specifically, we repeat our optimisation with steps 1-3 unchanged, however at step 4, we use a *single launch power level* equal to the optimal launch power established for section 1 in step 3. Thereafter, we continue the search with this fixed power only, optimising section after section and only once the map in the final section is optimised do we re-optimise the launch power for the whole line, whilst performing dispersion detuning at the Rx. This allows us to further reduce the parameter space required to optimise the whole link from (P_{in} x D1) + (P_{in} x D3) + (P_{in} x D5) + … + (P_{in} x D15), to a parameter space of (P_{in} x D1) + D3 + D5 + … + D15 + P_{in}, and therefore, for System 2A as an example, the number of numerical simulations from 1309 to 250 combinations, a massive reduction over a 2×10^{10} combination grid search. When we re-optimised System 1 with method B, the maps found in both the first two sections were identical to those identified by method A, the only difference being D5 = 60 SMF-km (as opposed to 70 SMF-km) in the third section but less than 0.1dB Q penalty which is within statistical variations in our numerics. In the first half of link 2A, the dispersion map (see Fig. 4.6) found using this revised methodology (method B) differs very little from that found using the full approach (method A). In the latter half of the line the maps vary slightly, particularly in sections 5 and 6. However, we also note that as our optimisation of these systems advances from section to concurrent section the choice of

dispersion scheme for each section becomes increasingly less important in terms of Q performance at the next receiving ROADM. The most critical maps (in terms of being optimised to their full performance potential) are the earliest in the light path and have the ability to affect the performance of the rest of the line to a greater extent as opposed to suboptimal maps in latter sections. Therefore, we find that by dropping the power- and dispersion-map co-optimisation feature of the technique then for System 2A at an optimal launch power of 5dBm (which is 1dBm lower than our primary technique), the modified methodology still allows for a 2dB Q-factor improvement over the 50/50 split and only a 0.25dB Q-factor performance reduction at the receiver than would be achieved by using the initial proposed method.

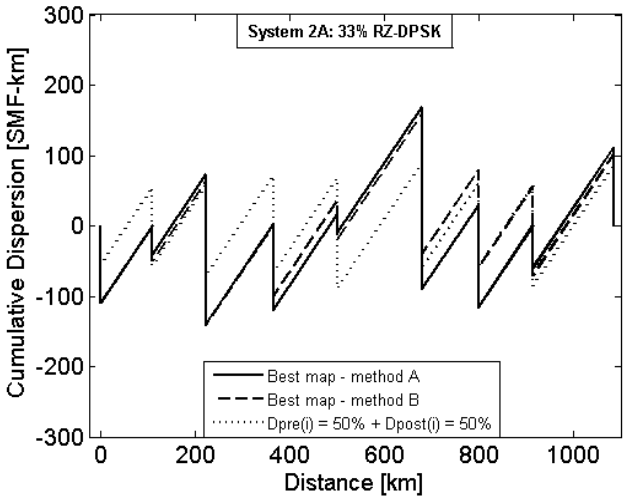

Figure 4.6: System 2a and 33% RZ-DPSK Signals

Finally, in the case of System 2B, our results show matching maps and equal Qs for methods A and B at the optimal launch power while giving a 1.5dB Q-factor improvement over the 50/50 split and a 2.3 dB improvement over the Singly Periodic Map.

4.7 Systems Analysis

Even although the overall system length is over 1000km, the inter-ROADM sections are of lengths between 100km and 150km. As each section has 100% dispersion compensation due to the ROADMs, bit overlapping effects due to pulse spreading (as seen in Chapter 3) will not dominate transmission impairments or influence the choice of dispersion map during simulations. In the numerical optimisations, the parameters which change with the dispersion map in each section are the gains, not-inline, but directly after the DCF at either end of the section. The input powers to the SMF and DCF are the same as the system launch power. Therefore, in essence, Method A has in these particular

system configurations, found by way of *Q*-factor measurements dispersion maps that distribute the gain values of the amplifiers as opposed to having high gains and/or multiple amplifiers lumped together. Of course the fixed benchmark dispersion maps do not have this degree of freedom and this explains to an extent why Method A produces better performing maps than the benchmarks. The best *Q*-factor during the optimisation process comes from a map which has an efficient trade-off between the OSNR level and the level of non-linear signal distortions.

4.8 Varying SMF and DCF Launch Power: Transmission Performance

Fibre nonlinearity and noise generation are two of the main effects which limit transmission performance in optical fibres. In this section we look at varying the launch power into the dispersion compensating fibre to understand the trade-offs between noise and non-linear transmission impairments for our dispersion maps and to gain insight into the performance of the proposed dispersion map optimisation technique. DCF has small effective area and with sufficiently high launch power into the DCF, the DCF will increase the total fibre nonlinearity present in the transmission line by adding its own nonlinear contribution. In this section we revisit Systems 1 and 2a, the optimal maps for each system (identified using method A) and the 50-50 split maps. The aim here is to clarify the system margins associated with these maps through a trade-off between the OSNR level and the level of non-linear distortions.

In these systems some constraints exist due to the presence of the ROADMs inline. Any attenuation of signal power away from its optimal value at a ROADM will reduce the signals *Q*-factor at that ROADM which would limit transparent transmission distance. As the dispersion map has already been optimised we know the optimal power given the dispersion scheme, but only in the regime of recovering span losses at the next EDFA, not when variable gains are introduced. By optimising the dispersion map as before, then optimising the DCF input power afterwards, we contain the combination of variable parameters which require simultaneous optimisation and thus maintain the theme of reducing the optimisation parameter space.

In these numerical simulations, the transmitter launch power is varied in order to vary the launch power into D1 (which changes the effect of the map on nonlinearity). The signal power is then amplified immediately after D1 which gives control over subsequent launch powers into the following SMF spans. After each ROADM, a variable optical attenuator (VOA) is employed, and in the case of System 1, reduces the launch powers into both D3 and D5 (see Figure 4.7). The attenuation is varied between 0 and 10dB in steps of 1dB. The amplifiers directly after D3 and D5 are used to control the launch powers into the SMF spans. In the case of 0 dB attenuation (no VOA), the launch power = D_{pre} input power in each section = SMF input power. In the inter-ROADM sections with two fibre

spans, the launch power into D_{post} (e.g. D2 and D4 in System 1) does not require adjustment as these launch powers are already very low due to losses from the preceding SMF spans. Within the inter-ROADM sections with three fibre spans, there exists an amplifier directly before the section D_{post} (e.g. D6 in System 1), so we choose to recover not all of the loss from the previous SMF span at this amplifier in order to lower the launch power into this DCF. The reduced gain (with respect to fully recovering the previous SMF loss) of this second last amplifier in the three span sections is equal to the attenuation level of the VOAs. The final amplifier in the three span section which follows these DCF recovers this unaccounted loss (by the amount equal to the reduction in gain at the previous amplifier).

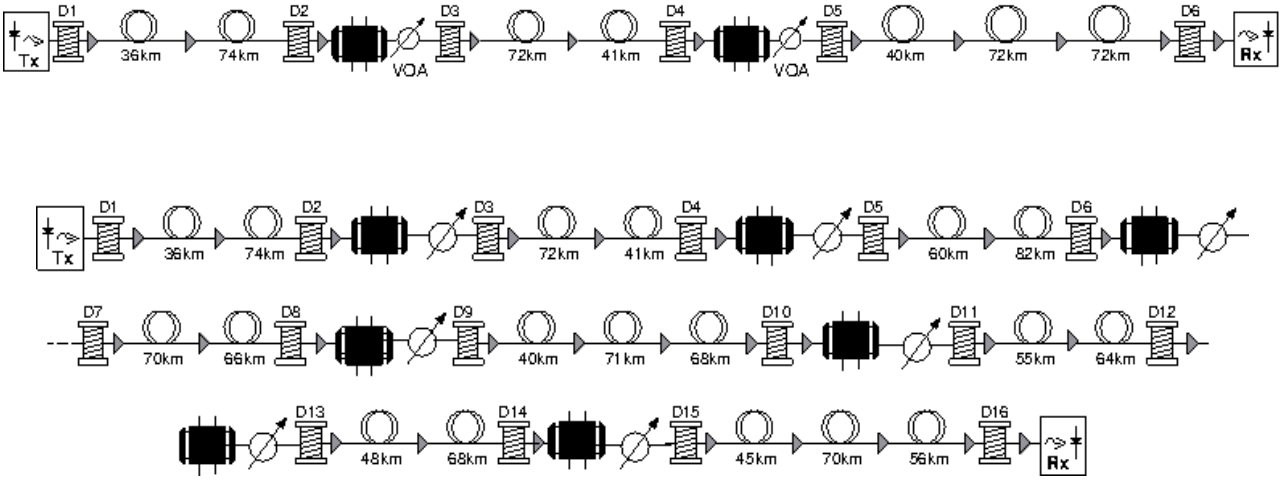

Figure 4.7: System 1 and 2a - VOA locations.

This technique allows variable attenuation of signal power before it is launched into the DCF, and by simultaneously re-optimising the launch power, which is varied between 0 and 10dBm, we also achieve variable launch power into the SMF. The decrease in signal power by each optical attenuator is equal for all VOAs. Note that the variable SMF launch power in this regime is still equal to the power of the signal when it arrives at each ROADM albeit this is now a variable, and is equal to the launch power from the transmitter. While maintaining system simplicity and avoiding any major structural overhaul, this technique allows a reduction of the impact of fibre non-linearity on system performance but at the expense of the OSNR. This is favourable to the opposite case of a good OSNR and a high nonlinear distortion. A main reason for this is that noise gradually accumulates in the system over its length and therefore slowly deteriorates system performance. As these networks have ROADMs inline, the signal can be dropped early in the line with only a small noise accumulation. Nonlinear distortions however have thresholds which when crossed can abruptly decrease the bit-error

rate of these systems. This is of increasing importance in the case where a signal is dropped at a ROADM onto a suboptimal dispersion map for that signal. Furthermore, operating at high distortions leaves little margin for any other possible impairments such as the ageing of a system and its components.

Presented in Figure 4.8 (a)-(d) are the results of these numerical simulations. In both System1 and System 2a, the best maps found by the optimisation technique method A do not benefit from lowering the DCF launch power, however the 50/50 maps gain some improvement in Q-factor. In neither system however does the Q improve enough for the 5050 map to compete with the performance of the Method A optimal maps.

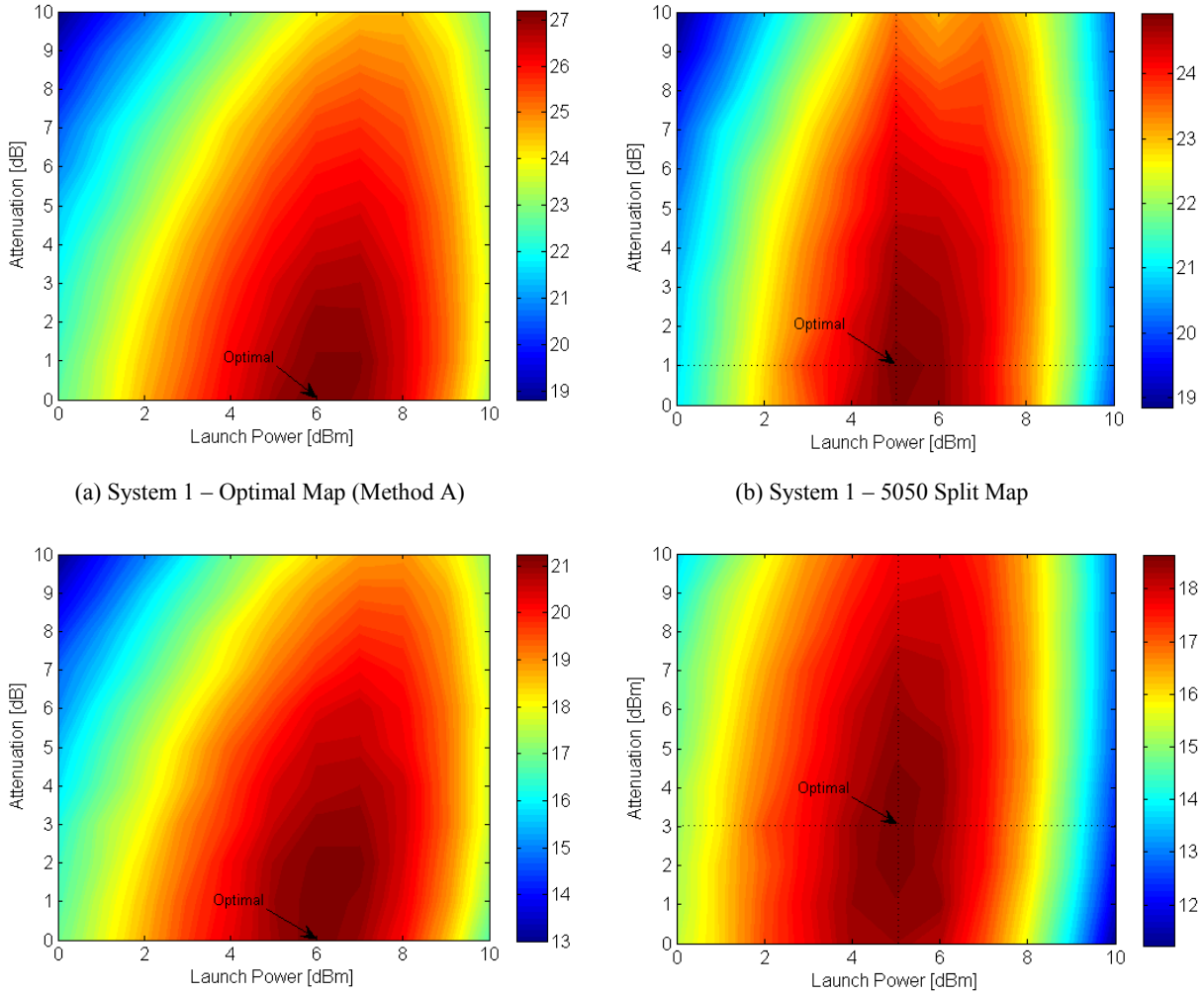

(a) System 1 – Optimal Map (Method A)

(b) System 1 – 5050 Split Map

(c) System 2A – Optimal Map (Method A)

(d) System 2A – 5050 Split Map

Figure 4.8: (a)-(d) Varying DCF launch power results

The Q-factors at the receiver compared to the previous runs without VOAs measured as follows - Optimal map in System 1: Q^2 = 27.26dB (no improvement), Optimal map in System 2a: Q^2 = 21.2dB (no improvement), 50-50 map in System 1: Q^2 = 24.78db increased to Q^2 = 25dB (0.22dB improvement) when 1dB attenuation is applied, and the 50-50 map in System 2a: Q^2 = 18.42dB increased to Q^2 = 18.72dB (0.3dB improvement) when 3 dB attenuation is applied. For both maps in each of the systems the optimal launch power from the transmitter were unchanged and remained 6dBm for the optimal maps of Method A and 5dBm for the 50-50 maps. This means that the optimal launch powers into the SMF have also remained unchanged. These results indicate that the 50-50 split maps in both systems benefit from reduced input power into the DCF in favour of a slightly increased noise loading. These are useful margins to realise for the 50-50 maps if they are to be used as a benchmark for performance. In the case of the optimal maps of Method A, it has been shown at least for these systems that the method finds maps which do balance very well the noise loading / nonlinear distortion trade-off.

4.9 Mesh Network Path

The configuration of amplification schemes and dispersion maps that a signal encounters in mesh networks can be greatly varied. An investigation into the performance margins of an additional mesh network path is presented in this section. The tendency in dispersion management is to optimise dispersion maps from one point in a network to another and from a transmitter to a receiver in a point-to-point fashion. A signal which has been sent by a transmitter in another part of the network, when encountering this dispersion map, will be affected more by propagation effects than if it was travelling on its original optimised path. It is therefore desirable to obtain knowledge of performance margins when a signal encounters a dispersion map not configured specifically for itself.

The performance of an additional path is tested by revisiting System 2a and sending 33% RZ-DPSK traffic from variable distances into System 2a at ROADM-1 (R1) and exiting at ROADM-3 (R3) as shown in Figure 4.9. The dispersion scheme (D3-D4 and D5-D6) is configured as per Table 4.1. Prior to the ROADM network the signal is transmitted over 90km SMF spans with dispersion pre-compensation DCF only. The EDFAs recover losses from the previous fibre. The signals are transmitted at different distances from the ROADM network as the number of spans prior to System 2a is varied between n = 1 to 5 to determine how the dispersion map from R1 to R3 affects the performance of the signal. Once the signal is dropped from System 2a at R3 it encounters another 90km SMF span with dispersion pre-compensation before reaching the receiver (Rx).

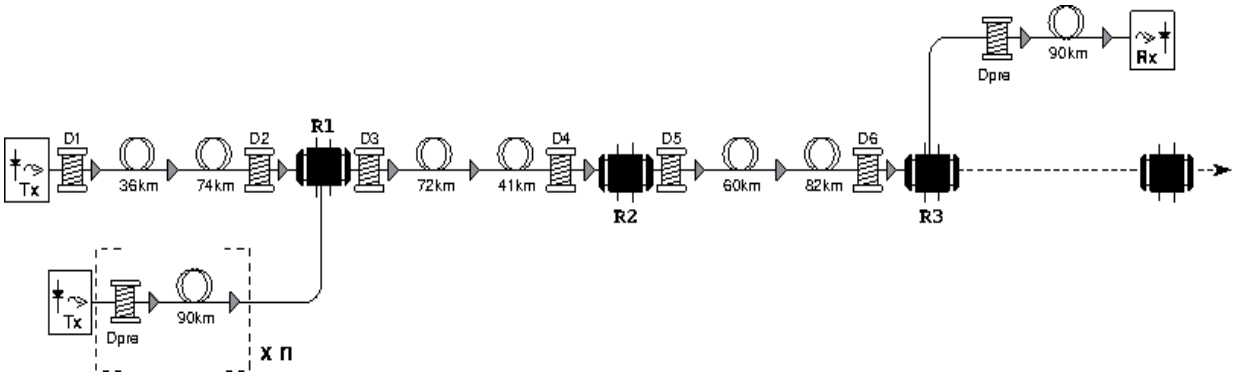

Figure 4.9: Configuration of mesh network path

The *Q*-factor is measured at various stages in the transmission path. When a signal is launched 90km (n = 1) from R1, the *Q*-factor is measured at R1, R2, R3 and the Rx. When a signal is launched further away, such as n = 5 spans from R1, then the Q-factor is measured at the start of span 4 (end of span n = 5), the start of spans 3, 2 and 1 and then, as before, at R1, R2, R3 and the Rx. The results of these numerical simulations are presented in Figure 4.10.

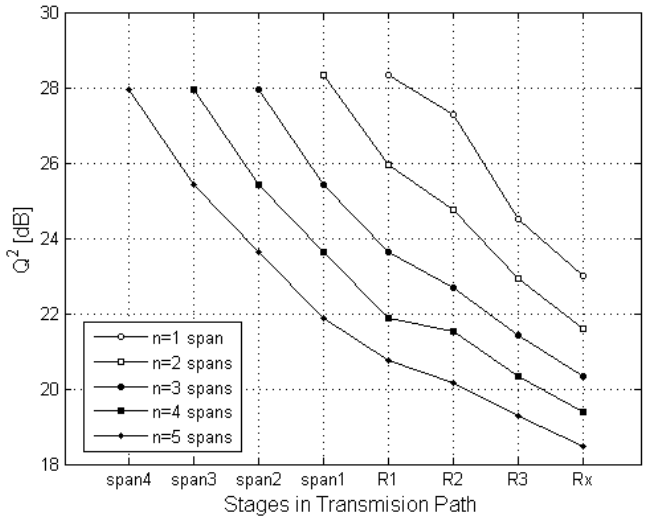

Figure 4.10: *Q*-factor at various stages in the transmission path

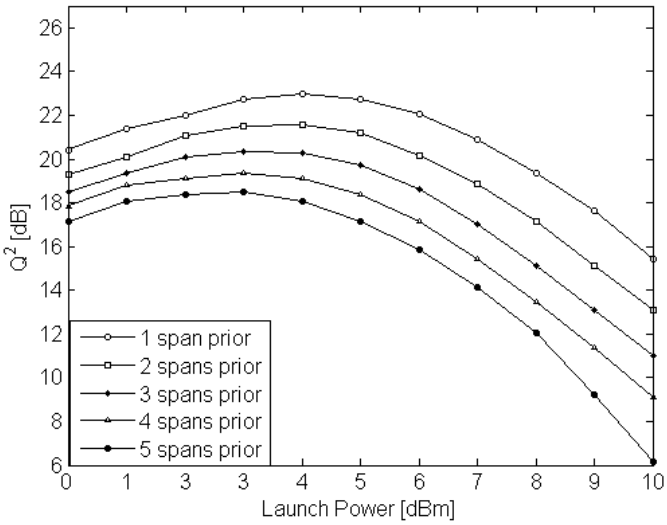

Figure 4.11: *Q*-factor variation vs. launch power from transmitter

In Figure 4.10, note that the optimal launch power (with respect to *Q* performance at the receiver) is 1 dB higher for the configurations with n = 1 and n = 2 prior spans and therefore the first *Q* measurement is slightly higher than the first *Q*-factor for the configurations where n > 2. The effect of the 'alien' (sub-optimal) map on the signal is observed in the differences between *Q*-factors at R1 (before entering this map) and the measurements at R2 and R3. There is certainly a tendency towards greater deterioration of the *Q* after propagation over the sub-optimal map when the signal is launched from a transmitter at closer distances.

Presented in Figure 4.11 is the *Q*-factor variation for various launch powers. As the number of prior spans to the ROADM line increases the non-linear tolerance decreases and the optimal power drops from 4 dBm to 3 dBm (at n = 3). Even after n = 5 spans, 2 sections of suboptimal map and the final 90km before the receiver, we are able to achieve a *Q* = 18 dB.

In Figure 4.10, when the system has n = 5 spans prior to System 2a, then as we advance towards the ROADMs the deterioration of the *Q*-factor becomes less aggressive. Similarly this is observed when comparing the 5 configurations together where the Q-factor at R3 and Rx has a smaller deterioration between these points as the distance propagated beforehand is increased. This is a common feature observed in dispersion management and occurs in many systems. In shows that in many cases the most critical part of a dispersion map (in terms of the map being optimised to obtain a systems full performance potential) are the parts of the map in the earlier sections of the transmission path and will

affect the general performance of the rest of the line to a greater extent than any suboptimal maps encountered later in transmission.

To establish the degrading effects of propagating the signal over the suboptimal map between ROADMs R1 to R3, we transmit a signal over n = 1 prior spans and re-optimise the dispersion map within the sections between R1 and R3 with method A. The re-optmised map had D3 = 50 SMFkm and D5 = 130 SMFkm. As shown in Figure 4.12, re-optmising the map leads to an increased optimal power of 5dBm and improved tolerance to non-linear propagation effects. The Q-factor is also improved by a margin of 0.4dB.

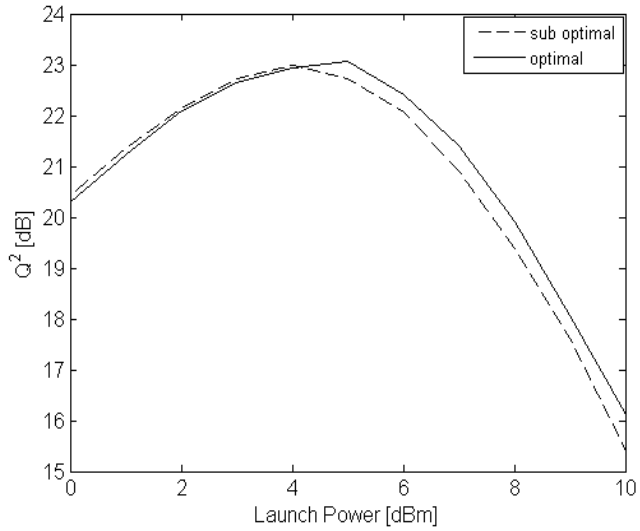

Figure 4.12: n = 1 span prior - sub optimal System 2a map and the re-optimised System 2a map

4.10 Conclusions

ROADMs provide flexibility in access bandwidth but pose new challenges in network design and dispersion management. Optimisation of dispersion maps for best performance can require many thousands of numerical simulations. A dispersion management method suitable for optimising 40G lumped dispersion compensating schemes in the standard mono mode fibre (G.652) sections of heterogeneous terrestrial optical networks was presented. The technique facilitates a vast reduction in the optimisation parameter space facilitating the general goal of lumped dispersion mapping. The maps found by the methodologies introduced are non-symmetric and perform better than the 50/50 map or indeed any of the other maps tested. This result also held for all system configurations under

test. Furthermore when the power co-optimisation was dropped from the technique leaving only the dispersion map optimisation the modified technique again found higher performing maps than the benchmarks.

The launch power for the SMF and DCF infrastructure was varied to determine the performance trade-offs between noise and non-linear transmission impairments for our dispersion maps and to gain insight into the performance of the proposed dispersion map optimisation technique. There was no improvement to the maps of the proposed technique indicating the proposed technique had performed very well and that the method finds maps which do balance very well the noise loading / nonlinear distortion trade-off.

An additional mesh network path was tested to obtain knowledge of performance margins when a signal encounters a dispersion map not configured specifically for itself. Margins were established between the suboptimal map and an optimised map which showed that RZ-DPSK is robust even to maps not originally configured for the light path in which the signal travels. It was shown that the tolerance and performance of RZ-DPSK to these maps will depend on the distance traveled before encountering the sub-optimal map and will also depend on how far the signal must travel on them.

Chapter 5

Dispersion Management in Dynamic Core Optical Networks

5.1 Long Haul Signals and Heterogeneous Rings

Link or node failures in today's high capacity optical networks have the potential to produce severe consequences. Fortunately random component failure events such as a fibre breakage (span failure), or ROADM / OXC breakdown (node failure) can be detected quickly through channel power monitoring at nodes. In the event that a component fails, it is necessary to switch the signal to a backup fibre (path based, end-to-end detouring) or reroute traffic around the failed component (link based, local detouring). End-to-end detouring is essentially a proactive protection technique where fault rescuing resources are allocated at the capacity planning phase. In this case, fibre or wavelength resources are "set-aside" for the purpose of rescuing partial network failure and re-establishing communication. This historically was a viable solution when dark fibres were abundant and had the advantage of fibres which were preconfigured for expected traffic. However, this approach becomes increasingly uneconomical as bandwidth demand steadily increases over time. Furthermore, component failures in practice do not usually occur often enough to warrant the full reservation of wavelengths let alone fibres. In this respect, reactive restoration of phase modulated signals with varied transmission history is very attractive as it has the advantage of low overhead costs in the absence of failures.

The main concern when detouring signals locally, or, rerouting traffic around failed components in heterogeneous networks, is that light paths with little historical commonality would travel over links not designed for variable signals. Although the varied signals may be encoded with the same modulation format and operate at the same line speed, the configuration of amplification schemes and dispersion maps that signals encounter both historically and in subsequent paths may be greatly varied. In order for the rerouting of traffic around failed components in legacy heterogeneous networks to take place, the signal must, primarily, be tolerant to encountered dispersion maps.

In the last chapter we demonstrated how careful node to node dispersion map optimisation can produce excellent maps for use in transparent heterogeneous ROADM networks and when designed with care, can afford a relaxation in receiver CD tolerance requirements allowing increased transparent transmittable distances in the absence of globally optimal dispersion maps.

It is desirable for optical networks to become increasingly mesh-like, so in this chapter we explore the feasibility of detouring signals locally into multi-path heterogeneous ring networks and establish the associated penalties imposed by the encountered non-optimal passive dispersion maps. These dispersion maps are optimised locally within the ring so that the dispersion map which the signal encounters on route to the ring has been optimised in a manner which is completely independent of the optimisation of the dispersion map configuration the signal encounters within the ring. Importantly, we assume that the investigated route is chosen from all potential routes in the network which avoid congestion. It is such then that the configuration of that route is of primary concern and transmission performance must be established. In this investigation we revisit System 2a which appeared in chapter 4, it is the 1086km link with non-uniform SMF lengths. We propagate an RZ-DPSK through this link and instead of receiving the signal at the links end, we detour the signal locally into a heterogeneous ring network with the aim of establishing system margins. These margins can be used to provide guidance in strategic CD management for RZ-DPSK signals in transparent heterogeneous terrestrial legacy networks where G.652, DCF fibres and EDFA infrastructure is in abundance.

Essentially we look to find out whether the System 2a when optimised with Method A can simply be adjoined to the Ring Network which itself has been independently optimised with Method A as in Figure 5.1 (the system configurations in Fig. 5.1 are for illustration purposes only).

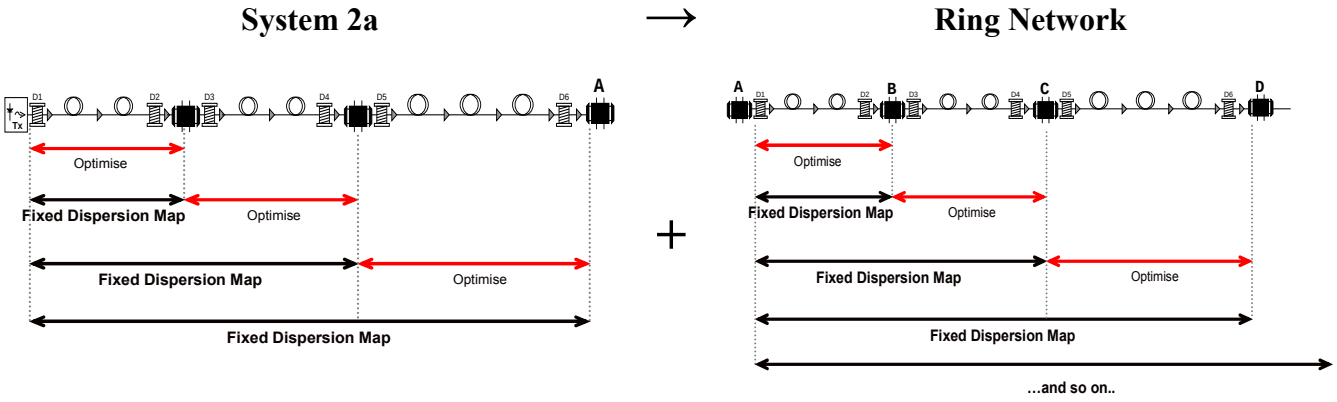

Figure 5.1: Combining independent optimisations of System 2a and a Ring network to extend transparent transmission

It is also interesting to find out how well the approach of concatenating systems optimised with Method A compares in performance to systems configured with 50-50 split type dispersion maps. The 50-50 split map performed well in the investigations in Chapter 4 and has the advantage of providing

uniform maps across the inter-node sections, a feature likely to be beneficial with regard to measured system performance when a signal enters at a random node and with a random history.

5.2 Ring Network Configuration

To begin this investigation we present the half-duplex transparent terrestrial ring in Figure 5.2 which has six nodes incorporating ROADMs. Between each of the node pairs are dispersion managed sections which require configuration. The single-stage EDFAs in the ring are conventional units that each have a noise figure of 4.5dB and recover losses from previous fibre sections. The ROADMs have 20dB insertion loss. The transmission fibre is G.652. Each DCF fibre is slope matched, has an Aeff = 30μm^2 and Loss = 0.65dB/km. Signals are 33% RZ-DPSK modulated in a train of $2^{\wedge 10}$ - 1 PRBS bits. All numerical simulations are performed at a 40 Gb/s line speed and the results averaged over 10 runs to eliminate minor statistical variations. In the dispersion map optimisations, the simultaneous optimisation of D_i and D_{i+1} DCF was performed for each inter-ROADM node link creating inter-node lumped dispersion compensation. At the receiving nodes, residual dispersion was fine tuned to maximise the signals *Q*-factor. Between A and F, the signal can take one of five paths around the ring, (i) A → B → C → D → E → F, (ii) B → C → D → E → F, or, (iii) C → D → E → F, (iv) D → E → F, and finally (v) E → F. Without loss of generality we will focus on the longest route and assume that the incoming signal from System 2a joins the ring network at node A and must travel to the ROADM at F to be either received or routed out of the ring onto an adjoining network.

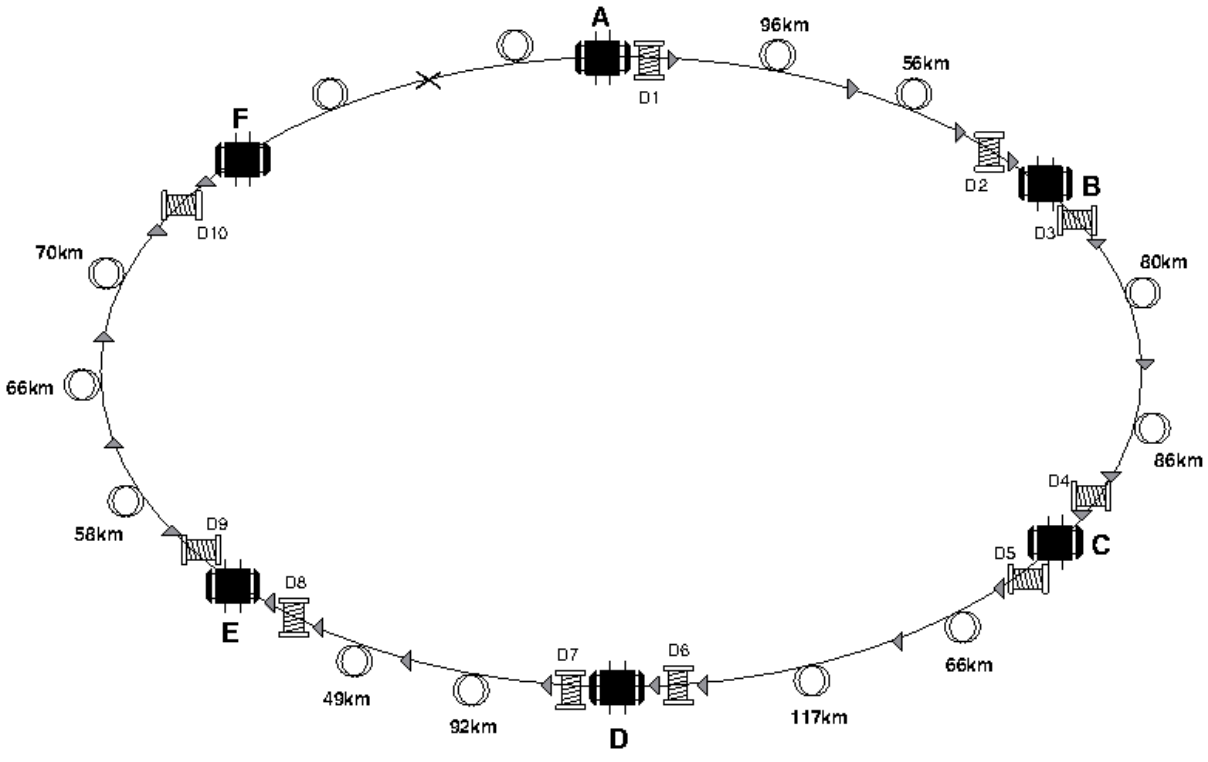

Figure 5.2: Six-node heterogeneous ring network

5.3 Standalone Ring - Optimisation Results

In this section the results of optimising the dispersion maps in the heterogeneous ring are presented. In Tables 5.1 and 5.2, the performance of Method A is compared to the 50-50 split dispersion map at each ROADM and the penalties imposed by transmission in the final column. In Figure 5.3, it can be seen that Method A achieves an optimal launch power of 8dBm and a *Q*-factor of 22.9 at node F, whilst in comparison the 50-50 split map provides an optimal launch power of only 7dBm and a Q-factor of 21.5 at this node. Figures 5.4(a) - 5.3(e) show the *Q*-factor (decibel) topology of the section precompensation (D1, D3, D5, D7, D9) versus launch power for each internode dispersion map in the Ring.

Table 5.1: Performance of Method A for the Heterogeneous Ring

Method A (PP=8 dBm)	Optimised DCM (SMF-km)	*Q* [dB] at following ROADM	*Q* [dB] at Rx	*Q* [dB] reduction
D1	70	29.9	-	-
D3	80	27.5	-	2.4
D5	40	24.0	-	3.5
D7	141	23.4	-	0.6
D9	100	-	22.9	0.6

Table 5.2: Performance of the 50-50 split for the Heterogeneous Ring

50-50 split (PP=7 dBm)	DCM Size (SMF-km)	*Q* [dB] at following ROADM	*Q* [dB] at Rx	*Q* [dB] reduction
D1	70	29.9	-	-
D3	80	27.5	-	2.4
D5	90	23.4	-	4.1
D7	80	22.7	-	0.7
D9	90	-	21.5	1.2

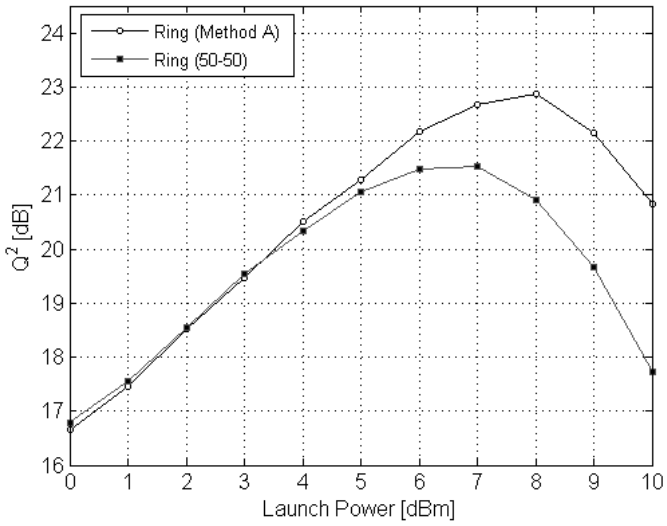

Figure 5.3 Heterogeneous Ring: Method A vs. 50-50 split at receiver.

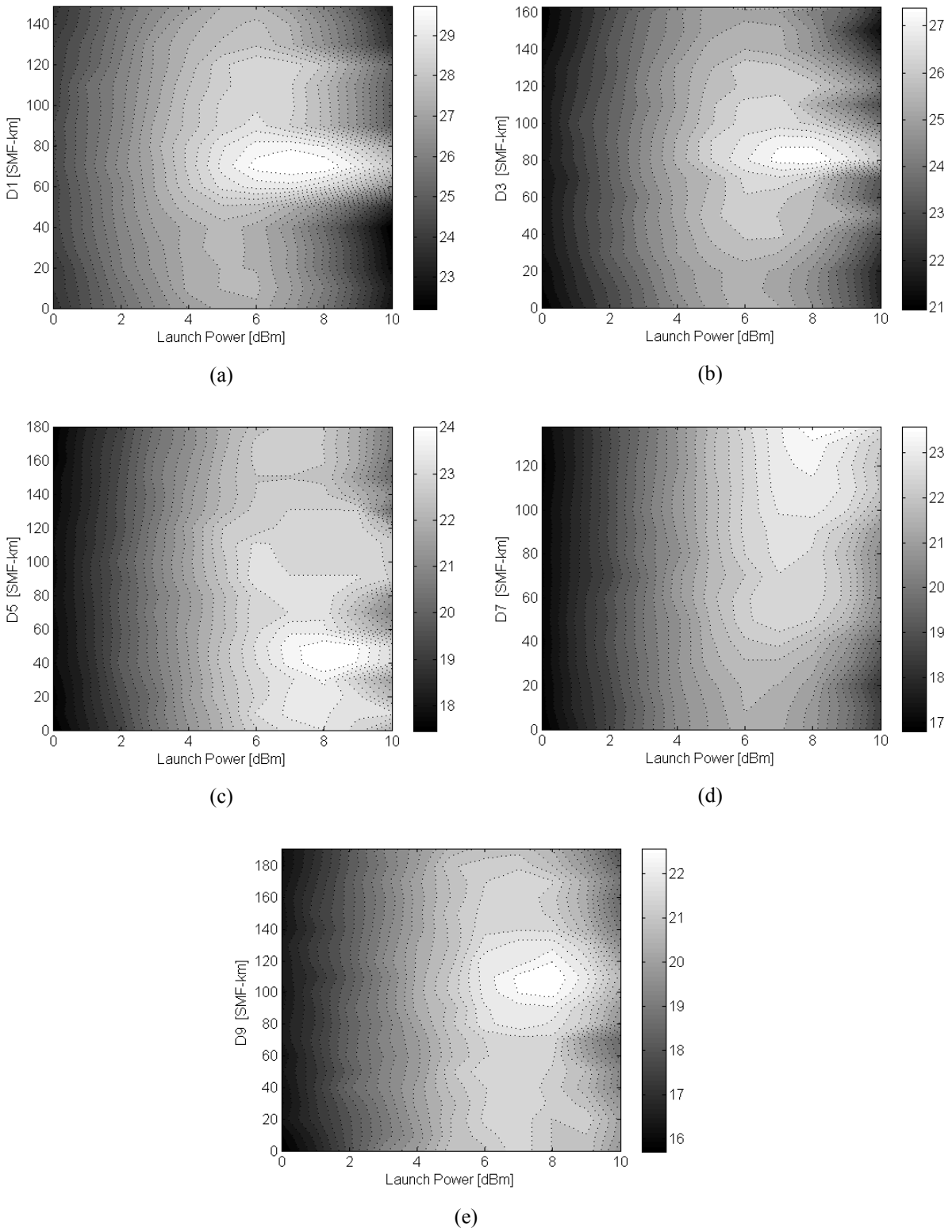

Figure 5.4: Heterogeneous Ring: (a) – (e) Q in the plane (DCM-pre, launch power) for inter ROADM sections.

Although the route from node A to node F is better configured through Method A than employing a 50-50 split map, this however does not necessarily mean that Method A's map is optimal for signals which arrive degraded from previous transmissions. The reason for this is that the encountered dispersion map becomes a little less important with respect to transmission performance as the transmission distance grows. This is an important margin to realise for it implies that the detrimental effect of propagating through a number of alien dispersion maps is related to the distance the signal has travelled before it enters the ring. This is a particularly useful feature in signal protection / network restoration and transparent mesh transmission, as the detriment to the signal imposed on by "local detouring" is not only determined by the dispersion maps that it encounters but on the length of the signals transmission history and the level of both noise accumulation and nonlinear distortion within the signal at that time. It is partly for this reason that the proposed methodology in chapter 4 works so well, as the best possible *Q*-factor is always achieved at the end of the first section, thus the signal gets off to the best possible start (where the dispersion map matters most) in the optimisation of the full transmission line.

5.4 Connected Networks – Propagation over System 2a then around the Ring

After establishing the performance of the standalone ring network with Method A and the 50/50 split map, we now transmit RZ-DPSK signals through System 2a (see chapter 4) but this time rather than receive the signal at the end of System 2a, we send the signal into the ring at ROADM A and propagate it around the ring until it reaches ROADM F. At this stage the signal is received at a combined distance of 1922km from the transmitter of System 2a. At ROADM F dispersion detuning is performed to improve the Q-factor.

In these numerical simulations, both System 2a and the Ring are preconfigured throughout with the optimal maps found by Method A, or, 50-50 split maps. When both systems are configured with Method A, the optimal maps from Table 4.1 and Table 5.1 are employed for System 2a and the Ring respectively.

In Figure 5.5, System 2a launch power versus the Q-factor performance versus after transmission through both System 2a and the Ring network is presented for these systems. The optimal peak power when both systems are configured with Method A is 6dBm and the Q-factor at the end of the combined links is 17.9dB. When both systems are configured with the 50-50 split maps the Q-factor at the receiver is 16.4dB, therefore Method A provides a performance increase of 1.5dB. As can be seen from the Q-factor curves in Figure 5.5, Method A has greater tolerance not only to noise but also helps maintain higher launch powers in into the system.

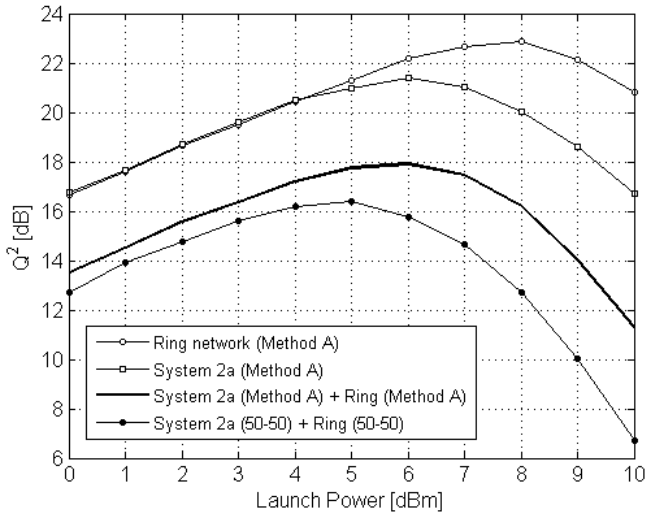

Figure 5.5: Q-factor after transmission through both System 2a and the Ring network.

5.5 Conclusions

In order for the rerouting of traffic around failed components in legacy heterogeneous networks to take place, the signal must, primarily, be tolerant to encountered dispersion maps. We explore the feasibility of detouring signals locally into multi-path heterogeneous ring networks and establish the associated penalties imposed by the encountered non-optimal passive independently configured dispersion maps. RZ-DPSK signals are propagated through System 2a but instead of receiving the signal at this links end, we detour the signal locally into a heterogeneous ring network with the aim of establishing system margins. The signal is received at the end of the ring at a distance of 1922km from the System 2a transmitter. In the UK, this distance would be equal to a return journey between the most southerly point in England and the most northerly point in mainland Scotland, or, in Germany, it would be sufficient in length to connect in a full ring configuration the major cities: Hamburg - Dusseldorf - Stuttgart - Munich - Dresden - Berlin and back to Hamburg.

Configuring both systems with Method A we still maintain a performance increase of 1.5dB after 1922 km, while the method also provides greater tolerance not only to noise but also helps maintain higher launch powers and improved tolerance to non-linear propagation effects.

Chapter 6

Conclusion

Network optimization and simplification is instrumental to the provision of new bandwidth and as such is the high level motivation for this research. Focus in this thesis was directed at terrestrial optical communications systems and the upgrade of fourth generation terrestrial core to metro legacy interconnects to fifth generation transmission system technologies. Retrofitting (without changing infrastructure) was considered for commercial applications. ROADM are crucial enabling components for future core network developments and make possible the transition from point to point links to mesh networks. Their switching capabilities now mean signals can be re-routed mid-link onto sub-optimally configured paths which raises new challenges in network management. System performance is determined by a trade-off between nonlinear impairments and noise, where the nonlinear signal distortions depend critically on deployed dispersion maps. Very large super-computing resources were employed so this thesis could present a comprehensive numerical investigation into the implementation of phase modulated signals in transparent reconfigurable wavelength division multiplexed fibre optic communication terrestrial heterogeneous networks.

In the first chapter, both historical and present developments of fibre optic communication network architectures were introduced along with the associated systems, system topologies and components which characterise the bulk of today's transparent terrestrial networks. This research is primarily centred on retrofitting transparent terrestrial networks with next generation phase modulated transmission technologies that permit faster line speeds and increased spectral efficiency. Therefore, the linear and nonlinear transmission propagation effects encountered during signal propagation through optical fibre were discussed in conjunction with select optical signal measurements which are used for analysing the performance of system designs.

In Chapter 2, some of the fundamental issues in dispersion management were presented in detail as a precursor to the research presented throughout this thesis. A review of dispersion compensating technologies was presented. Dispersion management methodologies proposed prior to this work were reviewed due to their employment in Chapter 4 where they were used as benchmarks against a novel optimisation methodology.

In Chapter 3, a highly economical solution to the dispersion management problem in 40 Gb/s Terrestrial Point to Point Links is presented. We explored the key issue of whether differential phase

encoded modulation formats are compatible with the cost optimised 10Gb/s system configurations. We determined how robust the transmission was to inevitable variations in the dispersion mapping and how large the margins were when suboptimal dispersion management was applied. We presented pragmatic trade-offs between inventory costs and system performance within acceptable performance margins and demonstrated that RZ-DPSK was a very robust and suitable candidate for lumped dispersion mapping with large granularity. We showed that for a particular considered system it is possible to replace five to eight existing DCFs with just one or two compensators with only a small penalty. This work demonstrates that drastic system overhauls can be avoided as RZ-DPSK is a very robust modulation format at 40Gb/s and its compatibility with the cost optimised, in-field, 10Gb/s dispersion managed system is superb.

We switch from using RZ-DPSK in point to point links to its application in heterogeneous networks in Chapter 4. Optimisation of dispersion management for best performance in these networks is advantageous, which if not constrained to follow a standard engineering rule, can require many thousands of time expensive numerical simulations. We present a novel DPSK dispersion map optimisation methodology which reduces drastically the optimisation parameter space and the many combinatory ways to deploy dispersion maps. This alleviates the strenuous task for even our modern super-computing resources and provides a uniform way to deal with dispersion and losses inherent in each section of these systems. Essentially the methodology further develops the results found in Chapter 3 as it provides a robust way to identify high performing lumped dispersion compensating schemes this time for use in heterogeneous 40Gb/s RZ-DPSK terrestrial meshed networks. We then develop a modified search algorithm which allows for further reduction in the number of calculations required to optimise the whole link from (P_{in} x D1) + (P_{in} x D3) + (P_{in} x D3) + … + (P_{in} x D15), to a parameter space of (P_{in} x D1) + D3 + … + D15 + P_{in}, and therefore, for system 2A as an example, the number of numerical simulations from 1309 to 250 combinations, a massive reduction over a 2×10^{10} combination grid search. We showed that by dropping the power- and dispersion-map co-optimisation feature of the technique then for System 2A the modified search algorithm still allowed for a 2dB Q-factor improvement over the 50/50 split and only a 0.25dB Q-factor performance reduction at the receiver than would be achieved by using the initial proposed method. This work was extended to show the viability of these maps in a Mesh network scenario where the methodology performed very well.

It is desirable for optical networks to become increasingly mesh-like. The reactive restoration of phase modulated signals with varied transmission history will be very attractive due to the advantage of low overhead costs in the absence of failures. In Chapter 5 we explore the feasibility of detouring signals locally into multi-path heterogeneous ring networks and established the associated penalties imposed by the encountered non-optimal passive dispersion maps. We show that System A when optimised

with Method A can simply be adjoined to the Ring Network which was independently optimised with Method A. In other words, the optimisation of the ring started where the optimisation of System 2A left off. This creates new possibilities for the use of Method A where concatenation of independent links (real or virtual topologies) can facilitate mesh networking and fault rescuing. Method A outperformed the 50-50 split within systems.

The possibility of future work could come from a number of places. An interesting extension would be to use the methodologies proposed in this thesis in submarine applications where periodic dispersion maps are often deployed for ease of application. The author suspects that Method A (presented in Chapter 4) may be useful in some existing systems to boost the performance of some of the earlier periods in such systems, which ultimately would boost the transmission performance throughout such lines.

Publications

C. French, W. Forysiak and S.K. Turitsyn, “40 Gb/s Optically Transparent Heterogeneous Networks: A Non-Distributed Dispersion Map Optimisation Methodology”, Optics Communications, 282, 2009, pp. 2707 – 2712.

R. Bhamber, C. French, S.K. Turitsyn, V. Mezentsev, W. Forysiak, J.H.B. Nijhof, “Lumped Dispersion Mapping and Performance Margins in Existing SMF–DCF Terrestrial Links”, Journal of Optical Networking, JOSA, Vol. 7, No.2, 2008, pp. 106 – 110.

R. Bhamber, C. French, S.K. Turitsyn, V. Mezentsev, W. Forysiak, J.H.B. Nijhof, “Migration from Periodic to Lumped Dispersion Mapping in Existing SMF/DCF Links”, Presented at the Conference on Lasers and Electro-optics (CLEO), Munich, 17–22 June, 2007.

Bibliography

[1] The Presidency of the Council of the European Union. (2nd December 2008) Vienna "e-Inclusion", Ministerial Conference: http://ec.europa.eu/information_society/events/e-inclusion/2008/doc/conclusions.pdf

[2] J.M.Simmons, "Survivable Passive Optical Networks Based on Arrayed-Waveguide-Grating Architectures", Journal of Lightwave Technology, Vol. 25, No. 12, December 2007, pp. 3658 3668.

[3] S.Bigo, "Multiterabit/s DWDM terrestrial transmission with bandwidth-limiting optical filtering", IEEE Journal of Selected Topics in Quantum Electronics, Vol. 10, Issue, 2, 2004, pp. 329-340.

[4] W.H.Loh, F.Q.Zhou, J.J.Pan, "Novel designs for sampled grating-based multiplexers demultiplexers," Optics Letters, 24, 1999, pp. 1457-1459.

[5] International Telecommunication Union, Series G: Transmission systems and media, ITU-T G.694.1 (06/2002).

[6] R.Dorward, "The Market, Rationale and Technology Options for Flexible Transparent Optical Networks", International Conference on Transparent Optical Networks (ICTON), 2009, paper Mo.B4.4.

[7] E.Desurvire, Erbium-Doped Fibre Amplifiers, Device and System Developments, Wiley-Interscience, August 2002.

[8] D.A.Fishman, J.Ying, X.Liu, S.Chandrasekhar, A.H.Gnauck, "Optical add/drop multiplexer with asymmetric bandwidth allocation and dispersion compensation for hybrid 10-Gb/s and 40- Gb/s DWDM transmission", Proceedings of the Optical Fibre Conference (OFC), 2006, paper OWI64.

[9] S.D.Robinson, "How ROADM Technology is Simplifying Network Management", presented at the OSA/IEEE Optical Fibre Communications & SPIE Nat'l Fibre Optic Engineers Conference (OFC/NFOEC), March 2005, paper NThP2.

[10] E.B.Basch, R.Egorov, S.Gringeri, S.Elby, "Architectural Tradeoffs for Reconfigurable Dense Wavelength Division Multiplexing Systems", Journal of Selected Topics in Quantum Electronics, Vol. 12, no. 4, 2006, pp. 615-626.

[11] C.K.Kao and G.A.Hockham, "Dielectric fibre surface waveguides for optical frequencies", Proc. IEE, vol. 113, 1966, pp. 1151–1151.

[12] G.P.Agrawal, Fibre-Optic Communication Systems, 3rd ed., Wiley, New York, 2002.

[13] G.P.Agrawal, Nonlinear Fibre-Optics, 4th ed., Wiley, New York, 2007.

[14] R.H.Stolen, C.Lin, "Self-phase-modulation in silica optical fibers", Phys. Rev. A 17, 1978, pp. 1448–1453.

[15] T.K.Chiang, N.Kagi, M.E.Marhic, L.G.Kazovsky, "Cross-phase modulation in fiber links with multiple optical amplifiers and dispersion compensators", Journal of Lightwave Technology, 14 (3), 1996, pp. 249-259

[16] H.J.Thiele, R.I.Killey, P.Bayvel, “Influence of fibre dispersion and bit rate on cross-phase-modulation-induced distortion in amplified optical fibre links”, Electronics Letters, 34 (21), 1998, pp. 2050-2051.

[17] G.P.Agrawal, Fibre-Optic Communication Systems, 4th ed., Wiley, New York, 2010.

[18] R.W.Tkach, “Four-Photon Mixing and High-speed WDM Systems”, Journal of Lightwave Technology, Vol. 13, No. 5, May 1995, pp. 841-849.

[19] J.P.Gordon and L.F.Mollenauer, “Phase noise in photonic communications systems using linear amplifiers”, Opt. Letters., vol. 15, no. 23, 1990, pp. 1351 – 1353.

[20] P.Winzer and R.Essiambre, “Advanced optical modulation formats”, Invited paper, ECOC 2003.

[21] S.Bigo, G.Charlet, E.Corbel, “What has hybrid phase/intensity encoding brought to 40Gb/s ultralong haul systems?” Invited paper, ECOC 2004.

[22] G.Charlet, A.Klekamp, “Optimum modulation format for high density and/or ultra long haul transmission at 40 Gb/s” Paper OTh13, 2003.

[23] I.Lyubomirsky, “Advanced Modulation formats for Ultra-Dense Wavelength Division Multiplexing”, White Paper, University of California, 2005.

[24] A.H.Gnauck, P.J.Winzer, “Tutorial: Phase shift keyed transmission“, Optical Fibre Communication Conference (OFC), 2004, paper: TuF5.

[25] D.Breuer, K.Petermann, “Comparison of NRZ and RZ modulation format for 40-Gb/s TDM standard-fibre systems”, IEEE Photonics Technology Letters, Vol. 9, No. 3, 1997, pp. 398–400.

[26] G.Mohs, C.Forst, H.Geiger, G.Fischer, “Advantages of nonlinear RZ and NRZ on 10 Gb/s single-span links”, Optical Fibre Communication Conference (OFC), 2000, paper FC2-1.

[27] H.Sunnerud, M.Karlsson, P.A.Andrekson, “A comparison between NRZ and RZ data formats with respect to PMD-induced system degradations”, IEEE Photonics Technology Letters, Vol. 13, No 5, 2001, pp. 448–450.

[28] A.Gnauck, P.J.Winzer, “Optical Phase-Shift-Keyed Transmission”, Journal of Lightwave Technology, Vol. 23, No 1, 2005, pp. 115 -130.

[29] R.J.Essiambre, B.Mikkelsen, G.Raybon, “Intra-channel cross-phase modulation and four-wave mixing in high-speed TDM systems”, Electronics Letters, 35, 1999, pp.1576.

[30] P.V.Mamyshev, N.A.Mamysheva, “Pulse-overlapped dispersion managed data transmission and intrachannel four-wave mixing”, Optics Letters, 24, 1999, pp 1454.

[31] A.V.Kanaev, G.G.Luther, V.Kovanis, S.R.Bickham, J.Conradi, “Ghostpulse generation suppression in phase-modulated 40-Gb/s RZ transmission”, Journal of Lightwave Technology, Vol. 21, No. 6, 2003, pp. 1486.

[32] M. J. Ablowitz, T. Hirooka, “Resonant intra-channel pulse interactions in dispersion-managed transmission systems”, IEEE Journal on Selected Topics in Quantum Electronics, Vol. 8, No. 3, 2002, pp. 603.

[33] G.Charlet, E.Corbel, J.Lazaro, A.Klekamp, R.Dischler, P.Tran, W.Idler, H.Mardoyan, A.Konczykowska, F.Jorge, S.Bigo, “WDM transmission at 6 Tbit/s capacity over transatlantic

distance, using 42.7Gb/s Differential Phase-Shift Keying without pulse carver", Optical Fibre Communication Conference (OFC), 2004, paper: PD36

[34] C.Xu, X.Liu, W.Xing, "Differential Phase-Shift Keying for High Spectral Efficiency Optical Transmissions", Journal of Selected Topics in Quantum Electronics" Vol. 10, No. 2, 2004, pp. 281-293.

[35] X.Liu, C.Xu, X.Wei, "Nonlinear phase noise in pulse-overlapped transmission based on return-to-zero differential-phase-shift-keying," in Proc. ECOC 2002, Copenhagen, Denmark, 2002, Paper 9.6.5.

[36] X.Wei, X.Liu. Analysis of intrachannel four-wave mixing in differential phase-shift keying transmission with large dispersion. Optics Letters, Vol. 28, No. 23, 2003, pp. 2300.

[37] L.Becouarn, G.Vareille, S.Dupont, P.Plantady, J.F.Marcerou, A.Klekamp, R.Dischler, W.Idler, G.Charlet, "42 x 42.7 Gb/s RZ-DPSK transmission over a 4820 km long NZDSF deployed line using C-band-only EDFAs", Optical Fibre Communication Conference (OFC), 2004, paper: PD37.

[38] A.Gnauck, P.Winzer, "Phase Shift Keyed Transmission", Proceedings of OFC 2004, Paper TuF5.

[39] M.Forzati, A.Berntson, J.Mårtensson, "IFWM Suppression Using APRZ With Optimized Phase-Modulation Parameters", Photonics Technology Letters, Vol. 16, No. 10, 2004, pp. 2368 – 2371.

[40] K.Yonenaga, S.Kuwano, S.Norimatsu, N.Shibata, "Optical duobinary transmission system with no receiver sensitivity degradation", Electronics Letters, Vol. 31, No. 4, 1995, pp. 302–304.

[41] K.Yonenaga, S.Kuwano, "Dispersion-tolerant optical transmission system using duobinary transmitter and binary receiver", Journal of Lightwave Technology, Vol. 15, No. 8, 1997, pp. 1530-1537.

[42] S.Walklin, J.Conradi, "On the relationship between chromatic dispersion and transmitter filter response in duobinary optical communication systems", Photonics Technology Letters, Vol. 9, 1997, pp. 1005–1007.

[43] A.Tan, E.Pincemin, "Performance Comparison of Duobinary Formats for 40-Gb/s and Mixed 10/40-Gb/s Long-Haul WDM Transmission on SSMF and LEAF Fibres", Journal of Lightwave Technology, Vol. 27, No 4, 2009, pp. 396-408.

[44] D.Penninckx, M.Chbat, L.Pierre, J.Thiery, "The phase-shaped binary transmission (PSBT): a new technique to transmit far beyond the chromatic dispersion limit", Photonics Technology Letters, Vol. 9, 1997, pp. 259 – 261.

[45] D.Penninckx, G.Vendrome, M.Maignan, J.C.Jacquinot, "Experimental verification of the phase-shaped binary transmission (PSBT) effect", Photonics Technology Letters, Vol. 10, 1998, pp. 612 – 614.

[46] D.Penninckx, "Enhanced-phase-shaped binary transmission," Electronic Letters, Vol. 36, 2000, pp. 478-480.

[47] G.Charlet, S.Lanne, L.Pierre, C.Simonnean, P.Tran, H.Mardoyan, P.Brindel, M.Gorlier, J.C.Antona, M.Molina, P.Sillard, J.Godin, W.Idler, S.Bigo, "Cost-optimised 6.3 Tbit/s-capacity terrestrial link over 17x100 km using phase-shaped binary transmission in a conventional all-EDFA SMF-based system", OFC, Feb, 2003, PD25.

[48] H.Bissessur, L.Pierre, J.P.Hamaide, “Enhanced PSBT: demonstration of dispersion tolerance and noise resistance over 300 km terrestrial link”, Electronic Letters, Vol. 37, No.1, 2001, pp. 45-46.

[49] I.Lyubomirsky, B.Pitchumani, “Impact of optical filtering on duobinary transmission”, Photonics Technology Letters, Vol. 16, No. 8, 2004, pp. 1969–1971.

[50] A.Tan, A.Bezard, E.Pincemin, Y.Jaouen, A.Tonello, S.Wabnitz, J.D.Ania-Castañòn, S.K.Turitsyn, “Performance comparison of duobinary modulation formats for 40 Gb/s long-haul WDM transmission”, ECOC, Sep. 2006, We3.P.94.

[51] G.Bosco, A.Carena, V.Curri, R.Gaudino, P.Poggiolini, “Quantum limit of direct receivers using duobinary transmission”, Photonics Technology Letters, Vol. 15, No. 1, 2003, pp. 102–104.

[52] P.Brindel, L.Pierre, G.Ducournau, O.Latry, M.Kétata, O.Leclerc, “Optical generation of 43 Gbit/s phase-shaped binary transmission format from DPSK signal using 50 GHz periodic optical filter”, ECOC, Sept. 2005, Vol. 4, pp. 847–848.

[53] K.S.Cheng, J.Conradi, “Reduction of pulse-to-pulse interaction using alternative RZ formats in 40 Gb/s systems”, Photonics Technology Letters, Vol. 14, No. 1, 2002, pp. 98-100.

[54] Y-H.Wang and I.Lyubomirsky, “Balanced Detection Schemes for Optical Duobinary Communication Systems”, Journal of Lightwave Technology, Vol. 29, No 12, 2011, pp. 1739.

[55] C.Wree, J.Leibrich, W.Rosenkranz, “RZ-DQPSK Format with High Spectral Efficiency and High Robustness Towards Fibre Non-linearities”, Proc. ECOC 2002, paper 9.6.6.

[56] R.A.Griffin, R.I.Johnstone, R.G.Walker, J.Hall, S.D.Wadsworth, K.Berry, A.C.Carter, M.J.Wale, J.Hughes, P.A.Jerram, N.J.Parsons, “10Gb/s optical differential quadrature phase shift key (DQPSK) transmission using GaAs/AlGaAs integration”, OFC 2002, paper FD6.

[57] R.A.Griffin, R.I.Johnstone, R.G.Walker, S.D.Wadsworth, A.C.Carter, M.J.Wale, “Integrated DQPSK Transmitter for Dispersion Tolerant and Dispersion Managed DWDM Transmission”, paper FP6, OFC 2003.

[58] R.A.Griffin, A.C.Carter, “Optical Differential Quadrature Phase Shift Key (oDQPSK) for High Capacity Optical Transmission”, paper WX6, OFC 2002.

[59] P.S.Cho, V.Grigoryan, Y.A.Godin, A.Salamon, Y.Achiam, “Transmission of 25Gbit/s RZ-DQPSK Signals with 25GHz Channel Spacing over 1000km of SMF28 Fibre”, IEEE Photonics Technology Letters, Vol.15, No.3, pp 473-475, March 2003.

[60] C.Wree, M.Serbay, W.Rosenkranz, “Towards 1.6 b/s/Hz spectral efficiency by strong optical filtering of RZ-DQPSK”, Post Deadline Paper, ECOC 03.

[61] C.Wree, N.Hecker-Denschlag, E.Gottwald, P.Krummrich, J.Leibrich, E.D.Schmidt, B.Lankl, W.Rosenkranz, “High Spectral Efficiency 1.6 b/s/Hz Transmission (8 x 40 Gbit/s with a 25 GHz Grid) Over 200km SSMF Using RZ_DQPSK and Polarisation Multiplexing”, IEEE Photonics Technology Letters, Vol.15, No.9, September 2003.

[62] G.Kramer, A.Ashikhmin, A.J.van Wijngaarden, W.Xing, “Spectral Efficiency of Coded Phase-Shift Keying for Fibre Optic Communication”, IEEE Journal of Lightwave Technology, Vol.21, No.10, pp 2438-2445, October 2003.

[63] T.Tokle, C.R.Davidson, M.Nissov, J.X.Cai, D.Foursa, A.Pilipetskii, “6500km Transmission of RZ-DQPSK WDM signals”, Electronic Letters, Vol.40, No.7, pp. 444–445, Apr. 2004.

[64] M.Serbay, C.Wree, W.Rosenkranz, “Implementation of Differential Precoder for High Speed Optical DQPSK Transmission”, Electronic Letters, Vol.40, No.20, September 2004.

[65] C.Wree, J.Leibrich, J.Eick, W.Rosenkranz, D.Mohr, “Experimental Investigation of Receiver Sensitivity of RZ-DQPSK Modulation Format using Balanced Detection”, OFC, 2003, paper ThE5.

[66] A.H.Gnauck, “Linear and Nonlinear Performance of 42.7-Gb/s Single-Polarization RZ-DQPSK Format”, IEEE Photonics Technology Letters, Vol. 18, No. 7, 2006, pp.883.

[67] D. van de Borne, S.L.Jansen, G.D.Khoe, H.de Waardt, E.Gottwald, “Line Optimisation in Long Haul Transmission Systems with 42.8-Gbit/s RZ-DQPSK Modulation”, OFC, 2006, paper OFD2.

[68] W.Idler, E.Lach, B.Junginger, W.Kuebart, K.Schuh, A.Klekamp, D.Werner, A.G.Steffan, A.Schippel, M.Schneiders, S.Vorbeck, R.Braun, “WDM field trial over 764 km SSMF with 16x112 Gb/s NRZ-DQPSK co-propagating with 10.7 Gb/s NRZ”, Proceedings Optoelectronics Communications Conference, 2010, pp.1-3.

[69] M.Alfiad, “111-Gb/s Transmission Over 1040-km Field-Deployed Fibre With 10G/40G Neighbours”, Photonics Technology Letters, Vol. 21, No. 10, 2009, pp.615.

[70] M.Duelk, “Next generation 100 Gb/s Ethernet,” ECOC, 2005, Paper Tu3.1.2.

[71] M.Batayneh, D.A.Schupke, M.Hoffmann, A.Kirstadter, B.Mukherjee, “Optical Network Design for a Multiline-Rate Carrier-Grade Ethernet Under Transmission-Range Constraints”, Journal of Lightwave Technology, Vol. 26, No. 1, 2008, pp. 121.

[72] M.Daikoku, I.Morita, H.Taga, H.Tanaka, T.Kawanishi, T.Sakamoto, T.Miyazaki, T.Fujita, “100Gb/s DQPSK transmission experiment without OTDM for 100G Ethernet transport”, OFC, 2006, Paper PDP36.

[73] P.J.Winzer, G.Raybon, C.R.Doerr, L.L.Buhl, T.Kawanishi, T.Sakamoto, M.Izutsu, K.Higuma, “2000-km WDM transmission of 10 x 107Gb/s RZ-DQPSK”, ECOC, 2006, Paper Th 4.1.3.

[74] P.J.Winzer, G.Raybon, S.Chandrasekhar, C.R.Doerr, T.Kawanishi, T.Sakamoto, K.Higuma, “10 x 107-gb/s NRZ-DQPSK transmission over 12 x 100 km including 6 routing nodes”, OFC, 2007, paper PDP24.

[75] P.Cho, “Investigation of 2-b/s/Hz 40Gbit/s DWDM Transmission over 4 x 100km SMF28 Fibre Using RZ-DQPSK and Polarisation Multiplexing”, IEEE Photonics Technology Letters, Vol.16, No.2, February 2004.

[76] D.van de Borne, S.L.Jansen, E.Gottwald, P.M.Krummrich, G.D.Khoe, H.de Waardt, “1.6-b/s/Hz Spectrally Efficient 40 x 85.6-Gb/s Transmission Over 1,700 km of Using POLMUX-RZ-DQPSK”, PDP34, OFC 2006.

[77] D.van de Borne, S.L.Jansen, G.D.Khoe, H.de Waardt, E.Gottwald, “A comparison between Multi-level Modulation Formats: 21.4-Gbit/s RZ-DQPSK and POLMUX-RZ-DPSK”, paper OThR2, OFC 2006.

[78] C.R.S.Fludger, T.Duthel, D. van den Borne, C.Schulien, E.D.Schmidt, T.Wuth, J.Geyer, E.De Man, G.D.Khoe, and H.de Waardt, “Coherent equalization and POLMUX-RZ-DQPSK for robust 100-GE transmission”, Journal of Lightwave Technology, vol. 26, no. 1, pp.64–72, Jan. 2008.

[79] D. van de Borne, V.Sleiffer, M.S.Alfiad, S.L.Jansen, T.Wuth, “POLMUX-QPSK modulation and coherent detection: the challenge of long-haul 100G transmission”, ECOC 2009, 20-24 September, 2009, Vienna, Austria.

[80] M. Alfiad, D.van de Borne, T.Wuth, M.Kuschnerov, H.de Waardt, “On the Tolerance of 111-Gb/s POLMUX-RZ-DQPSK to Nonlinear Transmission Effects”, Journal of Lightwave Technology, Vol. 29, No. 2, 2011.

[81] Michael G. Taylor, “Coherent Detection for Optical Communications using Digital Signal Processing”, OFC, 2007, Paper OMP1.

[82] Sebastien Bigo, “Coherent Detection: A Key Enabler for Next-Generation Optical Transmission Systems?”, ICTON, 2007, Paper Tu.B4.5

[83] E.Ip, A.P.T.Lau, D.J.F.Barros, J.M.Kahn, “Coherent detection in optical fibre systems”, Optics Express, Vol. 16, No. 2, 2008, pp.753.

[84] X.Liu, S.Chandrasekhar, A.Leven, “Digital self-coherent detection”, Optics Express, Vol. 16, No. 2, 2008, pp. 792–803.

[85] D.van den Borne, “POLMUX-QPSK modulation and coherent detection: the challenge of long-haul 100G transmission”, ECOC, 2009, Paper 3.4.1.

[86] P.A.Humblet, M.Azizoglu, “On the bit error rate of lightwave systems with optical amplifiers”, Journal of Lightwave Technology, Vol. 9, 1991. pp. 1576 – 1582.

[87] X.Wei, X.Liu, C.Xu, "Q factor in numerical simulations of DPSK with optical delay demodulation", Online Publication. http://arxiv.org/abs/physics/0304002

[88] X.Wei, X.Liu and C.Xu, "Numerical Simulation of the SPM Penalty in a 10-Gb/s RZ-DPSK System”, IEEE Photonics Technology Letters, Vol.15, No.11, 2004, pp.1636 - 1638.

[89] P.Becker, A.Olsson, R.Simpson, Erbium-Doped Fibre Amplifiers: Fundamentals and Technology, Toronto, Canada Academic Press, 1999.

[90] R.Schober, P.Bayvel, F.Di Pasquale, “Analytical model for the calculation of the optical signal-to-noise ratio (SNR) of WDM EDFA chains”, Optical and Quantum Electronics, 31, 1999, pp. 237-241.

[91] D.Marcuse, “Interdependence of waveguide and material dispersion”, Applied Optics, 18, 1979, pp. 2930 –2932.

[92] I.H.Malitson, “Interspecimen Comparison of the Refractive Index of Fused Silica”, Journal of the Optical Society of America (JOSA), Vol. 55, Issue 10, 1965, pp. 1205-1208.

[93] A.Antos, D.Smith, “Design and characterization of dispersion compensating fibre based on LP01 mode”, IEEE J. Lightwave Technology, 12, 1994, pp. 1739–1745.

[94] F.Gires, P.Tournois, "An interferometer useful for pulse compression of a frequency modulated light pulse", C. R. Academic Science, Paris, 258, 1964, pp. 6112–6115.

[95] X.Shu, K.Sugden, K.Byron, "Bragg-grating-based all-fibre distributed Gires Tournois etalons" Optics Letters, Vol. 28, 11, 2003, pp. 881-883.

[96] X.Shu, K.Sugden, P.Rhead, J.Mitchell, I.Felmeri, G.Lloyd, K.Byron, H.Zhijian, I.Khrushchev, I.Bennion, "Tuneable dispersion compensator based on distributed Gires-Tournois etalons", IEEE Photonics Technology Letters, Vol. 15, 8, 2003, pp. 1111-1113.

[97] D.Moss, L.Lunardi, M.Lamont, G.Randall, P.Colbourne, S.Chandrasekhar, L.Buhl, "Tuneable Dispersion Compensation at 10 Gb/s and 40 Gb/s Using Multicavity All-Pass Etalons," OFC 2003 Technical Digest, 2003, pp. 162-163.

[98] H.Ooi, K.Nakamura, Y.Akiyama, T.Takahara, T.Terahara, Y.Kawahata, H.Isono, G.Ishikawa, "40-Gb/s WDM Transmission with Virtually Imaged Phased Array (VIPA) Variable Dispersion Compensators," J. Lightwave Technol., Vol. 20, No. 12, 2002, pp. 2196-2203.

[99] F.Ouellette, "Dispersion cancellation using linearly chirped Bragg grating filters in optical waveguides", Optics Letters, 12, 1987, pp. 847–849.

[100] S.Watanabe, M.Shirasaki, "Exact Compensation for both Chromatic Dispersion and Kerr Effect in a Transmission Fibre Using Optical Phase Conjugation", IEEE J. Lightwave Technology, Vol. 14, 3, 1996, pp. pp. 243–249.

[101] J.McNicol, M.O'Sullivan, K.Roberts, A.Comeau, D.McGhan, L.Strawczynski, "Electrical Domain Compensation of Optical Dispersion", OFC, 2004, Paper OThJ3.

[102] K.O.Hill, F.Bilodeau, B.Malo, T.Kitagawa, S.Theriault, D.C.Johnson, J.Albert, "Aperiodic in-Fibre Bragg gratings for optical Fibre dispersion compensation", OFC 1994.

[103] K.O.Hill, S.Theriault, B.Malo, F.Bilodeau, T.Kitagawa, D.C.Johnson, J.Albert, K.Takiguchi, T.Kataoka, K.Hagimoto, "Chirped in-Fibre Bragg grating dispersion compensators: linearization of the dispersion characteristic and demonstration of dispersion compensation in a 100 km, 10 Gbit/s optical fiber link", Electronics Letters, Vol. 30, 1994, pp.1755–1756.

[104] J.A.R.Williams, I.Bennion, K.Sugden, N.J.Doran, "Fibre dispersion compensation using a chirped in-Fibre Bragg grating", Electronics Letters, Vol. 30, 1994, pp.985–987.

[105] K.O.Hill, F.Bilodeau, B.Malo, T.Kitagawa, S.Thériault, D.C.Johnson, J.Albert, K.Takiguchi, "Chirped in-Fibre Bragg grating for compensation of optical fibre dispersion", Optics Letters, Vol. 19, 1994, pp.1314–1316.

[106] F.Ouellette, P.A.Krug, T.Stephens, G.Dhosi, B.Eggleton, "Broadband and WDM dispersion compensation using chirped sampled fibre Bragg gratings", Electronics Letters, Vol. 31, No. 11, 1995, pp. 899-900.

[107] B.J. Eggleton, T. Stephens, P.A. Krug, G. Dhosi, Z. Brodzeli, F. Ouellette, "Dispersion compensation using a fibre grating in transmission", Electronics Letters, Vol. 32, No. 17, 1996, pp. 1610-1611.

[108] K.O.Hill, G. Meltz, "Fibre Bragg Grating Technology Fundamentals and Overview", Journal Of Lightwave Technology", Vol. 15, No. 8, 1997, pp.1263-1276.

[109] J.Brennan "Dispersion management with long-length fibre Bragg gratings", Optical Fibre Communication Conference (OFC), March 2003, paper FC1.

[110] Y.Painchaud, A.Mailloux, H.Chotard, E.Pelletier, M.Guy, "Multi-channel fibre Bragg gratings for dispersion and slope compensation", Optical Fibre Communication Conference (OFC), March 2002, paper TB3.

[111] D. van den Borne, “42.8-Gb/s RZ-DQPSK Transmission With FBG-Based In-Line Dispersion Compensation”, Photonics Technology Letters, Vol. 19, No. 14, 2007, pp. 1069 – 1071.

[112] A.Dochhan, S.Smolorz, H.Rohde, W.Rosenkranz, “FBG Dispersion Compensation in a 43 Gb/s WDM System: Comparing Different FBG Types and Modulation Formats”, ICTON, 2009, paper We.C2.5.

[113] Z.Pan, Y.W.Song, C.Yu, Y.Wang, Q.Yu, J.Popelek, H.Li, Y.Li, A.E.Willner, “Tuneable Chromatic Dispersion Compensation in 40-Gb/s Systems Using Nonlinearly Chirped Fibre Bragg Gratings”, Journal Of Lightwave Technology, Vol. 20, No. 12, 2002, pp.1263-1276.

[114] E.G.Turitsyna, S.Xuewen, S.K.Turitsyn, I.Bennion, “Design and Fabrication of Fibre Bragg Gratings With V-Shaped Dispersion Profile”, Journal Of Lightwave Technology, Vol. 25, No. 2, 2007, pp. 606 - 611.

[115] X.Shu, K.Sugden, I.Bennion, “Optically tuneable chromatic dispersion controller with coupled-cavity etalon structure,” Optics Letters, Vol. 30, No. 12, 2005, pp. 1440–1442.

[116] A.Corchia, C.Antonini, A.D'Ottavi, A.Mecozzi, F.Martelli, P.Spano, G.Guekos, R.Dall'Ara, “Mid-Span Spectral Inversion without Frequency Shift for Fibre Dispersion Compensation: A System Demonstration”, IEEE Photonics Technology Letters, Vol. 11, No. 2, 1999, pp. 275-277.

[117] G.S.He, “Optical Phase Conjugation: Principles, Techniques, and Applications,” Progress in Quantum Electronics, Vol. 26, No. 3, 2002, pp. 131-191.

[118] S.L.Jansen, D.van den Borne, B.Spinnler, S.Calabrò, H.Suche, P.M.Krummrich, W.Sohler, G.D.Khoe, H.de Waardt, “Optical Phase Conjugation for Ultra Long Haul Phase-Shift-Keyed Transmission”, IEEE Journal of Lightwave Technology, Vol. 24, No. 1, 2006, pp. 54 – 64.

[119] S.Jansen, D.van de Borne, G.D.Khoe, H.de Waardt, P.M.Krummrich, S.Spalter, “Phase Conjugation for Increased System Robustness”, Proc OFC, March 2006, paper OTuK3.

[120] R.J.Essiambre, P.J.Winzer, X.Q.Wang, W.Lee, C.A.White, E.C.Burrows, “Electronic predistortion and fibre nonlinearity”, Photonics Technology Letters, Vol. 18, No. 17, 2006, pp. 1804–1806.

[121] B.Franz, F.Buchali, D.Rösener, H.Bülow, “Adaptation techniques for electronic equalizers for the mitigation of time-variant distortions in 43 Gb/s optical transmission systems”, OFC, 2007, pp. 1–3.

[122] C.Xia, W.Rosenkranz, “Electrical Equalization for Duobinary and Phase Shift Keyed Modulation Formats”, Workshop on the Design of Next Generation Networks, Belgium, 6 Feb 2006.

[123] K.Fukuchil, T.Ito, “Electrical compensation technology for high speed signal and its feasibility study on 40-Gb/s transmission”, CLEO, 2007.

[124] M.E.McCarthy, J.Zhao, A.D.Ellis, P.Gunning, “Full-Field Electronic Dispersion Compensation of a 10 Gb/s OOK Signal Over 4 124 km Field-Installed Single-Mode Fibre”, Journal of Lightwave Technology., Vol. 27, No.23, 2009, pp. 5327-5334.

[125] R.I.Killey, H.J.Thiele, V.Mikhailov, P.Bayvel, “Reduction of intrachannel nonlinear distortion in 40-Gb/s-based WDM transmission over standard fibre”, IEEE Photonics Technology Letters, Vol. 12, No. 12, 2000, pp. 1624–1626.

[126] R.Essiambre, B.Mikkelsen, G.Raybon, “Intra-channel cross phase modulation and four-wave mixing in high-speed TDM systems”, Electronics Letters, Vol. 35, 1999, pp. 1576–1578.

[127] D.S.Govan, W.Forysiak, “Long-distance 40-Gbit/s soliton transmission over standard fibre by use of dispersion management”, Optics Letters, Vol. 23, 19, 1998, pp. 1523–1525.

[128] S.Banerjee, A.Agarwal, D.F.Grosz, A.P.Kung, D.N.Maywar, “Doubly Periodic Dispersion Maps for 10 and 40 Gbs Ultra-Long-Haul Transmission”, Electronics Letters, Vol. 40, No. 20, 2004.

[129] C.Xie, “A Doubly Periodic Dispersion Map for Ultra long-Haul 10- and 40-Gb/s Hybrid DWDM Optical Mesh Networks”, IEEE Photonics Technology Letters, Vol. 17, No. 5, 2005, pp. 1091-1093.

[130] M.Shtaif, “Ultrahigh Data-Rate Transmission Using a Dense Dispersion Map With Two-Fold Periodicity”, IEEE Photonics Technology Letters, Vol. 20, No. 8, 2008, pp. 620-622.

[131] J.H.B.Nijhof, W.Forysiak, “Investigation of Optimal Dispersion Management for Terrestrial 40Gbit/s RZ-DQPSK Transmission Systems”, presented at the Conference on Lasers and Electro-optics (CLEO), Long Beach, Calif. 21–26 May 2006, paper CThE.

[132] D. van de Borne, S.L.Jansen, E.Gottwald, G.D.Khoe, H. de Waardt, “Lumped Dispersion Management in Long-Haul 42.8-Gbit/s RZ-DQPSK Transmission”, Electronics Letters, Vol. 40, 22, 2004, pp. 1436.

[133] E.G.Shapiro, M.P.Fedoruk, S.K.Turitsyn, “Direct modelling of error statistics at 40 Gbit/s rate in SMF/DCF link with strong bit overlapping”, in ECOC Proc. 2006, Paper Mo3.2.2.

[134] R.S.Bhamber, S.K.Turitsyn, V.Mezentsev, “Effect of carrier reshaping and narrow MUX-DEMUX filtering in 0.8 bit/s/Hz WDM RZ-DPSK transmission”, Optical and Quantum Electronics, Vol 39, No. 8, 687-692, 2007.

[135] S.D.Robinson, “How ROADM Technology is Simplifying Network Management”, presented at the OSA/IEEE Optical Fibre Communications & SPIE Nat'l Fibre Optic Engineers Conference (OFC/NFOEC), March 2005, paper NThP2.

[136] P.Green, “Progress in Optical Networking”, IEEE Communications Magazine, Vol. 39, 1, 2001, pp. 54 - 61.

[137] B.Basch, R.Egorov, S.Gringeri, S.Elby, “Architectural Tradeoffs for Reconfigurable Dense Wavelength-Division Multiplexing Systems”, IEEE Journal of Selected Topics in Quantum Electronics, Vol. 12, No. 4, 2006, pp. 1 - 12.

[138] R.Bhamber, C.French, S.K.Turitsyn, V.Mezentsev, W.Forysiak, J.H.B.Nijhof, “Lumped Dispersion Mapping and Performance Margins in Existing SMF-DCF Terrestrial Links”, Journal of Optical Networking, Vol. 7, No. 2, 2008, pp. 106 - 110.

[139] R.Bhamber, C.French, S.K.Turitsyn, V.Mezentsev, W.Forysiak, J.H.B.Nijhof, “Migration from Periodic to Lumped Dispersion Mapping in Existing SMF/DCF Links” presented at the Conference on Lasers and Electro-optics (CLEO), Munich, 17th June 2007.

[140] D.Breuer, K.Jürgensen, F.Küppers, A.Mattheus, I.Gabitov, S.K.Turitsyn, “Optimal Schemes for Dispersion Compensation of Standard Monomode Fibre Based Links”, Optics Communications, 140, 1997, pp. 15-18.

[141] D.Breuer, F.Küppers, A.Mattheus, E.G.Shapiro, I.Gabitov, S.K.Turitsyn, "Symmetrical Dispersion Compensation for Standard Monomode-Fibre-Based Communication Systems with Large Amplifier Spacing", Optics Letters, Vol. 22, No. 13, 1997, pp. 982 - 984.

[142] F.Zhang, C.A.Bunge, K.Petermann, A.Richter, "Optimum Dispersion Mapping of Single-Channel 40 Gbit/s Return-to-Zero Differential Phase-Shift Keying Transmission Systems", Optics Express, Vol. 14, No. 15, 2006, pp. 6613 - 6618.

[143] X.Li, F.Zhang, C.Zhangyuan, X.Anshi, "Optimum Dispersion Mapping of 40 Gb/s RZ-DPSK WDM Transmission Systems with XPM-induced Nonlinear Phase Noise", International Nano-Optoelectronics Workshop (i-NOW), 2007, Poster Session 2, paper 37.

[144] X.Li, F.Zhang, Z.Chen, A.Xu, "Suppression of XPM and XPM-induced Nonlinear Phase Noise for RZ-DPSK Signals in 40Gbit/s WDM Transmission Systems with Optimum Dispersion Mapping", Optics Express, Vol. 15, No. 26, 2007, pp. 18247 – 18252.

[145] H.Taga, S.S.Shu, J.Yi.Wu, W.T.Shih, "A Theoretical Study of the Effect of Zero-crossing Points Within the Dispersion Map Upon a Long Haul RZ-DPSK System", Optics Express, Vol. 16, No. 9, 2008, pp. 6163 - 6169.

[146] O.Gaete, L.D.Coelho, B.Spinnler, E.D.Schmidt, N.Hanik, "Global Optimisation of Optical Communication Systems", presented at the European Conference on Optical Communications (ECOC), Brussels, 21–25 September 2008, paper P.4.17.

[147] D. van de Borne, S.L.Jansen, E.Gottwald, G.D.Khoe, H. de Waardt, "Lumped Dispersion Management in Long-haul 42.8 Gb/s RZ-DQPSK Transmission", presented at the European Conference on Optical Communications (ECOC), Cannes, France 24–28 September 2006, paper Mo3.2.2.

[148] X.Chen, C.Kim, L.Guifang, Z.Bingkun, "Numerical Study of Lumped Dispersion Compensation for 40-Gb/s Return-to-Zero Differential Phase-Shift Keying Transmission", IEEE Photonics Technology Letters, Vol. 19, No.8, 2007, pp. 568 - 570.

[149] S.Ramachandran, Springer Series: Optical and Fiber Communications Reports 5, 429, 2007.